CLARA conceptual design report

2014 JINST 9 T05001

(http://iopscience.iop.org/1748-0221/9/05/T05001)

PUBLISHED BY IOP PUBLISHING FOR SISSA MEDIALAB
RECEIVED: *January 21, 2014*
ACCEPTED: *March 25, 2014*
PUBLISHED: *May 9, 2014*

TECHNICAL REPORT

CLARA conceptual design report

J.A. Clarke,[a,b,*] **D. Angal-Kalinin,**[a,b] **N. Bliss,**[a] **R. Buckley,**[a,b] **S. Buckley,**[a,b] **R. Cash,**[a] **P. Corlett,**[a,b] **L. Cowie,**[a,b] **G. Cox,**[a] **G.P. Diakun,**[a,b] **D.J. Dunning,**[a,b] **B.D. Fell,**[a] **A. Gallagher,**[a] **P. Goudket,**[a,b] **A.R. Goulden,**[a,b] **D.M.P. Holland,**[a,b] **S.P. Jamison,**[a,b] **J.K. Jones,**[a,b] **A.S. Kalinin,**[a,b] **W. Liggins,**[a,b] **L. Ma,**[a,b] **K.B. Marinov,**[a,b] **B. Martlew,**[a] **P.A. McIntosh,**[a,b] **J.W. McKenzie,**[a,b] **K.J. Middleman,**[a,b] **B.L. Militsyn,**[a,b] **A.J. Moss,**[a,b] **B.D. Muratori,**[a,b] **M.D. Roper,**[a,b] **R. Santer,**[a,b] **Y. Saveliev,**[a,b] **E. Snedden,**[a,b] **R.J. Smith,**[a,b] **S.L. Smith,**[a,b] **M. Surman,**[a,b] **T. Thakker,**[a,b] **N.R. Thompson,**[a,b] **R. Valizadeh,**[a,b] **A.E. Wheelhouse,**[a,b] **P.H. Williams,**[a,b] **R. Bartolini,**[c,d] **I. Martin,**[c] **R. Barlow,**[e] **A. Kolano,**[e] **G. Burt,**[b,f] **S. Chattopadhyay,**[b,f,g,h] **D. Newton,**[b,g] **A. Wolski,**[b,g] **R.B. Appleby,**[b,h] **H.L. Owen,**[b,h] **M. Serluca,**[b,h] **G. Xia,**[b,h] **S. Boogert,**[i] **A. Lyapin,**[i] **L. Campbell,**[j] **B.W.J. McNeil**[j] **and V.V. Paramonov**[k]

[a] *STFC Daresbury Laboratory, Sci-Tech Daresbury, Warrington, U.K.*
[b] *Cockcroft Institute, Sci-Tech Daresbury, Warrington, U.K.*
[c] *Diamond Light Source, Oxfordshire, U.K.*
[d] *John Adams Institute, University of Oxford, U.K.*
[e] *University of Huddersfield, U.K.*
[f] *University of Lancaster, U.K.*
[g] *University of Liverpool, U.K.*
[h] *University of Manchester, U.K.*
[i] *John Adams Institute at Royal Holloway, University of London, U.K.*
[j] *University of Strathclyde, U.K.*
[k] *Institute for Nuclear Research of the RAS, Moscow, Russian Federation*

E-mail: jim.clarke@stfc.ac.uk

ABSTRACT: This report describes the conceptual design of a proposed free electron laser test facility called CLARA that will be a major upgrade to the existing VELA accelerator test facility at Daresbury Laboratory in the UK. CLARA will be able to test a number of new free electron laser schemes that have been proposed but require a proof of principle experiment to confirm that they perform as predicted. The primary focus of CLARA will be on ultra short photon pulse generation which will take free electron lasers into a whole new regime, enabling a new area of photon science to emerge.

KEYWORDS: Accelerator modelling and simulations (multi-particle dynamics; single-particle dynamics); Beam dynamics; Accelerator Subsystems and Technologies; Instrumentation for FEL

*Corresponding author.

doi:10.1088/1748-0221/9/05/T05001

Contents

2014 JINST 9 T05001

2014 JINST 9 T05001

Acknowledgments

The authors gratefully acknowledge the support we have received from the international accelerator and FEL communities in the development of the conceptual design of CLARA. Special thanks are due to colleagues at the Paul Scherrer Institute for their very helpful advice and input to this report and their support of CLARA in general. The authors are also extremely grateful to colleagues at the Laboratoire de l'Accélérateur Linéaire for sharing their experience of RF photoinjectors. Finally, we would like to thank the University of Strathclyde for kindly providing the RF photoinjector, klystron and other equipment for the VELA project.

2014 JINST 9 T05001

Chapter 1

Introduction and motivation

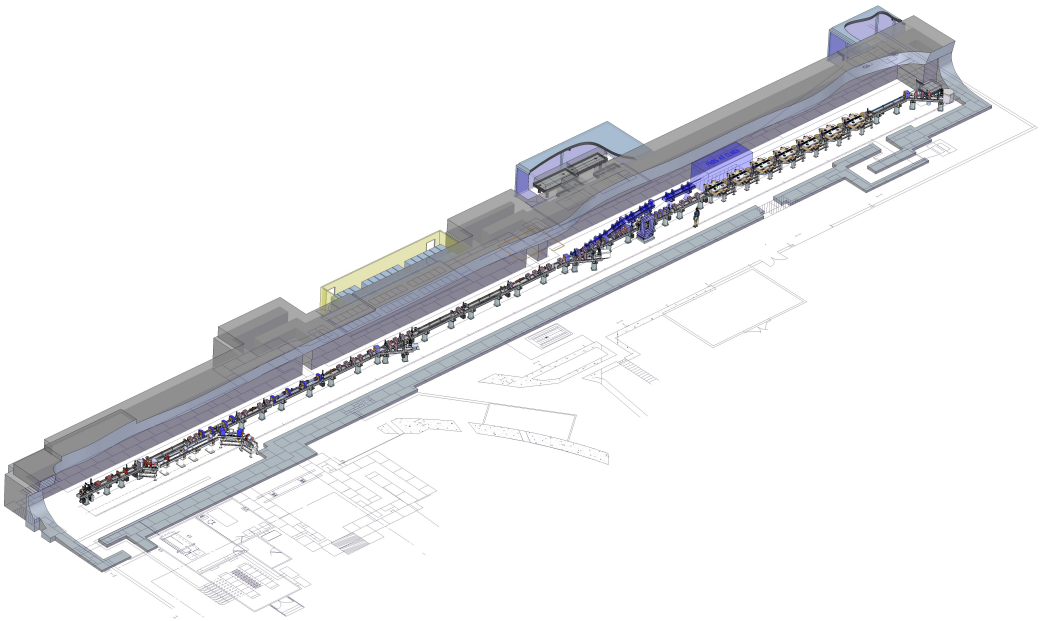

Figure 1.1. CLARA — the Compact Linear Accelerator for Research and Applications.

Free-electron lasers (FELs) have made huge advances in the past few years with the first successful demonstration of an X-ray FEL at LCLS in the USA in 2009 [1], followed by similar success at SACLA in Japan in 2011 [2]. New X-ray facilities are currently under construction in Germany [3], Switzerland [4], and elsewhere and soft X-ray FELs, such as FLASH in Germany [5] and FERMI@Elettra in Italy [6], are also operating for users routinely. Whilst the new X-ray FELs are remarkable in their performance the potential for improvements is enormous. Many suggestions have been made by FEL experts for improving the FEL photon output in terms of temporal coherence, wavelength stability, increased power, intensity stability and ultra-short pulse generation. Unfortunately, given the low number of operating FELs and the pressure to dedicate significant time for user exploitation it is not surprising that very few of these ideas have been tested experimentally. This Conceptual Design Report describes the design of CLARA (Compact Linear

2014 JINST 9 T05001

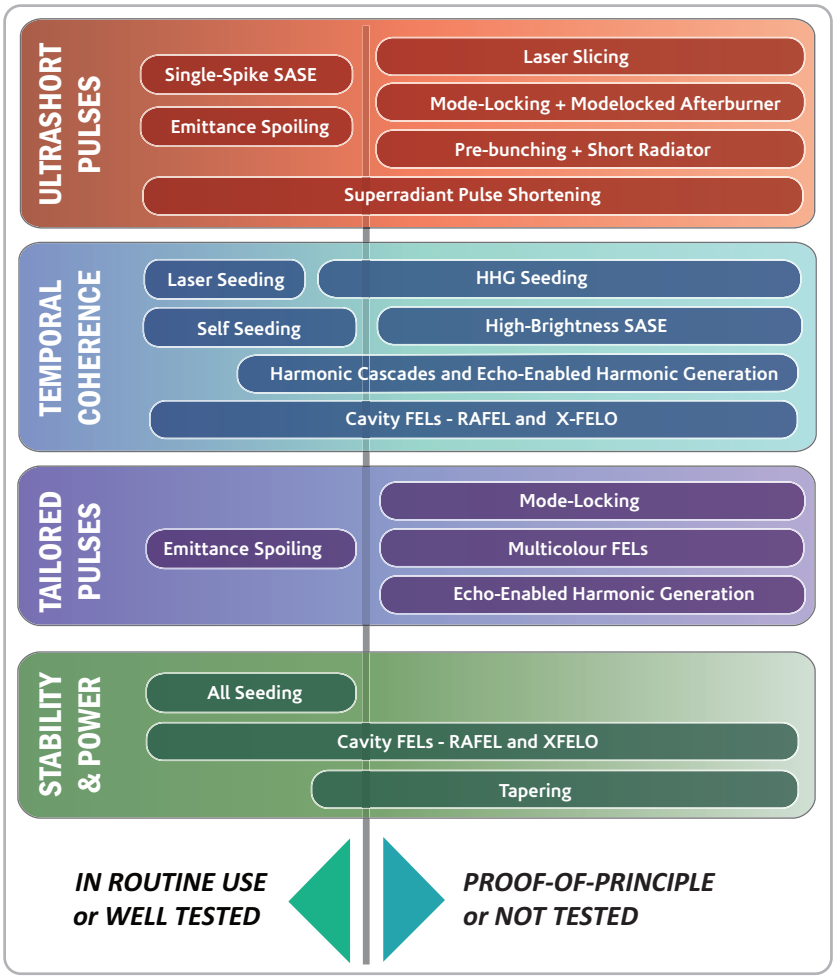

Figure 1.2. Schematic representation of the FEL landscape in terms of potential improvements to particular output properties against progress to date.

Accelerator for Research and Applications), a dedicated flexible FEL Test Facility, which will be able to test several of the most promising of the new schemes. Figure 1.1 shows a three-dimensional representation of CLARA. The successful proof of principle demonstration with CLARA will be a vital stepping stone to the implementation of any new scheme on an existing or planned FEL facility.

Of course CLARA will not operate in isolation and existing FELs are already dedicating machine development time for the testing of new ideas, such as self seeding or harmonic generation, and this is sure to continue given the strong call from users for ever higher quality light output. We have carefully assessed the short term focus of existing FELs and have strategically decided that CLARA should have a longer term vision and be targeted at proving concepts which will not just have an incremental impact on FEL performance but take FELs into a whole new regime. We believe that this will ensure that the international impact of CLARA will be maximized and place the UK in a vanguard position should it choose to develop its own future FEL facility. The landscape showing the potential improvements currently identified for FELs is presented schematically

2014 JINST 9 T05001

in figure 1.2. It is clear that whilst significant progress has been made recently in making FELs operational, there are many major areas where the potential of FELs remains untapped. We aim to release this potential to open up further new fields of science for investigation and exploitation.

Our vision for CLARA is that it should be dedicated to the production of ultra-short photon pulses of high-brightness coherent light. Existing X-ray FELs are already capable of generating pulses of light that are only tens of femtoseconds in duration (tens of thousands of optical cycles) but FEL experts have proposed several schemes which have the potential to generate pulses that are two or three orders of magnitude shorter than this (hundreds or tens of attoseconds) [7–15] and a recent paper has even proposed a novel idea for sub-attosecond pulse generation from a FEL (a few optical cycles) [16]. The science which is enabled by ultra-short photon pulses was described in detail in the NLS Science Case [17] and reviews of science carried out using attosecond pulses are also available [18–20]. Many exciting applications of attosecond pulses have already been demonstrated, including coherent X-ray imaging, femtosecond holography, real-time observations of molecular motion and capturing the movement of electrons in atoms and molecules. Attosecond X-ray science could revolutionise how we understand and control electron dynamics in matter.

In order to achieve this vision for ultra-short pulse generation, CLARA must be able to implement advanced techniques, such as laser seeding, laser-electron bunch manipulation, and femtosecond synchronisation. These can only be achieved by developing a state-of-the-art accelerator with the capability to drive current FEL designs. CLARA is therefore of direct relevance to the wider international FEL community and will also ensure that the UK has all the skills required should it choose to develop its own future FEL facility. This underpinning foundation requirement is shown in figure 1.3.

In detail the goals, opportunities and benefits of CLARA will be:

- Proof-of-principle demonstrations of ultra-short 'attosecond' photon pulse generation (of order of the coherence length or less, typically less than 100 optical cycles) using schemes which are applicable to X-ray FELs (such as laser slicing, mode locking, or single spike Self-Amplified Spontaneous Emission (SASE)) and with extreme levels of synchronisation.

- The ability to test novel schemes for increasing the intrinsic FEL output intensity stability, wavelength stability, or longitudinal coherence using external seeding, self seeding or through the introduction of additional delays within the radiator section.

- The ability to generate higher harmonics of a seed source using Echo Enabled Harmonic Generation (EEHG), High Gain Harmonic Generation (HGHG), or other novel schemes.

- The generation and characterisation of very bright (in 6D) electron bunches and the subsequent manipulation of their properties with externally injected radiation fields, and the testing of mitigation techniques against unwanted short electron bunch effects.

- The development and demonstration of advanced accelerator technologies, with many wide ranging applications well beyond FELs, such as a high repetition rate normal conducting Radio Frequency (RF) photoinjector, novel undulators, RF accelerating structures and sources, single bunch low charge diagnostics, and novel photocathode materials and preparation tech-

2014 JINST 9 T05001

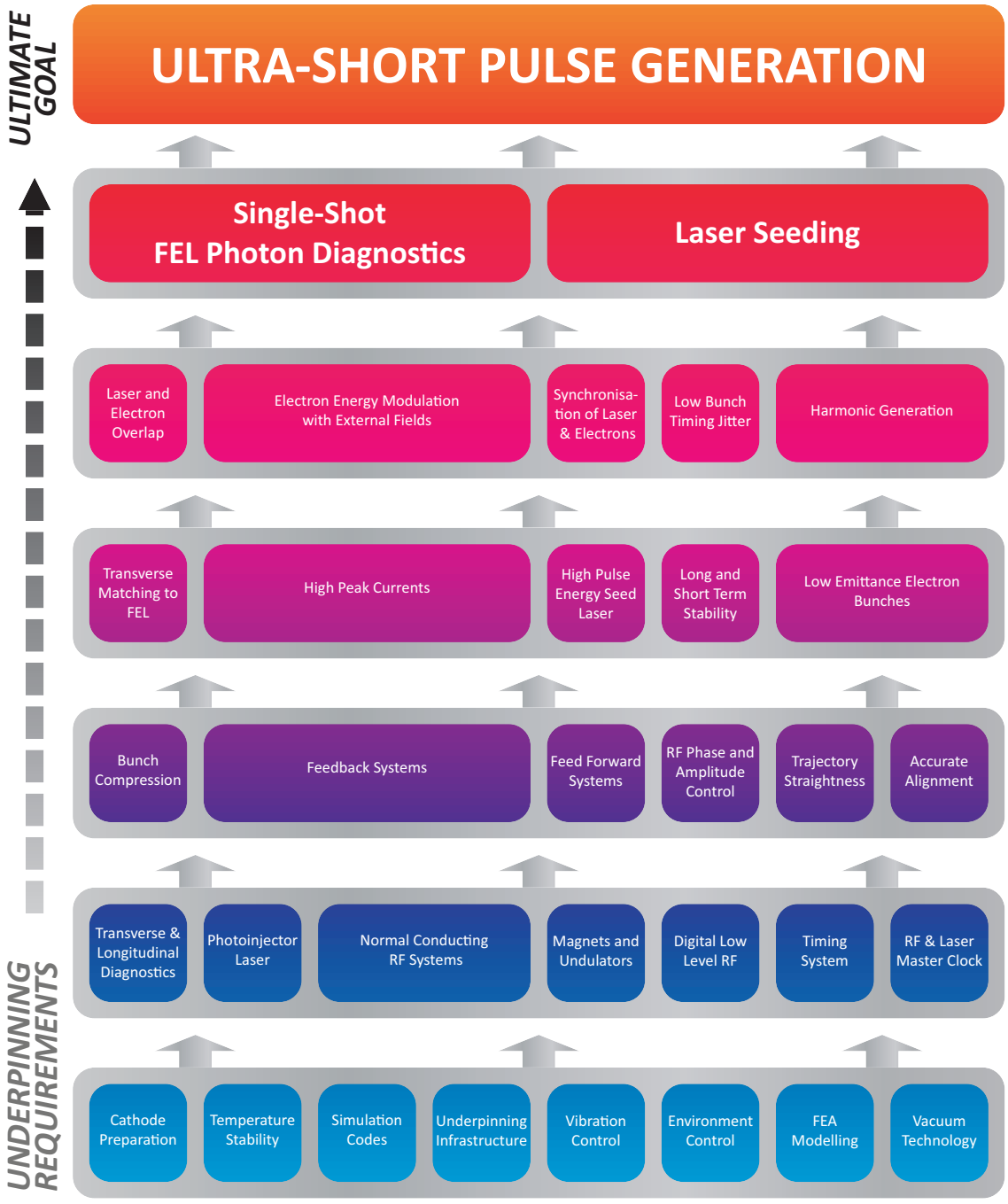

Figure 1.3. To achieve the primary goal of CLARA will require the mastery and understanding of many other techniques and technologies.

niques. The potential to test the new generation of plasma-based accelerators as drivers of FELs is also a significant consideration.

- The enhancement of VELA (Versatile Electron Linear Accelerator) [21], in terms of energy, beam power, and repetition rate, enabling additional industrial applications of electron beams that are currently excluded.

- A flexible, high quality, electron test accelerator available to the entire UK accelerator community on a proposal-driven basis, enabling wide ranging, high impact accelerator R&D.

- The development and retention of vital skills within the UK accelerator community, including providing excellent opportunities for attracting the best PhD students and early stage researchers to work on a world class accelerator test facility.

- The possibility to use the high quality bright electron beam for other scientific research applications such as ultra-fast electron diffraction experiments, plasma wakefield accelerators (as a witness bunch or a drive bunch), as the drive beam for a Compton scattering source of X-rays or gamma photons, and for other novel acceleration schemes such as dielectric wakefield accelerators and exotic storage rings.

We recognise the dynamic nature of FEL research and aim not just to demonstrate and study the novel concepts of today but also be well positioned to prove the novel concepts of tomorrow. For these reasons we have planned a number of different CLARA operating modes, each of which is designed to be appropriate for a different class of FEL experiments. The complete set of experiments discussed in this design report impacts on every area of the future FEL landscape presented in figure 1.2. This flexibility of approach also extends to advanced technological aspects, such as retaining the ability to implement and test alternative RF systems in the future, for example C-band linac structures or even superconducting RF cavities, as required by the needs of the UK accelerator programme.

CLARA will be well placed to test emerging ideas for fifth generation light sources based on laser or electron driven plasma accelerators, such as those put forward by the FACET-II proposal [22]. The experimental testing of such advanced ideas, that scale well to larger projects, can result in leaps forward in capability.

The ability to simulate coherent light sources driven by plasma accelerators requires different computational models from those used to simulate light sources driven by conventional accelerators. A new simulation code has been developed by ASTeC in collaboration with researchers at the University of Strathclyde [23]. This is the only such code currently available and is generating significant international interest resulting in collaborations developing with international groups that wish to use both laser and electron beam driven plasma accelerators as FEL drivers.

These collaborations offer the potential for CLARA to develop into an international focal point for such research. The embedded excellence of ASTeC staff in the design of electron beam transport systems and start-to-end modelling capability would ensure that any plasma driven research towards a FEL would be internationally leading.

Since CLARA is intimately linked to the existing VELA facility, much of the essential infrastructure for the project already exists. This will significantly reduce the time required to implement

2014 JINST 9 T05001

CLARA. We believe that within 3 years of funding we could procure and install all of the equipment and commence beam commissioning.

International Context

Currently there are only four dedicated single pass FEL test facilities worldwide, one in the US (NLCTA), one in Asia (SDUV-FEL) and two in Europe (SPARC and MAX). We have assessed the capabilities and programmes of each of these facilities in turn and have confirmed that CLARA will offer unique capabilities and have a complementary programme to the other test facilities.

The **NLCTA** at SLAC is a low energy (120 MeV) test accelerator deliberately focussing on near term Research and Development (R&D). The main goal of this facility is the development and optimization of EEHG for the improvement of temporal coherence, indeed this facility was the first to demonstrate EEHG experimentally. The primary objective now appears to be the establishment of very high order harmonic generation with the EEHG scheme.

The **SDUV-FEL** in Shanghai is the only dedicated test facility in Asia. They first observed SASE lasing in 2009 and this has been followed by seeded FEL experiments, EEHG, and other techniques for generating high harmonics from a seed laser, such as HGHG.

The **SPARC** test FEL at Frascati currently operates at 150 MeV with a planned upgrade to take it to 250 MeV. SASE lasing has been demonstrated and characterised, and direct High Harmonic Generation (HHG) seeding is being studied. SPARC has also carried out some short pulse experiments including energy chirped electron beams and undulator tapering and seeded superradiance.

The **MAX-lab** test FEL in Sweden will close at the end of 2013 after carrying out a final experiment exploring seeding by an HHG source at lower harmonics.

In summary, there are currently four FEL test facilities with similarities to CLARA. Improved temporal coherence using various seeding techniques dominate the programmes but one of the facilities has also carried out some promising experiments aimed at short pulse generation.

Two other pioneering facilities, previously dedicated to FEL development, have now evolved into larger projects due to the high demand for their output from users. The **FLASH** facility in Germany operates at 1.25 GeV, generating light down to 4 nm, and has operated for user experiments since 2005. **SCSS** in Japan operates at 250 MeV and routinely delivers 50–60 nm light for user experiments. Other accelerator test facilities, such as the **ATF** at Brookhaven, have broader programmes not concentrated on FEL development.

2014 JINST 9 T05001

Chapter 2

Benefit to VELA

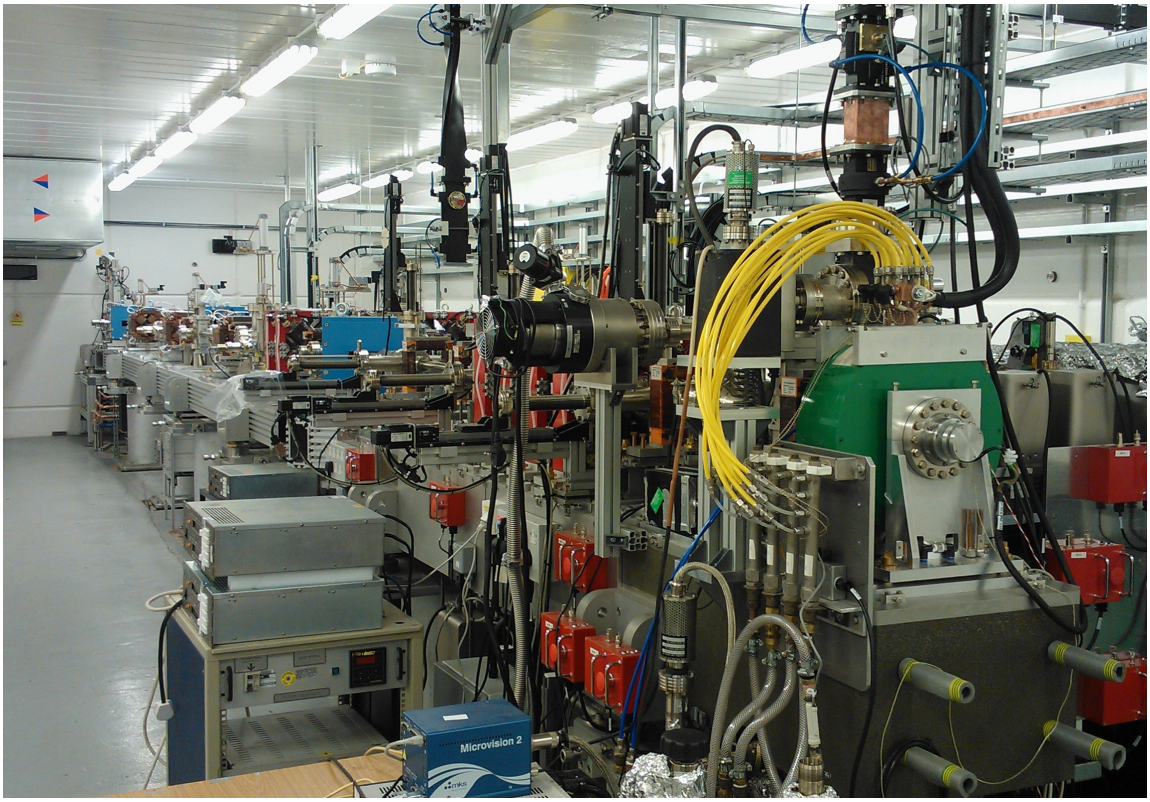

Figure 2.1. Photograph of the existing VELA facility at Daresbury Laboratory.

The upgrade of the VELA facility [21] (shown in figure 2.1) to incorporate CLARA will be of considerable benefit to VELA itself. The CLARA project has been carefully designed to minimize disruption to the operation of VELA during the installation and commissioning phases by making a number of key design choices. First, the CLARA components will be assembled onto individual girder modules offline in the Engineering Technology Centre at Daresbury Laboratory. This approach was used successfully by VELA and other projects and has been shown to be an efficient method of assembly, allowing easy access to each module for hardware installation and

2014 JINST 9 T05001

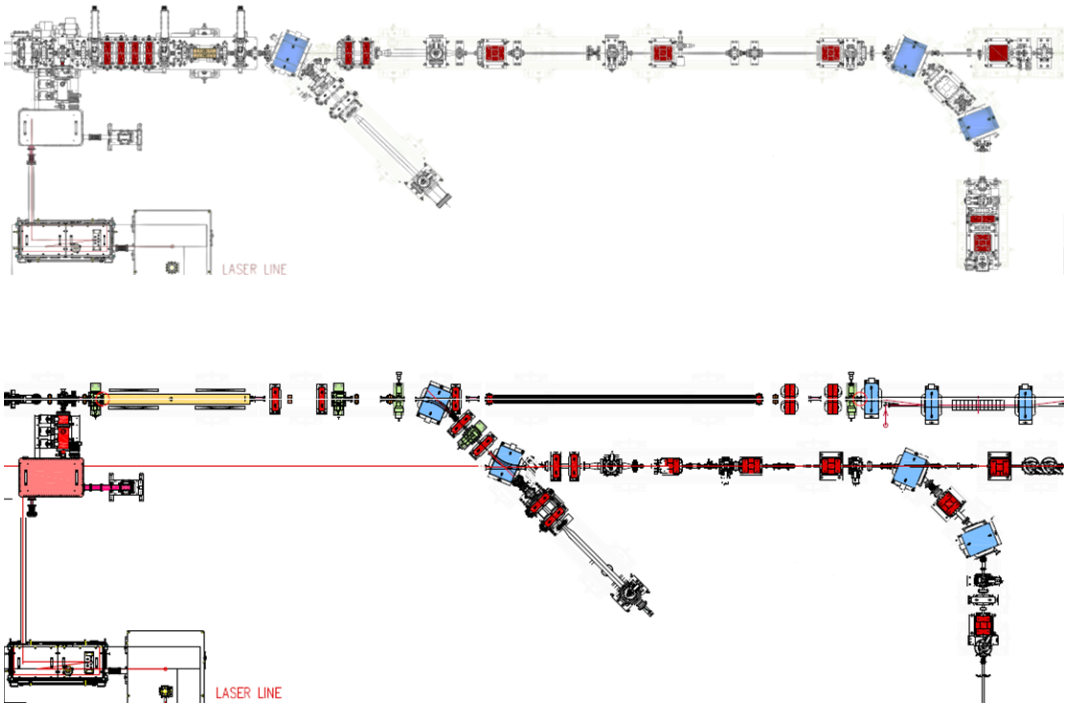

Figure 2.2. Engineering layouts of (top) the existing VELA facility and (bottom) VELA and the front end of CLARA once CLARA is fully installed.

commissioning and enabling accurate alignment of individual components on each module. Second, CLARA will be permanently installed parallel to VELA, spaced approximately one meter from the current VELA beam axis. This will mean that, with careful scheduling of installation activities, VELA will be able to continue to operate for users in parallel with CLARA installation. Indeed, the majority of CLARA is well away from VELA and this can be installed simultaneously to VELA operations with no disruption at all. There will, of course, have to be a scheduled shutdown of VELA for final installation which will include: the reconfiguration of the radiation shielding into a single tunnel; the transfer of the photoinjector gun cavity across to the CLARA front end, along with modifications to the associated RF waveguide and photoinjector laser transport systems; breaking of the VELA machine vacuum to join the two facilities together with a short dogleg electron beam transport line between the CLARA beam axis and the existing VELA axis. This last aspect is another deliberate design choice which will mean that the VELA user areas will benefit from enhanced electron beam parameters post-CLARA installation.

Figure 2.2 shows the current VELA engineering layout and the layout once the installation of CLARA is complete. Both facilities will then be served by a single photoinjector, mounted on the CLARA beam axis. Initially this will be the existing VELA gun but will later be replaced by a more advanced gun, capable of a much higher repetition rate (400 Hz compared with 10 Hz). For VELA operation the dogleg transfer line will be energised and beam delivered to either the straight ahead or perpendicular user beam areas. Clearly this operating scheme does not allow simultaneous operation of both VELA and CLARA but since VELA is not scheduled to run 24 hours a day it is likely that both facilities can operate successfully in this mode with intelligent scheduling of

2014 JINST 9 T05001

beam time. However, if the user demand for both facilities cannot be met, it would be relatively straightforward to implement a dedicated electron gun for VELA in the space vacated by removing the existing photoinjector cavity. In this case it is likely that a thermionic electron gun would be implemented. The option for the highest quality bunches from the CLARA photoinjector would still be available as required. The added benefit of transferring electron bunches from CLARA to VELA is that they are able to undergo further acceleration before the dogleg and so higher energy electrons will be available to VELA users once CLARA is installed. At present VELA will deliver up to 5 MeV electrons. Following the CLARA installation VELA will be able to offer up to 25 MeV electrons. This will increase the beam power available by a factor of five. The subsequent implementation of the high repetition rate photoinjector will increase the beam power by another factor of 40. Hence, VELA users will see a factor of 200 beam power increase following the full installation of CLARA. If the additional upgrade of a thermionic gun is implemented later the beam power will be increased even further due to the very high number of bunches per macropulse that will be possible. Note that increased beam power has been identified during an extensive market survey as one of the key parameters from which users of VELA would benefit most [24].

2014 JINST 9 T05001

Chapter 3

FEL design

3.1 Introduction

As discussed in chapter 1 CLARA has been designed to be a dedicated flexible FEL test facility, which will be able to test several of the most promising of the new FEL schemes. The successful proof of principle demonstration with CLARA will be a vital stepping stone to the implementation of any new scheme on an existing or planned FEL facility.

In this chapter we discuss the main parameters for CLARA, before detailing a number of different CLARA operating modes each of which is designed to be suitable for a different class of FEL experiments. We then summarise the layout of the FEL systems before giving details of a selection of the FEL schemes we will be able to study on CLARA, including some predictions of the FEL output properties. We broadly divide the research topics into two main areas, each of which is intended to demonstrate new schemes for the improvement of FEL output beyond that available from the SASE process [25, 26]. The first area is the generation of ultra-short pulses and the second area is improvement of temporal coherence. The physics of the FEL mechanism is not described in this report but is covered in a number of texts [27–29]. A number of review articles give a clear overview of the worldwide FEL status and future prospects [30–32].

CLARA has been designed and optimised so that the FEL wavelengths are in the visible and VUV. This has tremendous advantages for the operation of the FEL and diagnosis of the output. Our emphasis for the short pulse schemes is to generate pulses with as few optical cycles as possible with durations of the order of, or shorter than, the FEL cooperation length. These are our figures of merit and we aim to study the essential physics of the schemes which can often therefore be independent of the FEL wavelength.

Of course ultimately many of the schemes we study are intended for application at X-ray FELs. In this case the absolute pulse durations will scale in some way with the wavelength and in the final section of the chapter we indicate the potential of the schemes we study when applied at shorter wavelengths. Of course at these wavelengths there could be technological issues, tolerance criteria or disruptive effects which scale with absolute electron bunch length or beam energy. In the final section we also discuss these issues to understand the wavelength scalability of the research we plan to undertake.

2014 JINST 9 T05001

3.2 Parameter selection

The wavelength range chosen for the CLARA FEL is 400–100 nm, appropriate for the demonstration of advanced FEL concepts on a relatively low energy accelerator. Key drivers for this choice are the availability of suitable seed sources for interacting with the electron beam, as required by many of the FEL topics we propose to study, and the availability of single shot diagnostic techniques for the characterisation of the FEL output.

We propose to study short pulse generation over the wavelength range 400–250 nm, where suitable nonlinear materials for single shot pulse profile characterisation are available. For schemes in this regime it is often necessary to produce a periodic modulation in the properties of the electrons along the bunch such that it can be arranged (using a variety of methods, depending on the scheme) that only some sections of the beam can lase. Often the scale length of each independent FEL interaction is given by the slippage in one gain length, known as the cooperation length l_c, so the modulation of the electron bunch properties should have a period λ_M significantly longer than this to enable an independent temporally-separated interaction for each period of the modulation. This means we require $\lambda_M \gg l_c$. For the lasing wavelength range 400–250 nm for the short pulse schemes this leads to the requirement that to cover most of the research topics the modulating laser should have wavelength $\lambda \simeq 20$–$50\ \mu$m with the possibility of extending the wavelength to 120 μm later on.

For schemes requiring only spectral characterisation (for example producing coherent higher harmonics of seed sources, or improving the spectral brightness of SASE) the operating wavelength range will be 266–100 nm, with the possibility of output down to 80 nm at a later stage. For these schemes the most appropriate seed source (if required) is an 800 nm Ti:sapphire laser from which we can generate coherent harmonics up to the 8th harmonic, or 10th harmonic later on.

To operate at shorter wavelengths than 80 nm would currently offer little advantage, but many complications. The wavelength would in fact have to be significantly shorter than 80 nm to enable pulse profile characterisation and this would have to be done using photoionisation in gases as the nonlinear medium for the cross-correlation. Such a technique is complex and would not provide single-shot measurements, so is not acceptable. The photon diagnostic beamlines would also be more complex and require more floor space because low incidence angle optics would be necessary. Finally, the CLARA energy would need to be upgraded and the undulator beamline extended.

The required electron beam energy and undulator parameters depend on the required tuning range. The FEL wavelength λ_r is given by

$$\lambda_r = \frac{\lambda_w}{2\gamma^2}\left(1+\frac{K^2}{2}\right)$$

where λ_w is the period of the FEL undulator and γ is the electron energy in units of its rest mass. K is the undulator parameter which is proportional to the on-axis field which depends on the undulator gap. As the gap is extended the field decays until K falls below a level that gives useable FEL interaction. This sets a soft limit for the shortest wavelength. As the gap is reduced the field increases until the minimum gap imposed by the vacuum vessel is reached. This sets the longest wavelength. For CLARA we set the minimum useful undulator parameter to be $K \simeq 1$ (in common with other FEL facilities) and the minimum undulator gap to 6 mm. For a hybrid planar undulator,

2014 JINST 9 T05001

and a tuning range of 400–100 nm, this uniquely defines the required electron beam energy to be $E = 228$ MeV and the undulator period to be $\lambda_w = 27$ mm. However, we have designed the CLARA accelerator to provide a maximum beam energy of 250 MeV. This allows sensible contingency in three areas. First, it allows the full wavelength tuning range to be achieved at a slightly reduced linac gradient. Second, it allows the linac cavities to be operated further off-crest for added flexibility. Third it allows us to push the FEL wavelength to around 80 nm with only a slight reduction in undulator parameter enabling us to generate even higher harmonics of the seed sources.

Table 3.1. Main parameters for CLARA operating modes.

	Operating Modes			
Parameter	**Seeding**	**SASE**	**Ultra-short**	**Multibunch**
Max Energy (MeV)	250	250	250	250
Macropulse Rep Rate (Hz)	1–100	1–100	1–100	1–100
Bunches/macropulse	1	1	1	16
Bunch Charge (pC)	250	250	20–100	25
Peak Current (A)	125–400	400	∼1000	25
Bunch length (fs)	850–250 (flat-top)	250 (rms)	<25 (rms)	300 (rms)
Norm. Emittance (mm-mrad)	≤ 1	≤ 1	≤ 1	≤ 1
rms Energy Spread (keV)	25	100	150	100
Radiator Period (mm)	27	27	27	27

3.3 Operating modes

The approach we have adopted is to design a flexible, well-diagnosed facility for testing a variety of advanced FEL concepts. This flexibility will be built into the accelerator itself, as discussed in chapter 4 and also incorporated into the systems specific to the FEL. We recognise the dynamic nature of FEL research and aim not just to demonstrate and study the novel concepts of today but also be well positioned to prove the novel concepts of tomorrow. For these reasons we have planned a number of different CLARA operating modes, each of which is designed to be appropriate for a different class of FEL experiments. The complete set of experiments discussed in this design report spans every area of the future FEL landscape presented in chapter 1. The parameters for the different operating modes are summarised in table 3.1.

3.3.1 Seeding mode

This mode is designed for any FEL scheme where a seed source interacts with the electron beam. For schemes at 100 nm wavelength the accelerator has been optimised to produce an electron bunch with a relatively flat-top current profile of duration ≃250 fs. The specification for the flatness of the current within this region is $\sigma_I/I \leq 7\%$, as discussed in section 3.3.5. The reason for the flat top is to make the FEL performance insensitive to up to ±100 fs temporal jitter between the electron bunch and seeding laser. The required peak current to reach saturation at 100 nm in a sufficiently compact undulator section, taking into account the expected emittance and energy spread in the beam, is

2014 JINST 9 T05001

400 A. These requirements lead to a necessary bunch charge of 250 pC of which approximately 100 pC is within the flat top region and the remainder is in the head and tail.

For schemes where the beam is modulated with the long wavelength seed the bunch length must be longer. This is because of the slippage that occurs between the seed field and the electrons in the modulator undulator — every period of the undulator the electrons slip back one wavelength. For a 50 μm seed interacting in a 4-period modulator the slippage time is $\simeq$650 fs so the flat region of the bunch must be at least this duration. Adding contingency for $\pm$100 fs temporal jitter the flat top region must be $\gtrsim$850 fs duration. Fortunately, the gain length is shorter at longer wavelengths so the peak current to reach saturation in the same length of undulator as required for 100 nm operation is only 125 A. The charge in the flat top region is therefore 100 pC as before, so a total charge of 250 pC is well matched to the requirements.

In this mode it is important to keep the energy spread small so that the ratio between the energy modulation applied by the laser and the beam energy spread is as high as possible to enable strong bunching to be generated at high harmonics.

3.3.2 SASE mode

This mode is designed for operating the FEL in SASE mode. This is the 'base' FEL operation mode because no seed fields or optics are required but will be an essential mode of operation for validating the performance of the accelerator, the properties of the electron bunch and the alignment within the undulator sections. In addition, many of the schemes proposed for CLARA aim to improve the temporal coherence and/or stability of SASE so it is important to be able to use SASE as a control. The bunch charge and peak current have already been set by the requirements of the Seeding Mode so we adopt the same maximum charge and peak current for SASE mode. There is however, no requirement for a flat-top profile so this mode of operation will be easier to demonstrate. The SASE FEL performance is quite insensitive to energy spread at the 25–100 keV level so in this mode we allow the energy spread to be higher than in the seeding mode.

3.3.3 Ultra-short pulse mode

This mode is specific to research into ultra-short bunch generation and transport, and the use of such bunches for single spike SASE FEL operation, where the bunch length must be shorter than the typical SASE spike separation of $2\pi l_c$. The cooperation length l_c depends strongly on the peak current, which itself of course depends on the bunch charge and bunch duration. To generate and transport very short bunches is only possible if the charge is quite modest. A study of the parameter space has led to the conclusion that a bunch charge of 20-100 pC is appropriate for single-spike SASE FEL operation at 100 nm wavelength with a peak current requirement of up to 1000 A.

3.3.4 Multibunch mode

This mode is designed to allow research into short-wavelength oscillator FELs, a topic currently undergoing a resurgence of interest within the FEL community for short wavelengths, with interest in the Regenerative Amplifier FEL (RAFEL) which is a low-feedback high gain oscillator [33–38], and also the high feedback low gain X-ray FEL Oscillator (X-FELO) [39, 40].

To operate the FEL in oscillator mode would require some rearrangement of components to install an appropriate optical cavity, but we recognise the potential importance of this research area

2014 JINST 9 T05001

and make cost-neutral design choices which do not unnecessarily exclude this mode. The proposed scheme is to demonstrate a RAFEL for the generation of transform limited pulses at wavelengths as short as 100 nm. Such a system requires only a very low feedback optical cavity. Our initial studies show that the undulator length needs only be one third of the SASE saturation length, therefore even using only five of the seven radiator undulators we can afford to increase the gain length significantly and reduce the peak current to a modest 25 A. We also require that the electron bunch is longer than the slippage length giving required length of ≈ 300 fs rms and hence minimum bunch charge of 15 pC.

The bunch repetition rate must be matched to the ≈ 17.5 m optical cavity round trip time (a 17.5 m cavity assumes the first and last radiators are removed and replaced with cavity mirrors and electron beam chicanes to divert the beam around the mirrors) giving $f = 8.5$ MHz and bunch spacing 120 ns. Typically 8 cavity round trips are required to reach saturation so the minimum macropulse duration is 1 μs. We therefore specify a macropulse duration of 2 μs to allow time to diagnose the FEL output (and its stability) at saturation. The total charge in the macropulse is thus 250 pC which is consistent with other operating modes. The average power demands on the accelerator systems are therefore no greater than in any other operating mode.

3.3.5 Electron beam stability requirements

The stability of the FEL output will depend on the stability of the electron bunch parameters, particularly the energy and the peak current. To develop a complete specification each FEL scheme needs to be studied in detail. For now we specify, as an absolute minimum, that the energy jitter in the electron bunch should translate to an rms FEL wavelength jitter of less than half the SASE bandwidth. This will allow practical characterisation of unseeded schemes and ensures that for seeded schemes, for which the seed wavelength jitter should be relatively small, the seed always falls within the gain bandwidth of the FEL. From time-dependent `GENESIS 1.3` [41] simulations of SASE operation at 100 nm the FWHM bandwidth at saturation is $\Delta\lambda/\lambda \simeq 5 \times 10^{-3}$ so the required wavelength stability is $\sigma_\lambda/\lambda \leq 2.5 \times 10^{-3}$. From the resonance condition, energy jitter and wavelength jitter are related by $\Delta E/E = \Delta\lambda/(2\lambda)$ so for $\sigma_\lambda/\lambda \leq 2.5 \times 10^{-3}$ we require $\sigma_E/E \leq 1.25 \times 10^{-3}$.

We also state, in line with the specification proposed for the NLS [42], the requirement that the relative rms shot-to-shot FEL pulse energy jitter should be less than 10%. For SASE the pulse energy will fluctuate anyway due to the intrinsic nature of the process, but for schemes aiming to improve the temporal coherence of SASE the intrinsic SASE fluctuation will be removed. The FEL power scales with peak current as $P \propto I^{4/3}$ therefore to achieve 10% stability we require the rms variation of the peak current to be better than $\sigma_I/I \simeq 7\%$. Equivalently, for a constant bunch charge, we require the rms bunch length jitter to be better than 7%.

For seeding schemes the temporal jitter in the electron bunch will cause the seed to align longitudinally with different sections of the bunch. We therefore require that the temporal jitter is less than the flat-top region of the bunch, and that within this flat-top region the current variation is again less than $\sigma_I/I \simeq 7\%$.

It is emphasised that study of the CLARA tolerances is at an initial stage. The stability specification stated here is a minimum requirement, but as seen in chapter 4 it is consistent with the initial

2014 JINST 9 T05001

tolerance studies made of the accelerator systems. Further iteration will strengthen the stability specification consistently with the predicted performance of the accelerator.

3.4 FEL layout

The schematic layout of the FEL systems is shown in figure 3.1. The proposed research topics require interaction with seed lasers in a modulator undulator then amplification in radiator undulators.

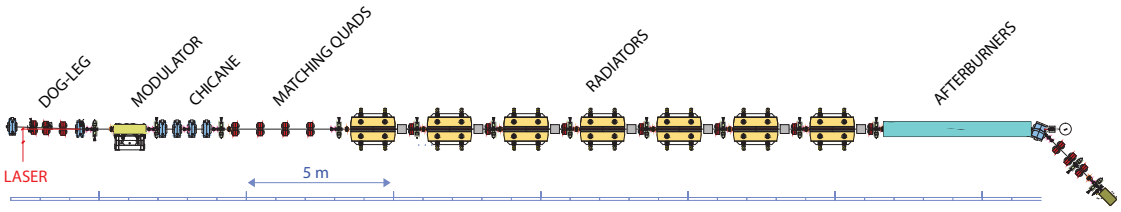

Figure 3.1. FEL layout.

3.4.1 Modulator section

Our initial studies have indicated that sufficient energy modulation can be obtained at 50 μm using only four undulator periods, assuming the pulse energy of the seed laser is 10–20 μJ. In order to maintain a resonant interaction between a 250 MeV electron beam and seed lasers covering the range 120 μm to 800 nm the undulator period should be around 200 mm with minimum gap 20 mm to allow the longest wavelength seed to be focussed at the centre of the modulator with an optimum Rayleigh length equal to half the modulator length and negligible diffraction loss on the internal vacuum vessel aperture. Hence the minimum modulator length is 1.0 m (this allows an extra period at each end for suitable termination of the field). Further study may indicate that at shorter wavelengths it would be useful and practical to utilise more periods in the modulator — in this case the design can be revised accordingly. A practical economic solution is to use an existing multipole wiggler which was previously installed on the Synchrotron Radiation Source (SRS) at Daresbury. This has length 1 m, period 200 mm and minimum gap 20 mm, so is quite well matched to CLARA requirements. For the present layout we assume the use of this device and intend to study its performance in this role in more detail. For schemes which require an additional modulator, for example EEHG which is discussed in section 3.5.3, the first radiator can be replaced by a short modulator and chicane. We intend the engineering design to allow such configuration changes to be made quickly and conveniently.

The seeds will be injected onto the FEL axis via an insertable mirror in the dog-leg immediately upstream of the modulator. The seed optical transfer lines will have the flexibility to focus the seed to a Rayleigh length of 0.35–1.25 m with a variable waist position. The optimum Rayleigh length, for strongest interaction between seed and electron beam, is approximately one half the modulator undulator length, so this flexibility allows optimum use of modulator undulators of length 0.7–2.5 m.

2014 JINST 9 T05001

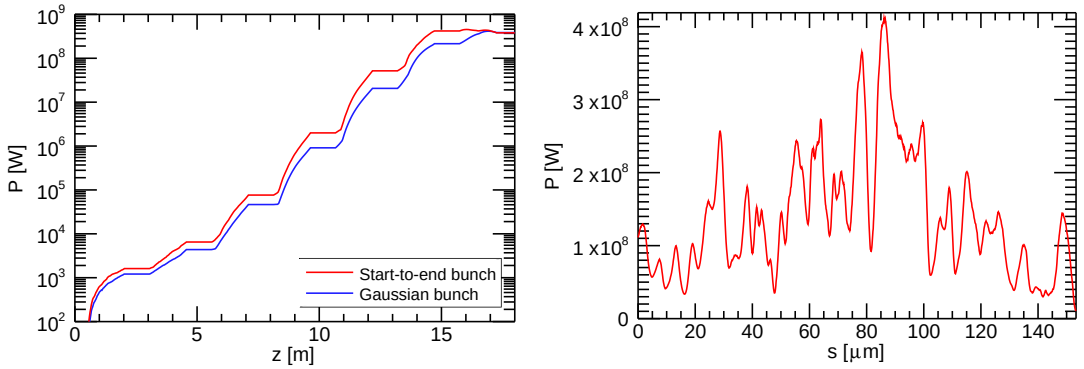

Figure 3.2. Results of 100 nm SASE simulations. The left hand plot shows the evolution of power along the undulator lattice for the s2e and gaussian bunches, and the right hand plot shows the photon pulse longitudinal profiles for the s2e bunch after 7 undulator modules.

In some of the schemes proposed it is necessary to convert the imposed energy modulation into a density modulation. This will be done using a 4-dipole chicane immediately downstream of the modulator. The parameters for this chicane are dependent on the maximum required longitudinal dispersion (or R_{56}). We anticipate that the EEHG scheme [43, 44] will place the strongest demand on this chicane. A thorough study of EEHG applied to CLARA (section 3.5.3) has shown the maximum R_{56} will be 40 mm, and this can be achieved with a four-dipole chicane of magnet and drift lengths of 200 mm and peak field 0.7 T. The total footprint of this chicane (including magnet coil overhangs) is thus 1.5 m. Beyond the chicane are four quadrupoles for matching the Twiss parameters into the radiator section.

3.4.2 Radiator section

The radiator section comprises seven 1.5 m long radiator undulators of planar hybrid design with the arrays aligned vertically (so that the magnetic field on-axis is horizontal). In this way the polarisation of the FEL output is vertical allowing much improved transmission using horizontal reflections to the photon diagnostic beamline. The undulator modules are arranged within a Focus-Drift-Defocus-Drift (FODO) lattice, with a single quadrupole between each module. The gaps between undulator modules are 1.1 m to allow sufficient space for diagnostic and vacuum components and a compact 0.3 m electron beam delay/phase shifter with a maximum delay capability of 50 μm. The period of the FODO lattice is therefore 5.2 m. A substantial study has been made to optimise the FODO period. The conclusion is that $\sim$5 m is the longest period that allows periodically matched Twiss parameters over the full wavelength range of the FEL while maintaining high electron beam energy. For longer FODO periods it becomes necessary to reduce the electron beam energy to maintain a matched solution for longer wavelengths, which means that the undulator parameter must also be reduced to maintain FEL resonance. These effects have a doubly detrimental effect on the FEL performance — the efficiency of the FEL at converting electron beam power to radiation power is decreased because of the reduced K and the beam power itself is reduced because of the lower energy.

2014 JINST 9 T05001

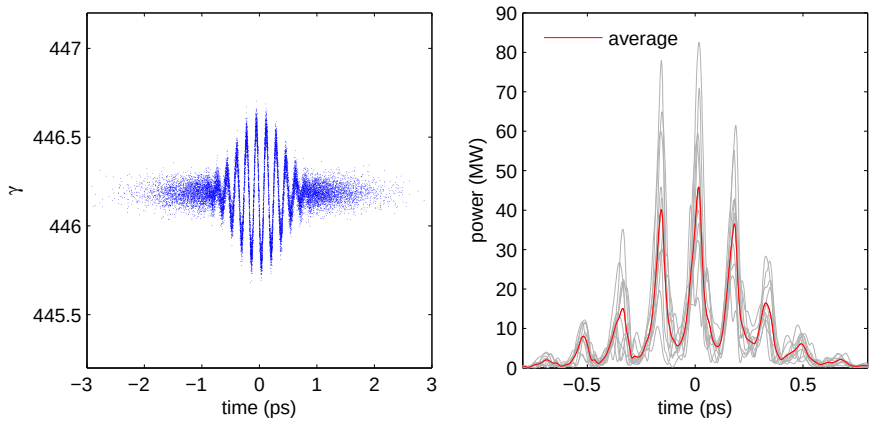

Figure 3.3. (Left) Energy modulation given to the electron beam by a 50 μm, 10 μJ, 500 fs seed laser. (Right) FEL power at saturation for 10 shot-noise seeds.

3.4.3 Afterburner

Beyond the final radiator we have allocated a space of 5 m for the installation of afterburner undulators. These can be used for generation of shorter wavelengths than the FEL resonance, to investigate novel methods for polarisation control, or as part of an exotic scheme for short pulse generation. Possible applications are discussed in section 3.5.4. Allocation of this dedicated space will also allow CLARA to be an excellent facility for testing advanced undulator designs, as discussed further in section 5.7.

3.5 FEL schemes

In this section we present further details of a number of FEL research topics that could be studied using CLARA. We include simulation results of the schemes applied to CLARA to illustrate the flexibility of the accelerator and FEL systems and give indications of the expected FEL output. The schemes presented cover the full range of the FEL landscape as presented in chapter 1. Of course unknown schemes lie beyond the horizon and we intend to maintain the long-term flexibility of CLARA to enable rapid study of future ideas proposed by the FEL community.

3.5.1 SASE

This is the base scheme, which we must be able to demonstrate in order to show the improvement over SASE available from the more advanced schemes. This scheme has been simulated, with the FEL operating at its shortest design wavelength of 100 nm, using the well-benchmarked standard FEL code `GENESIS 1.3`. Electron bunch distributions from the simulation codes used to model the accelerator and beam transport have been imported into the FEL simulation. The simulation is therefore a complete 'start-to-end' (s2e) simulation.

The electron bunch properties are listed for the SASE mode in table 3.1. This bunch is non-uniform, having developed some structure through the processes used to generate and transport it, so a comparative study has been made of the FEL performance using an ideal bunch with a Gaussian current profile and uniform emittance and energy spread along the bunch (with these

2014 JINST 9 T05001

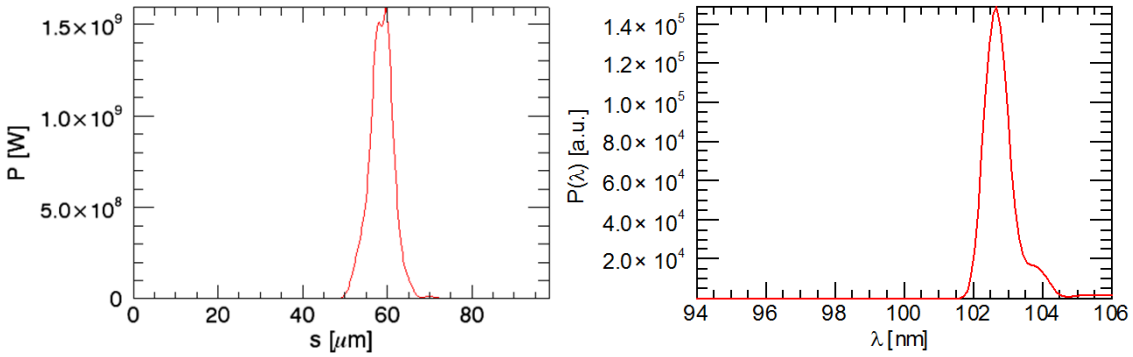

Figure 3.4. 100 nm Single Spike SASE Pulses: Power and Spectrum.

values set to match that of the s2e bunch at the position of maximum peak current). The results of the simulations for these two electron bunches are shown in figure 3.2. The left hand plot shows the evolution of power along the undulator lattice for the s2e and gaussian bunches, and the right hand plot shows the photon pulse longitudinal profiles for the s2e bunch after 7 undulator modules. It is seen that both the s2e bunch and gaussian bunch reach FEL saturation before the end of the 7th undulator module at a distance of 16.5 m from the start of the radiator section. These results demonstrate that the electron bunch properties and undulator lattice design are sufficiently good. Many of the FEL schemes to be studied on CLARA will reach saturation earlier in the radiator section, either because they will be tested at longer wavelengths where the gain length is shorter, or because the electron bunch will enter the radiator pre-bunched due to manipulations in the modulator section and chicane.

3.5.2 Generation of short pulses

The generation of short pulses is one of the important research themes for CLARA. Our aim is to generate pulses with as few optical cycles as possible with durations of the order of, or shorter than, the FEL cooperation length l_c. The cooperation length is the slippage in a gain length and therefore an intrinsic scale length for the FEL process. It is therefore difficult to generate high intensity FEL pulses of duration less than l_c. The SASE process generates spikes of duration $\simeq \pi l_c$ with each SASE spike developing independently from the shot noise in the electron beam. Many of the short pulse schemes aim to slice out, or isolate, a single SASE spike and the duration of the output pulse is therefore typically no shorter than πl_c. One gain length in a FEL is typically one hundred undulator periods, so the cooperation length is therefore typically 100 wavelengths and pulse durations possible from slicing schemes are of this order. In the first two parts of this section we discuss two schemes with this level of potential: Slicing and Single-Spike SASE. To generate shorter pulses than $\simeq \pi l_c$ requires fundamentally altering the FEL process. Two such schemes, Mode-Locking and the Mode-Locked Afterburner are discussed later in this section. For each scheme in this section we indicate the predicted pulse durations, and lengths in μm, number of optical cycles and number of cooperation lengths. Of course other schemes will be proposed in the future and the flexibility of CLARA will make us well placed to investigate these schemes in due course.

2014 JINST 9 T05001

Slicing schemes

One promising scheme for ultra-short pulse generation is the energy chirp plus tapered undulator scheme [13] and we have studied the implementation on CLARA in some detail [45] following earlier assessment for implementation on the UK's NLS proposal [46]. In this scheme, a few-cycle seed laser is used to modulate the electron beam energy to an amplitude greater than the natural bandwidth of the FEL. By tapering the gap of the undulator, only the sections of the electron bunch where the energy chirp is correctly matched to the undulator taper will experience high FEL gain. The final FEL pulse therefore consists of a train of individual SASE spikes, each separated by the seed laser period. The number of spikes can be controlled by varying the number of cycles in the seed laser and periods in the modulator undulator — by using a single-cycle laser and a single period modulator a solitary spike can be generated which would be the ultimate aim for implementing this scheme at short wavelengths.

For CLARA it is not feasible to provide a single cycle seed of appropriately long wavelength and pulse energy but we can demonstrate the physics of the mechanism by generating a train of spikes. The scheme has been studied using a combination of `elegant` [47] and `GENESIS 1.3` assuming Gaussian electron bunch distributions with parameters as given in table 3.1.

Simulations were carried out for both 400 nm and 266 nm FEL wavelengths. For the 400 nm case, a seed laser of 50 μm wavelength looks optimal, with a 500 fs/10 μJ pulse providing sufficient energy modulation to restrict the growth of the SASE radiation spikes to the energy-chirped regions. For the 266 nm case, a similar seed laser pulse energy would be required, but the wavelength should be reduced to 40 μm in order to give a good match between the length of the energy chirps in the electron bunch and the width of the SASE radiation spike ($\simeq \pi l_c$). Assuming these conditions can be met, numerical simulations suggest FEL pulses of the order 50 MW peak power and 50 fs/15 μm/55 cycles FWHM can be expected.

Figure 3.3 shows the calculated energy modulation given to the electron bunch, along with the FEL pulse profile at saturation for 10 different shot-noise seeds. The taper in radiator gap was applied in steps, with constant gap for each undulator module.

The EEHG scheme discussed later can also be used to control the length of the FEL pulse by varying the length of the second seed laser, keeping the electron energy modulation amplitude fixed. Studies of this option using a 40 fs FWHM laser indicate the scheme will work just as well as when using the 500 fs seed, generating a temporally coherent FEL pulse of >100 MW peak power and 25-40 fs FWHM duration at 100 nm.

Single spike SASE

The idea of the single-spike SASE scheme is simple. In a SASE FEL the spacing between the SASE spikes is $\Delta s \leq 2\pi l_c$. If the electron bunch $L_b > 2\pi l_c$ then the number of SASE spikes N in the FEL output will be $N = L_b/2\pi l_c$ [48]. If however the electron bunch is of length $L_b \simeq 2\pi l_c$ then only one SASE spike can develop, hence the term single-spike SASE. For $L_b < 2\pi l_c$ then again only one SASE spike will develop, but the saturation power will be reduced because the radiation will slip out of the front of the electron bunch before it can be fully amplified.

We have investigated this scheme using an electron bunch compressed via the velocity bunching scheme and an initial simulation result using a tracked bunch imported into `GENESIS 1.3` is shown in figure 3.4. The FWHM pulse length obtained at 100 nm is 23 fs/7 μm/70 cycles.

2014 JINST 9 T05001

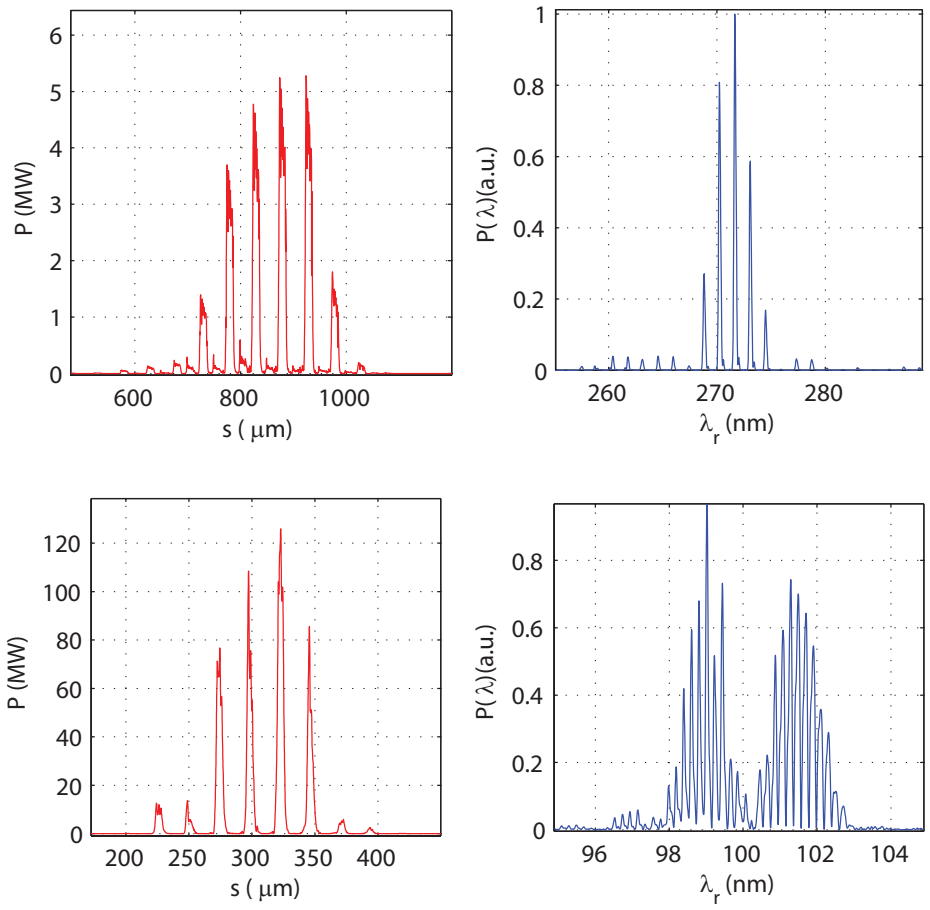

Figure 3.5. Mode-locked output pulses and spectra using the standard CLARA configuration, at 266 nm (top) and 100 nm (bottom).

Mode-Locking

The Mode-Locking scheme [15, 49, 50] requires the use of delay sections between the radiator undulator modules to periodically delay the electron bunch with respect to the radiation. This generates a set of sideband modes in the radiation spectrum which correspond in the time domain to a strong modulation in the radiation pulse envelope with a period equal to the slippage in one undulator module plus the added delay. If a periodic modulation is added to the electron bunch current or energy, with a frequency equal to the spacing between the sideband modes, then these modes develop their own sidebands which overlap and phase lock with the neighbouring modes. The process is analogous to mode-locking in a conventional laser. In the time domain the output then comprises a train of evenly spaced phase-locked spikes, with a duration potentially far shorter than the FEL cooperation length. In the frequency domain the radiation modes extend out to the full bandwidth of a single undulator module, which is far greater than the bandwidth of a normal SASE FEL. The mode-locking technique therefore has two applications of interest — generation of ultra-short pulses and generation of simultaneous multi-colour FEL output with a wide and variable frequency separation.

2014 JINST 9 T05001

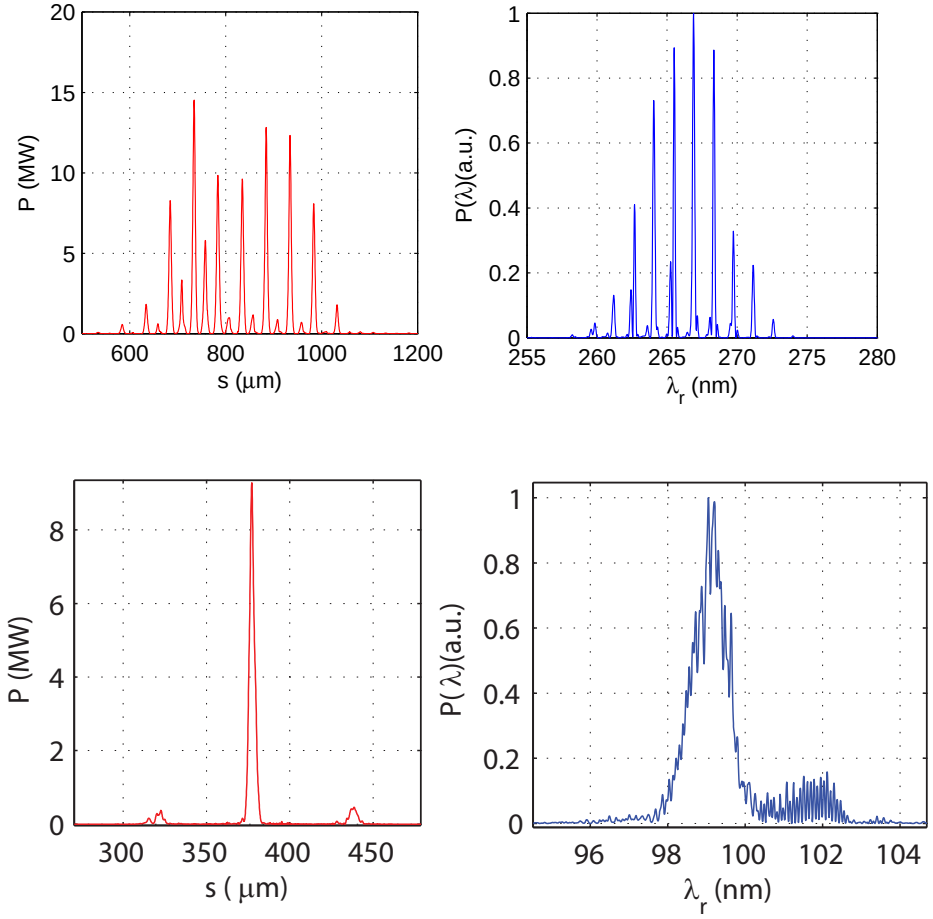

Figure 3.6. Mode-locked output pulses in the second phase of the research. Output at 266 nm with extra delays within standard undulators (top) and single-spike mode-locked output at 100 nm with 120 μm modulation (bottom).

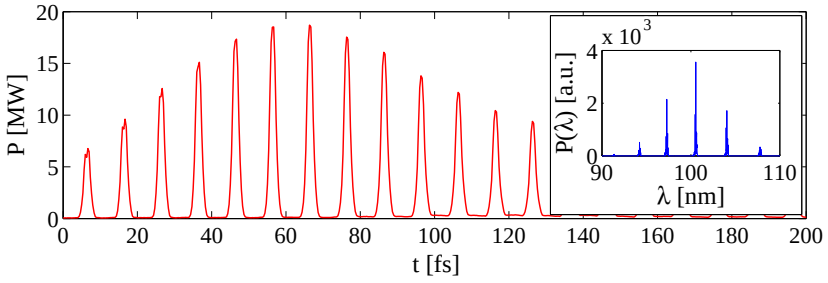

Figure 3.7. Simulation results of the Mode-Locked Afterburner operating at 100 nm.

The scheme has been studied for implementation in two phases. In the first phase the scheme has been simulated for CLARA parameters, using the standard undulator lattice, with the delays imparted via the phase-shifters between undulator modules. We would aim to demonstrate initially at 266 nm, where the single shot temporal diagnostics are available and we would also characterise

2014 JINST 9 T05001

the output spectrally. We would then reduce the wavelength to 100 nm and rely on the spectral diagnostics only, looking for equivalent spectral profiles at 266 nm and 100 nm to prove the scheme. The simulation results at 266 nm and 100 nm are shown in figure 3.5. A 50 μm energy modulation has been added to the beam, and the delays are set so that total slippage in undulator module and delay is also 50 μm. The results indicate that in this phase the scheme can be proven in principle. For the results shown here, the FWHM pulse lengths (of individual pulses within the train) are 43 fs/13 μm/50 cycles at 266 nm and 18 fs/5 μm/50 cycles at 100 nm. For comparison $\pi l_c \simeq 20\,\mu$m at 266 nm and $\pi l_c \simeq 10\,\mu$m at 100 nm. The spectra show that the output is also discretely multichromatic over a full 7% bandwidth which is far broader than the SASE bandwidth.

In the second phase the aim would be to reduce pulse durations further to below the FEL cooperation length, using additional delays which would be inserted within the undulator modules — from the scalings given in [15] this would enable a broader gain bandwidth supporting more modes and thus the synthesis of even shorter pulses within the train. Simulation results of this setup, operating at 266 nm, are shown in figure 3.6. The pulse length obtained is 17 fs/5 μm/20 cycles, more than a factor of two shorter than possible with the standard configuration.

Another interesting possibility, also shown in figure 3.6, is an extension scheme where it might be possible to generate isolated pulses. The modulation wavelength is longer here, at 120 μm. The motivation for this is by obtaining the correct ratio between electron bunch length and modulation period it is possible to preferentially amplify only a single pulse within the train. The pulse duration obtained here is 14 fs/4 μm/40 cycles. Further study is required of this concept but the hope is to eventually demonstrate the production of isolated mode-locked pulses. It may in fact be possible to do this with a 50 μm beam modulation if the electron bunch is compressed to the appropriate length.

Mode-Locked Afterburner

The Mode-Locked Afterburner scheme [16] is a development of the mode-locked amplifier FEL concept and promises to deliver ultra-short pulses. It retains the baseline radiator stage of the CLARA FEL, with short pulses generated in a relatively short 'afterburner' comprising several few-period undulators separated by chicanes. For CLARA the electron bunch would be modulated with period 3 μm using an Optical Parametric Amplifier (OPA) driven by the Ti:sapphire laser. Simulation results using `GENESIS 1.3` are shown in figure 3.7 using the following afterburner parameters: each undulator module has 8 periods and the chicanes comprise four 2.9 cm length, 0.25 T dipoles. FWHM pulse durations of 1.6 fs/0.5 μm/5 cycles are predicted, with peak power reaching $\simeq$ 20 MW in 10 undulator-chicane modules, so the total afterburner length is just over 4 m. The spectrum shows clearly separated distinct wavelengths, over a broad bandwidth of $\sim$13%.

Summary of pulse durations

For each scheme in this section the predicted pulse durations are summarised in table 3.2 in units of fs, μm, number of optical cycles and number of cooperation lengths. For reference the cooperation length $l_c \simeq 7$ μm at 266 nm and $l_c \simeq 3\,\mu$m at 100 nm. It is seen that the Slicing/Taper, EEHG and Single Spike SASE schemes would produce pulses of around 55–75 cycles FWHM or just over two cooperation lengths. The Phase I Mode-Locking scheme would generate pulses slightly

2014 JINST 9 T05001

shorter (but in a train) of around 50 cycles or just less than 2 cooperation lengths. With the Mode-Locking scheme upgraded in Phase II pulses would come down to around 20 cycles (in the train) or less than one cooperation length, or for the case where an isolated pulse could be produced about double this number of cycles. Finally, the Mode-Locked Afterburner may produce pulses of only 5 cycles, nearly an order of magnitude less than the cooperation length.

Table 3.2. Predicted pulse durations for CLARA Short Pulse Schemes.

			FWHM Pulse Duration			
Scheme	**Pulse Type**	**Wavelength (nm)**	fs	μm	#cycles	$\#l_c$
Slice/Taper	Single	266	50	15	56	2.2
EEHG	Single	100	25	8	75	2.6
Single-Spike SASE	Single	100	23	7	70	2.3
Mode-Locking Phase I	Train	266	43	13	49	1.9
	Train	100	18	5.3	50	1.8
Mode-Locking Phase II	Train	266	17	5.1	20	0.7
	Single	100	14	4.1	41	1.4
Mode-Locked Afterburner	Train	100	1.6	0.5	5	0.16

3.5.3 Improving temporal coherence

Currently the full potential of X-ray FELs is not realised because they operate in SASE mode for which the temporal coherence is relatively poor. For this reason, their spectral brightness is typically two orders of magnitude lower than that that of a transform limited source. Improvement of SASE FEL temporal coherence would greatly enhance scientific reach and allow access to new experimental regimes. There are a number of methods for improving SASE coherence, many of which have been tested or are already in routine use. Existing methods fall into two classes. In the first class, an externally injected seed source of good temporal coherence 'seeds' the FEL interaction so that noise effects are reduced. This seed field may be either at the resonant radiation wavelength, where available, or at a subharmonic which is then up-converted within the FEL. These methods, which include HGHG [51–54] and EEHG [43, 44], rely on a synchronised external seed at the appropriate wavelength, pulse energy and repetition rate. In the second class, the coherence is created by optical manipulation of the FEL radiation itself, for example by spectrally filtering the SASE emission at an early stage for subsequent re-amplification to saturation in a self-seeding method [55–58], or via the use of an optical cavity [33–40]. Methods in this class rely on potentially complex material-dependent optical systems which limit the ease and range of wavelength tuning. If an optical cavity is used, the electron source repetition rate should also be in the MHz regime to enable a practical cavity length. A third, more recently proposed class of methods, rely on artificially increasing the slippage between FEL radiation and electron bunch to slow down the electrons which extends the coherence length [59–61] or even completely 'delocalises' the FEL interaction allowing the radiation coherence length to grow exponentially [62].

Schemes in all three classes can be optimised, validated or even demonstrated for the first time on CLARA, as discussed in the remainder of this section.

2014 JINST 9 T05001

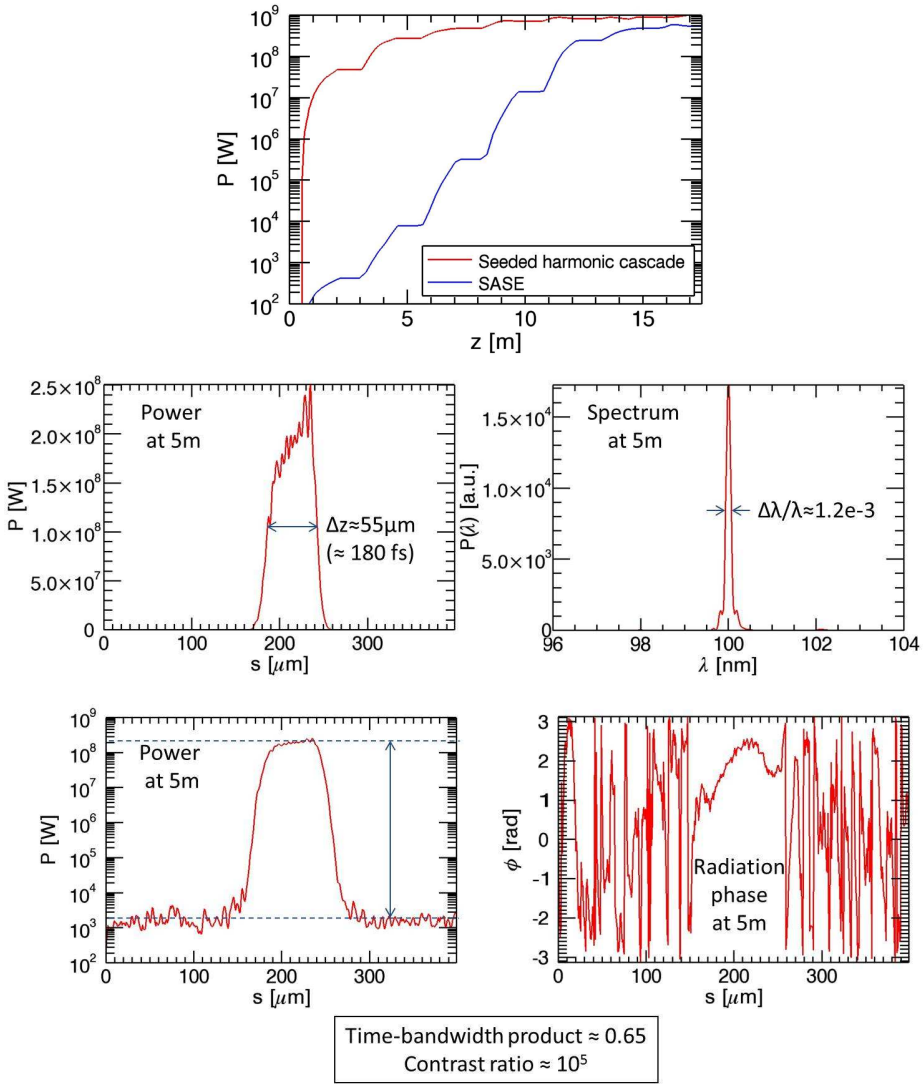

Figure 3.8. Simulation results for the seeded harmonic cascade scheme, showing peak power along the radiator compared to an equivalent SASE case (top), and the pulse properties at saturation (bottom).

Seeded harmonic cascade

When using injected seed sources to improve FEL temporal coherence, an important aspect is to extend the seeding effect beyond the wavelength range of available seed sources towards the much shorter wavelengths achievable with FELs. Methods to do this involve operating the FEL in stages, with harmonic up-conversion to shorter wavelength at each stage. The use of multiple such stages is termed a 'seeded harmonic cascade', and is a key underlying technique of the recently commissioned FERMI@Elettra facility [6] and also for the proposed UK NLS project [42, 63].

There are several variants on the technique. Here we investigate the one proposed for the shortest wavelength of the UK NLS project which involves two harmonic steps. To study this on CLARA we would seed with the 800 nm source in the first stage before conversion to the second harmonic (400 nm) in the second stage, followed by a further fourth harmonic conversion for

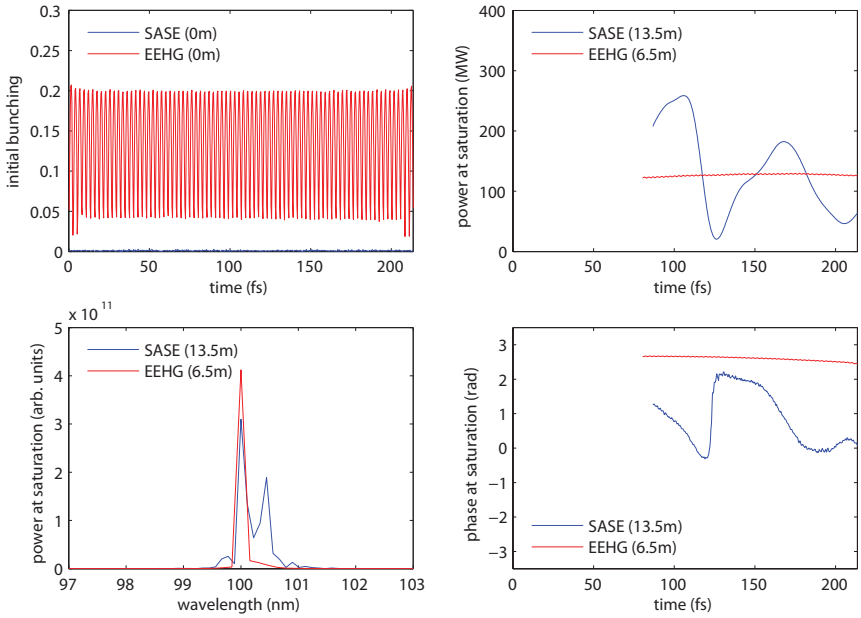

Figure 3.9. EEHG: comparing the final FEL pulse to a standard SASE simulation, the FEL pulse generated using EEHG shows a more uniform peak power at saturation, reduced bandwidth and constant radiation phase, combined with a substantial reduction in saturation length.

100 nm FEL operation. The seed imprints a sinusoidal energy modulation on the electron beam within the modulator undulator, then chicanes convert this into a density modulation (or 'bunching') containing higher harmonic components. The induced energy spread must be sufficiently low to allow FEL lasing in the final stage.

A two stage harmonic cascade could be demonstrated with the baseline CLARA layout by using the first radiator undulator as a modulator. `GENESIS 1.3` simulations were carried out and the results are shown in figure 3.8. An 800 nm seed with 200 fs FWHM duration and 0.5 MW peak power was used in the modulator to apply an energy modulation $\Delta\gamma/\sigma_\gamma \approx 1$. The chicane was set for $R_{56} \approx 200\ \mu$m, giving a bunching factor of $\sim$2% at 400 nm. This is deliberately less than optimum — the first radiator stage used as a modulator resonant at 400 nm is relatively long, so the relatively low bunching factor acts to keep the induced energy spread sufficiently low in this stage. Energy modulation of $\Delta\gamma/\sigma_\gamma \approx 6$ was applied, giving $\sim$20% bunching factor at 100 nm, using the inter-module electron delay chicanes to apply a relatively low compression ($R_{56} \approx 60\ \mu$m). The remainder of the radiator is resonant at 100 nm and the FEL saturates after only two undulator modules with excellent temporal coherence and contrast ratio over the SASE background, as shown in figure 3.8.

Saturating so early in the radiator opens up the possibility of investigating other FEL methods such as undulator tapering [64] to enhance the output power, or superradiance [65–67], in which sub-cooperation length pulses can be generated as the FEL interaction proceeds deep into saturation.

2014 JINST 9 T05001

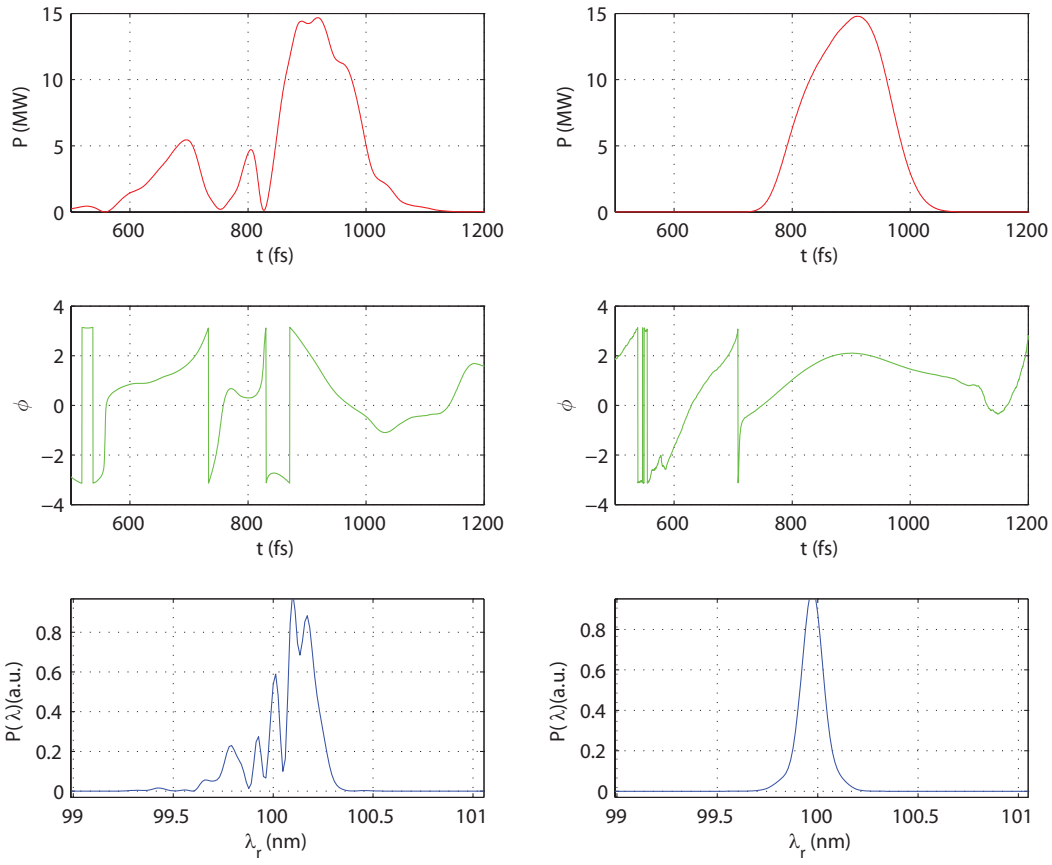

Figure 3.10. Results of 100 nm RAFEL simulations. The left hand column shows the control case without an optical cavity, i.e. normal SASE, whereas the right hand column shows the effect of adding the feedback — the output pulse is cleaned up both spectrally and temporally. The pulse is shown after 11 cavity round trips.

Echo-enabled harmonic generation

The EEHG scheme has been proposed as a way to improve the temporal coherence of FEL pulses, and works by combining two energy modulation stages with two chicanes to induce a fine-structure density modulation in the electron bunch [43]. The electron bunch is then sent through a radiator section resonant at the density modulation wavelength, ultimately generating a temporally coherent FEL pulse at a wavelength many times shorter than the initial seed lasers. Initial studies of this scheme [68] assumed both modulators were identical, with 65 mm period and 1 m total length but for implementation on CLARA the first radiator would be replaced by an additional short modulator and weak chicane. We expect performance to be similar in this configuration.

The optimal seed laser wavelength for investigating EEHG on CLARA is 800 nm. Based on the analytic equations derived in [44] and the above modulator parameters, maximum bunching at wavelengths from 100 nm down to 8 nm (8th to 100th harmonics of the seed lasers) can be

achieved using seed lasers of up to 100 μJ pulse energy with 500 fs rms pulse duration. The maximum requirements placed on the two chicanes would be R_{56} values of 41 mm and 0.5 mm respectively.

To complement the analytical studies, numerical simulations have been carried out at λ_{FEL} = 100nm (8th harmonic) using `elegant` for the two modulator and chicane sections, and `GENESIS 1.3` for the radiator section. The tracking in `elegant` was carried out with and without coherent and incoherent synchrotron radiation emission in the chicane dipoles. In the simulations, a 250 fs long section of the electron bunch was studied, with sufficient particles to account for the individual electrons (>590M particles). The seed laser pulse energy was 10 μJ. Comparing the final FEL pulse to a standard SASE simulation, the FEL pulse generated using EEHG shows a more uniform peak power at saturation, reduced bandwidth and constant radiation phase, combined with a substantial reduction in saturation length, as shown in figure 3.9.

For the study of coherent bunching at very high harmonics, i.e. at wavelengths shorter than 100 nm where it will not be possible to demonstrate lasing, methods for generating coherently enhanced radiation from the electron beam may be used as a diagnostic. This is a subject for further study.

RAFEL

Simulations have been done of a RAFEL driven by CLARA operating in multibunch mode, with electron bunch parameters given in table 3.1. The one-dimensional FEL oscillator simulation code `FELO` [69] was employed. Although this code does not model the radiation propagation in the cavity, employing instead a simple radiation feedback factor, its predictions of the longitudinal radiation characteristics and build up from shot noise have been shown previously to agree well with fully three-dimensional simulations of RAFEL systems using `GENESIS 1.3` and dedicated optical propagation codes [70].

Only five of the seven radiator undulators are required. The radiation feedback factor F to maximise the output power and longitudinal coherence [38] is given by $F = 25\exp(-\sqrt{3}G)$ where $G = 4\pi\rho N_w$ with ρ the usual FEL parameter and N_w the number of undulator periods. For the electron bunch parameters as listed in table 3.1 it is found that $F = 1.8\times10^{-3}$ showing that only a very small fraction of the emitted radiation needs to be fed back via the optical cavity to the start of the undulator. The scheme is in effect a self-seeded FEL rather than an oscillator FEL because there is no requirement to build up a stable optical mode in the resonator.

The simulation results are shown in figure 3.10 where the RAFEL has reached saturation after 11 cavity round trips. The left hand plot shows the control case for these parameters without an optical cavity, i.e. normal SASE, whereas the right hand plot shows the effect of adding the feedback — the output pulse is cleaned up both spectrally and temporally with time bandwidth product $(\Delta\lambda/\lambda^2)c\Delta t = 0.58$ which is close to that of a transform limited pulse. Simulations for 266 nm and 400 nm output also show near transform limited output using optimum feedback factors of $F = 4.5\times10^{-6}$ and $F = 3.5\times10^{-7}$ respectively.

The emphasis here has been the use of a RAFEL to improve SASE temporal coherence, but it should be noted that theoretical work has also indicated the potential of RAFEL systems for the generation of stable attosecond pulses [71]. This is another research topic that could be investigated experimentally on CLARA.

2014 JINST 9 T05001

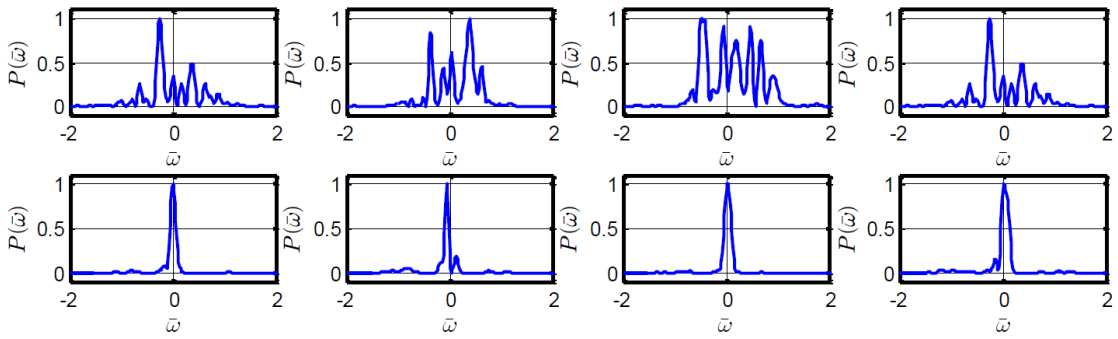

Figure 3.11. HB-SASE: the spectra (in scaled frequency $\bar{\omega} = (\lambda - \lambda_r)/2\rho\lambda_r$) of four statistically independent 100 nm SASE pulses on the top row, and the spectra of four statistically independent HB-SASE pulses on the bottom row.

High-brightness SASE schemes

A recently proposed class of methods rely on artificially increasing the slippage between FEL radiation and electron bunch to enhance the SASE FEL longitudinal coherence and hence improve the spectral brightness. This can be done by using chicanes to apply a series of unequal delays to the electron bunch as it propagates though the undulator [59]. Variations of the scheme have been studied in some detail and named High-Brightness SASE (HB-SASE) [62] and Improved SASE (iSASE) [72]. For CLARA the delays can be applied via magnetic chicanes between undulator sections, using the same hardware as required for the Mode-Locking scheme discussed in section 3.5.2. A proof-of-principle experiment to demonstrate the concept has already been done successfully at the LCLS using detuned undulator sections as delays, but this only allowed a limited slippage enhancement [73]. Another proposal called purified SASE (p-SASE) [61] suggests using subharmonic undulators as 'slippage-boosted' sections. Theoretical work on HB-SASE and iSASE has shown that by using magnetic chicanes to delay the beam and optimising the delay sequence it may be possible to significantly extend the radiation coherence length. Further advantages are that the efficiency of a taper can be much enhanced and that the shot-to-shot stability of the output power in the presence of electron beam energy fluctuation should be improved compared to a self-seeding scheme using optics [60].

The scheme has been studied for implementation on the standard CLARA lattice, with delays based on a prime number sequence [74]. The results indicate we could generate transform limited pulses at 100 nm. Figure 3.11 shows the spectra of four statistically independent SASE pulses on the top row, and the spectra of four statistically independent HB-SASE pulses on the bottom row. The particular areas of research that could be done on CLARA are: study and optimisation of the delay sequence; statistical studies of output stability; tolerance studies of sensitivity to accelerator jitter; enhancing tapering efficiency. A later phase of research (which could run parallel to the extended research on mode-locking) would investigate: impact on FEL output of extra in-undulator delays; demonstration of novel compact isochronous delays [75]; use of mixed non-isochronous and isochronous delays; study of a 'correction chicane' with negative R_{56} [76].

2014 JINST 9 T05001

3.5.4 Afterburner schemes

A number of schemes which use afterburner undulators could be tested:

Short wavelength generation. This is done by exploiting the electron beam bunching at harmonics which are higher than the FEL resonance. This harmonic bunching occurs naturally within the beam due to the FEL interaction. By propagating the beam into a short afterburner which is tuned to this harmonic the beam can be made to emit a pulse of coherently enhanced radiation at a wavelength shorter than the FEL wavelength. This burst of radiation undergoes a sharp initial power growth (quadratic with distance through the afterburner) which rapidly saturates — the energy spread induced in the beam by the previous FEL interaction prohibits exponential growth and lasing, but the emitted power can still be orders of magnitude greater than incoherent spontaneous undulator emission. Such afterburner schemes are of interest to many FEL facilities as a way of extracting useful short wavelength radiation from an otherwise 'spent' beam. The research interest is in the use of compact novel undulators for this purpose.

Exotic short pulse generation. A proof of principle experiment could be done for the 'mode-locked' afterburner concept, which is a new proposal for generating FEL pulses in the zeptosecond regime from existing X-ray FELs via a compact afterburner extension. This idea was explained further in section 3.5.2.

Polarisation control. To generate circularly polarised radiation via the crossed undulator scheme. This requires two undulators as the final FEL radiators with orthogonal linear polarisation [77]. Alternatively a single variably polarised undulator could be used as the final radiator to demonstrate high intensity variably polarised emission from an electron beam strongly pre-bunched in the previous planar undulators [63].

3.6 Scaling to short wavelengths

The CLARA wavelength range, in the visible and VUV, has been chosen to enable easy diagnosis of the output. For many schemes we are concerned only with the underlying physics of the mechanism which is often wavelength-independent — the wavelength only becomes an issue when considering those factors specific to the scheme in question which may mitigate performance at shorter wavelengths. However, scalability to shorter wavelengths is important to understand because the R&D done at CLARA will be applied at FELs which operate at shorter wavelengths than CLARA can access. This will benefit UK scientists whether they are current users of short-wavelength FEL facilities abroad or future users of a short-wavelength FEL facility in the UK.

In general the parameter tolerances are more demanding as the wavelength decreases. The required geometrical emittance is proportional to the wavelength, the tolerances on energy spread and field quality scale with the FEL ρ parameter which is smaller at shorter wavelengths, and the tolerances on electron beam trajectory control scale with the size of the electron beam which reduces due to adiabatic damping at the higher beam energies required for shorter wavelengths. These issues must be addressed for the FEL to lase *even in SASE mode* so do not directly affect the scalability of CLARA results — the issues we are concerned with are only those relating to the extra manipulation required to convert SASE output to short pulse output or temporally coherent output.

2014 JINST 9 T05001

For example, in many schemes one or more magnetic chicanes are used, either to longitudinally shear the electron bunch or delay it with respect to the radiation. Often some wavelength-specific tolerances on the stability of these chicanes have been determined in the original papers (see for example [15]). Sometimes more specific issues have been raised which need further study, such as: the effect of R_{51} leakage smearing the imparted modulation in EEHG; the degrading effect of Coherent Synchrotron Radiation (CSR) emission in the chicanes; the washing out of FEL induced microbunching during beam transport; the discrepancy between the EEHG model, which assumes each harmonic has a δ-function linewidth, and reality where the harmonics all have a width which depends on laser pulse length, chirp, laser phase noise and electron beam shot noise. All of these effects will become relatively more significant for the finer beam manipulations and structures required at shorter wavelengths. Using CLARA we will be uniquely placed to actively study the impact of these effects by progressively changing the input parameters and carefully assessing the FEL performance. For example we can add errors to magnet angles, add jitter to magnet power supplies, adjust the laser heater settings to control the beam microbunching, propagate bunched beams over variable distances before diagnosing the bunching degradation via Coherent Optical Transmission Radiation (COTR) screens, adjust the laser chirp and pulse duration, and so on. In this way we can obtain invaluable data which can be used to prioritise schemes for future implementation at X-ray wavelengths.

As a last comment, we consider how the pulse durations for the CLARA short pulse schemes would scale if implemented on an X-ray FEL. For the Slice/Taper scheme and the Single Spike SASE scheme the pulse duration would be expected to scale with the cooperation time $t_c = l_c/c$. An estimate for t_c at 0.15 nm wavelength is $t_c \simeq 80$ as, so from table 3.2 which gives the pulses lengths in units of the cooperation length we would expect pulse durations of order 180 as at 0.15 nm. For the Mode-Locked schemes the pulse durations would be expected to scale with the number of cycles, so at 0.15 nm we would expect FWHM pulse durations of 10–25 as for Mode-Locking, and around 2.5 as for the Mode-Locked afterburner. Both of these estimates are in agreement with the published 3D simulations of these schemes at this wavelength [15, 16]. What is clear then is that if the schemes we test on CLARA are one day applied in the X-ray they may enable a transformative change in the utility of the free-electron laser as a scientific tool.

2014 JINST 9 T05001

Chapter 4

Accelerator design

4.1 Layout overview

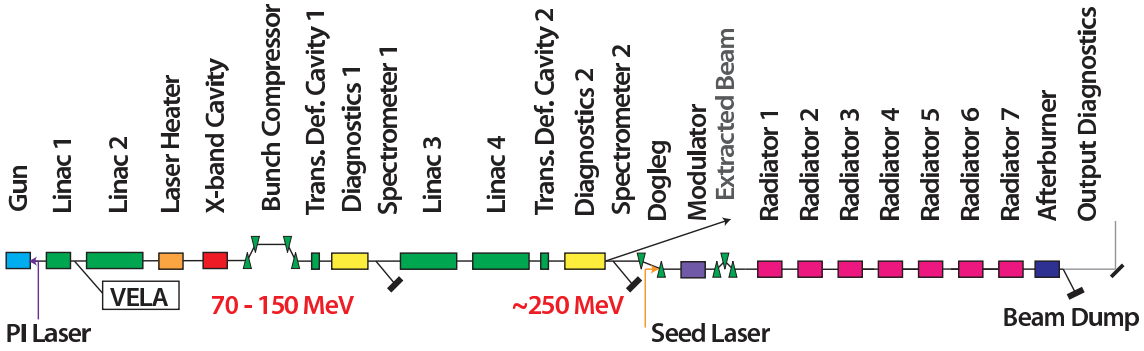

Figure 4.1. CLARA layout overview.

The design approach for CLARA is to build in flexibility of operation, enabling a wide exploration of FEL schemes. To this end a range of possible accelerator configurations have been considered. A major aim is to test seeded FEL schemes. This places a stringent requirement on the longitudinal properties of the electron bunches, namely that the slice parameters should be nearly constant for a large proportion of the bunch length. In addition, CLARA should deliver high peak current bunches for SASE operation and ultra-short pulse generation schemes, such as velocity compressed bunches. This flexibility of delivering tailored pulse profiles will allow a direct comparison of FEL schemes in one facility.

The proposed layout of CLARA is shown in figure 4.1. The S-band (2998.5 MHz) RF photocathode gun [78] is followed by Linac 1. This is a ∼2 m long structure that may be used in acceleration or bunching configurations. A spectrometer line which also serves as injection to VELA branches at this location. Linac 2 follows which is ∼4 m long and can accelerating up to 150 MeV. Space for a laser heater is reserved provisionally at this point. Initially this will not be installed however we expect that in the ultra-short bunch mode the beam properties will be degraded by microbunching instability (predominantly driven by longitudinal space-charge impedance). This effect will be quantified and the necessity and optimum location of the laser heater determined in the future.

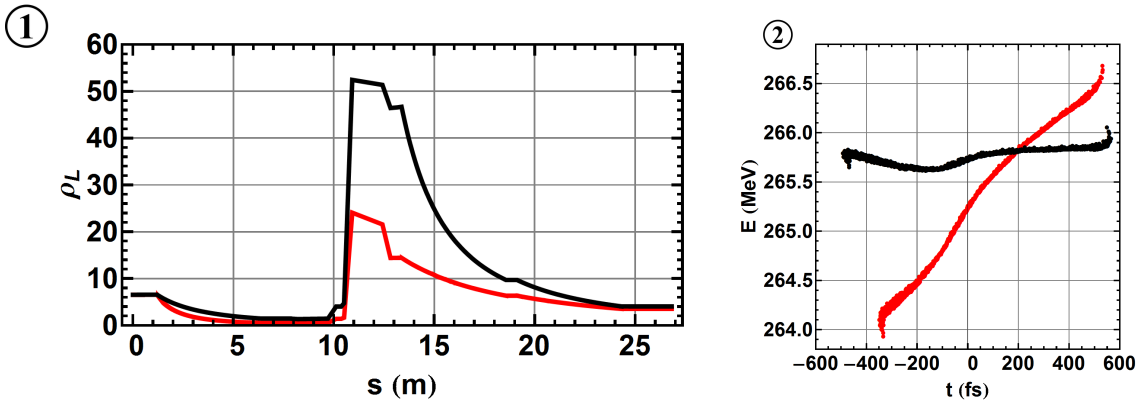

Figure 4.2. (1) Laminarity (black/red) in the 10% of charge slice containing the peak current with compression at 70 MeV/130 MeV (for an indicative layout). (2) Longitudinal phase space (black/red) with compression at 70 MeV/130 MeV.

A fourth harmonic linearising X-band cavity (11994 MHz) [79] is situated before the magnetic compressor to correct for longitudinal phase space curvature. A variable magnetic bunch compressor is then followed by the first dedicated beam diagnostics section, incorporating transverse deflecting cavity and spectrometer, enabling measurement of emittance, bunch length and slice properties. Linacs 3 & 4 (each $\sim$ 4 m long) accelerate to 250 MeV. These are followed by a second diagnostics section. It has also been proposed to divert this high energy beam for other applications. The beamline then passes a dogleg, offsetting the FELs from the linacs transversely by $\sim$ 50 mm to enable co-propagation of long wavelength laser seeds. Immediately following the dogleg is the FEL modulator undulator and chicane. A dedicated matching section ensures that periodic optics is achievable in the radiators for the entire wavelength range. Seven FEL radiators and a space for a FEL afterburner complete the accelerator and the beam is then dumped.

4.1.1 Phase space linearisation

Magnetic compression of electron bunches requires that some attention be given to the removal of the curvature imposed on the longitudinal phase space of the bunch by the accelerating RF. For CLARA, a harmonic linearising cavity was compared with non-linear magnetic correction in the chicane [80]. The additional complication of a harmonic cavity was shown to be justified by the ability to predictably tailor the longitudinal phase space.

4.1.2 Energy at magnetic compressor

The seeded FEL schemes to be demonstrated at CLARA require small correlated energy spread at the undulators, therefore when magnetic compression is to be used the compressor must be situated at substantially less than full energy. This ensures that the chirp needed at compression can be adiabatically damped or suppressed through running subsequent accelerating structures beyond crest. This requirement must be balanced against the fact that compressing at low energy exacerbates

Table 4.1. Specification of variable bunch compressor.

	Value	Unit
Energy at compressor	70 - 150	MeV
Min. : Max. bend	0 : 200	mrad
Bend magnetic length	200	mm
Max. bend field	0.5	T
Min. : Max. offset	0 : 300	mm
Separation of dipoles 1 & 2	1500	mm
Separation of dipoles 2 & 3	1000	mm
Max. bellows extension	260	mm
Min. : Max. R_{56}	0 : -72	mm
Beam size from δ_E ($\pm 6\sigma$)	0 : 20	mm
Beam size from β_x ($\pm 6\sigma$)	3.0	mm

space-charge effects. To quantify this we use the laminarity parameter

$$\rho_L = \left(\frac{I/(2I_A)}{\epsilon_{th}\gamma\gamma' \sqrt{1/4+\Omega^2}} \right)^2$$

where I is the current in the slice under consideration, I_A is the Alfven current, ϵ_{th} is the thermal emittance, $\gamma' = d\gamma/ds$ and Ω is a solenoidal focusing field (zero in the case considered).

When this parameter is greater than 1, we should consider space-charge effects in the bunch evolution. To inform this we select two candidate configurations, one with magnetic compression at 70 MeV and one at 130 MeV. An indicative bunch was tracked through both configurations, setting the machine parameters to produce a zero chirp 250 pC bunch of peak current 350 A at 250 MeV. Tracking was carried out with `ASTRA` [81, 82] to the exit of the first linac section to include space-charge, followed by `elegant` [47, 80] taking into account the effect of cavity wake-fields, longitudinal space-charge (LSC) and CSR emittance dilution. Figure 4.2 shows the resultant laminarities and final bunch longitudinal phase spaces.

We see that in both cases space-charge should be considered. However compression at 130 MeV does not allow us to subsequently de-chirp the bunch (for the same energy gain). A dedicated de-chirping cavity at full energy has been considered and rejected due to technical immaturity and lack of space. Note that we go no further than 30° beyond crest in the final accelerating structures in order to avoid large jitter effects. As we wish the facility to be flexible we select a nominal compressor energy of approximately 70 MeV, but we achieve this by reducing the gradient in the accelerating structure before the compressor (and increasing the gradient required in Linacs 3 and 4 to 23 MV/m). This gives us the option of compressing at higher energy in regimes where a de-chirped bunch is not required.

The `elegant` LSC model is used in all tracking and the achieved compression will be compared with other codes in further studies allowing differences between 1D and full 3D space charge effects up to full energy.

2014 JINST 9 T05001

4.1.3 Variable bunch compressor

With the above considerations in mind the specifications for the CLARA variable bunch compressor are shown in table 4.1.

For flexibility, the compressor has a continuously variable R_{56} and is rated for maximum energy of 150 MeV. Physical movement of the elements transversely allow for a small aperture beam pipe in the central section. This enables energy feedback on Linacs 1, 2 and the X-band lineariser via a high resolution cavity Beam Position Monitor (BPM) situated in the high dispersion region. A screen and collimator are also situated in this section. The ability to set a straight-through path also allows the use of velocity compressed bunches. Optics are kept such that β_x is minimised at the last dipole, thereby minimising CSR. Residual dispersion arising from non-identical compressor dipoles will then be corrected using trim coils informed by recent experience at FERMI@Elettra and LCLS.

4.1.4 Diagnostic sections

Dedicated beam diagnostics sections are situated after the bunch compressor at $70-150$ MeV, and again after Linac 4 at 250 MeV. The transverse and longitudinal properties of the compressed bunch will be analysed immediately post compression in the first section, and those at full energy in the second section.

Specifically we intend to measure the Twiss functions, emittance, energy, energy spread, bunch length, slice emittance and slice energy spread. This is achieved with a five quadrupole system together with transverse deflecting cavity (TDC) and spectrometer line. This arrangement has been used with success at, for instance, FERMI@Elettra [83, 84]. The large relative energy spread required at the bunch compressor, of $\mathcal{O}(2\%)$, dictates that the quadrupole integrated strengths in this section are limited by chromatic aberration to $kl \simeq 0.7$ m^{-1}. This in turn implies that these sections are relatively long.

Figure 4.3 shows the optics of these diagnostic sections (starting at 0 m and 19 m respectively). β_x is small at the start to minimise the CSR induced emittance growth in the preceding bunch compressor. Large β_y at the TDC and vertical phase advance of $\sim 90^\circ$ is chosen to maximise the vertical size of the streaked beam on a screen situated after the fifth quadrupole, The following four quadrupole telescope ensures that CLARA can drive the FEL without changing optics from the diagnostic configuration. This ensures minimal intervention from running mode, and allows the possibility of online diagnostics on the upgrade of the spectrometer dipole to a pulsed magnet.

We estimate the achievable slice resolution following the method of Craievich [85]. Figure 4.4 shows that we are able to resolve 10 fs slices in the low energy diagnostics line at 70 MeV with a TDC deflecting voltage of 5 MV.

Figure 4.5 shows the long pulse bunch tracked through the low energy diagnostics section. The bunch is sliced in 0.1 ps time slices at the TDC, and the screen image with TDC on and off is shown. Figure 4.6 shows the same information, but with the screen now in the spectrometer line after the fifth quadrupole. The screen is at the same path length from the TDC as the non-dispersive screen with $|\eta_x| = 0.5$ m, allowing energy and energy spread determination. With the TDC on, the resolution of slice parameters is seen.

2014 JINST 9 T05001

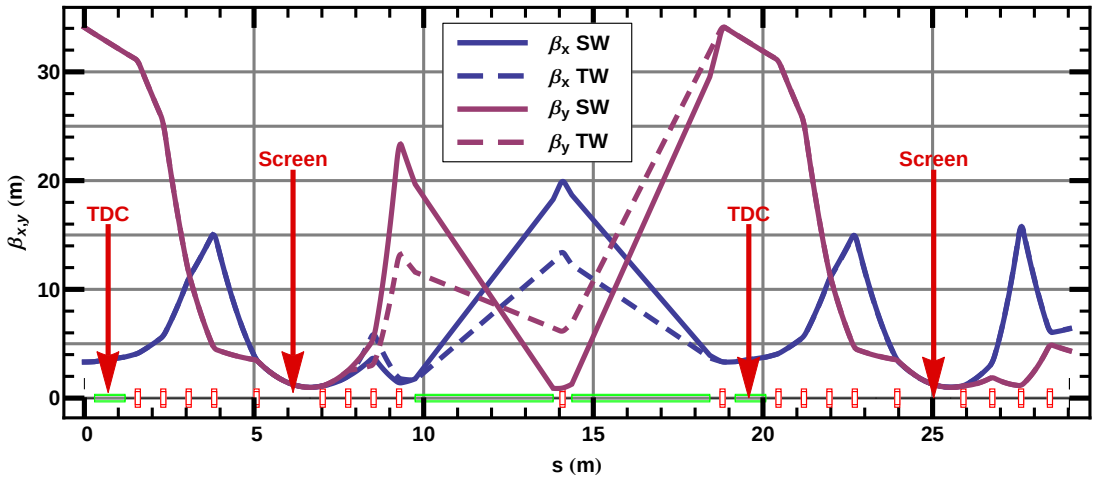

Figure 4.3. Optics of CLARA from bunch compressor exit (at 24.5 m from the cathode) to dogleg entrance, comprising low and high energy diagnostics lines with Linacs 3 & 4 separating. Matches for both standing wave (SW) and travelling wave (TW) linac focussing are shown. Between each TDC and subsequent screen there is a vertical phase advance of $\pi/2$.

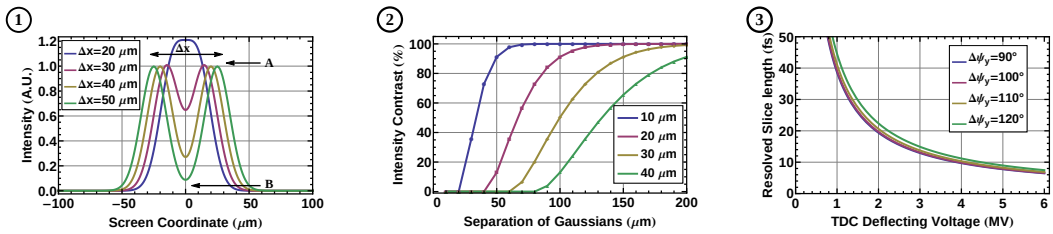

Figure 4.4. (1) Two features on a screen modelled as Gaussians separated by Δx with screen resolution of $10\,\mu$m. Intensity contrast (IC) is then defined as $\frac{(A-B)}{A}$. (2) IC as a function of the separation of the two Gaussian features for 4 screen resolutions from $10\,\mu$m to $40\,\mu$m. (3) Resolved slice length in low energy diagnostics line as a function of TDC deflecting voltage assuming a screen resolution of $10\,\mu$m and IC of 70%.

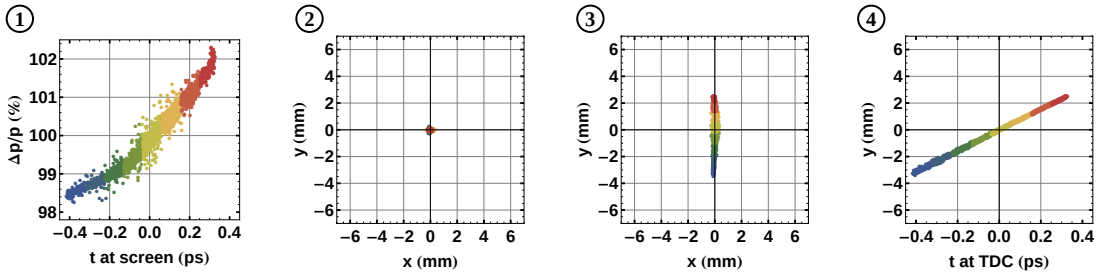

Figure 4.5. Long pulse bunch streaked by TDC in low energy diagnostics line: (1) Long. phase space at screen; (2) Screen image with TDC deflecting voltage = 0 MV; (3) Screen image with TDC deflecting voltage = 5 MV; (4) Correlation between arrival time at TDC and vertical position on screen.

2014 JINST 9 T05001

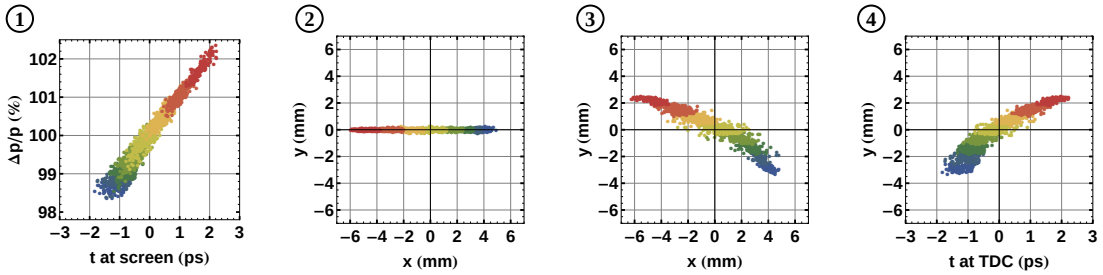

Figure 4.6. Long pulse bunch streaked by TDC in low energy diagnostics spectrometer line: (1) Long. phase space at screen; (2) Screen image with TDC deflecting voltage = 0 MV; (3) Screen image with TDC deflecting voltage = 5 MV; (4) Correlation between arrival time at TDC and vertical position on screen.

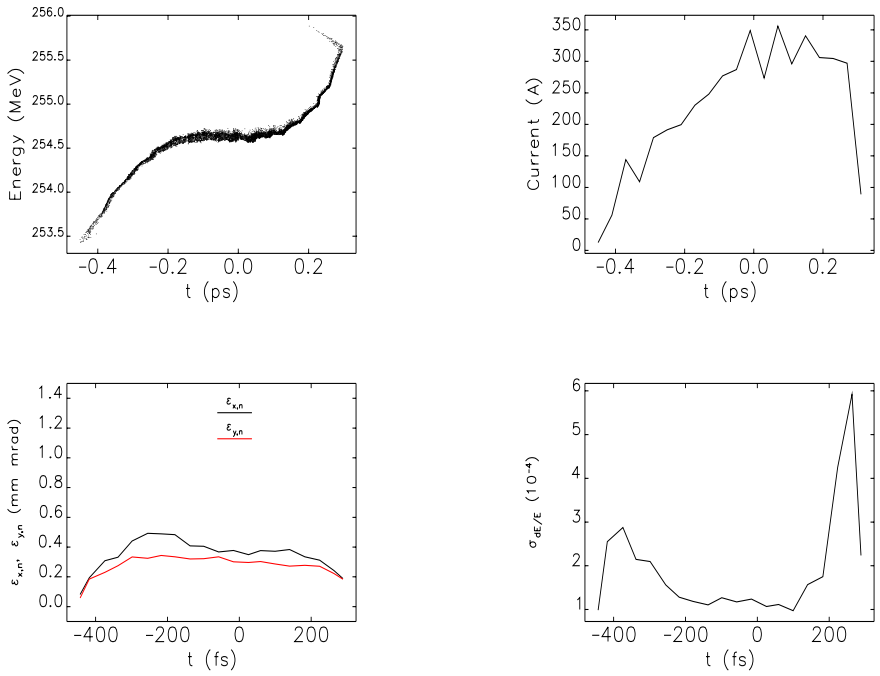

Figure 4.7. Seeded bunch longitudinal phase space, current profile, normalised slice emittance and slice energy spread.

A similar analysis in the high energy diagnostics line at 250 MeV produces similar results for a TDC with deflecting voltage of 10 MV. The possibility of moving (or inserting an additional) TDC and diagnostics section after the FEL will be investigated as an upgrade.

4.2 Beam dynamics

The beam was simulated from the cathode until the exit of Linac 1 using `ASTRA` to include the effects of space-charge. Wakefield effects have not yet been included. The rest of the machine was then tracked using `elegant` [47]. Linac wakefields, longitudinal space-charge and coherent radiation effects were included.

Table 4.2. Optimised machine parameters for seeded bunch (gradients are specified at on-crest levels).

	Value	Unit
Gun Gradient	100	MV/m
Gun ϕ	-25	$^\circ$
Linac 1 V	21.0	MeV/m
Linac 1 ϕ	-20	$^\circ$
Linac 2 V	11.5	MeV/m
Linac 2 ϕ	-31	$^\circ$
Linac X V	7.3	MeV/m
Linac X ϕ	-168	$^\circ$
BC θ	95.0	mrad
Linac 3 V	22.5	MeV/m
Linac 3 ϕ	$+0$	$^\circ$
Linac 4 V	22.5	MeV/m
Linac 4 ϕ	$+0$	$^\circ$

4.2.1 Electron source

The electron source of CLARA will initially be the VELA 2.5 cell S-band normal conducting gun, as detailed in chapter 5. A solenoid surrounds the gun cavity and an additional bucking coil cancels the magnetic field on the cathode plane. The design peak field is 100 MV/m, which equates to a maximum beam energy of 6.5 MeV. For all simulations, an intrinsic transverse emittance from the copper photocathode is included as per LCLS measurements of 0.9 mm mrad per mm rms of a flat-top laser spot [86]. A laser diameter of 1 mm has been assumed with Gaussian longitudinal laser profile of duration 76 fs rms. This short pulse length allows the gun to operate in the so-called 'blow-out' regime, where the bunch length expands due to space-charge. For the long pulse mode a 250 pC bunch expands to 1.3 ps rms in the gun and does not evolve afterwards until the magnetic bunch compressor. The blow-out regime has been demonstrated experimentally and compared to simulations [87]. Full characterisation of this scheme and the beam properties achievable with the CLARA gun will be tested using VELA. There is also the possibility of adding pulse stackers to stretch the laser pulse to the required length if the blow-out regime is found experimentally to not provide the required beam properties. A solenoid surrounding Linac 1 is used for transverse focussing and emittance compensation and Linac 1 is operated off-crest to provide part of the chirp required for magnetic bunch compression.

4.2.2 Optimisation of seeded mode

The seeded operating mode is the most challenging as it requires that the bunch slice properties at the entrance to the FEL are constant for a large fraction of the bunch length, i.e. 250 fs out of 500 fs FW, and that the peak current is above 400 A for this fraction, without significant energy chirp. This is to ensure that the FEL output performance is tolerant to jitter between the laser seed and the electron bunch.

2014 JINST 9 T05001

To achieve this an optimisation [88] was performed on the longitudinal phase space of the bunch at the FEL. At each step a transverse rematch was necessary to preserve the projected emittance. The optimisation variables are the voltages and phases of the S-band linacs and X-band linac, and the bunch compressor bend angle. The optimisation constraints were that there exists a 300 fs window where the mean current exceeds 400 A, and in that window:

- the minimum current in a 20 fs slice is greater than 370 A,
- the standard deviation of the charges in a 20 fs slice is less than 20 pC and
- the chirp is no larger than 1% of the energy spread in the 20 fs slice at the centre of the window.

In figure 4.7 we show the optimised longitudinal phase space, current profile, slice emittance and slice energy spread at the FEL. The optimisation constraints are broadly met. The standard deviation of the charges in the window is marginal. This may be due to insufficient numerics in the simulations thus far produced. The transverse matching along the bunch is also suboptimal and will be the subject of further study.

Table 4.2 shows the optimised machine parameters. The relatively low gradient in Linac 2 and high gradients in Linacs 3 and 4 arise from the requirement to minimise the chirp. This will not be the case in other modes, therefore flexibility in operation of linac gradients is required.

4.2.3 Other operating modes

An alternative to magnetic compression is to use velocity bunching in the low energy section of the accelerator. Linac 1 is set to the zero crossing phase to impart a time-velocity chirp along the bunch. The bunch then compresses in the following drift space. Linac 2 then rapidly accelerates the beam and 'captures' the short bunch length. Solenoids are required around Linac 1 to control the transverse beam size and prevent emittance degradation.

Simulations suggest that this mode of compression can produce a similar bunch profile to that produced by the magnetic compression scheme if the fourth harmonic cavity is not used for linearization. Thus both compression modes can be used to meet the SASE mode of CLARA operation.

Velocity bunching can also be used to drive the ultra-short mode of operation. Preliminary simulations suggest that for a 100 pC bunch, a peak current $\sim$ 1 kA can be achieved, with a FWHM bunch of 100 fs. At the slice of the peak current, the energy spread is $\sim$ 250 keV rms and the slice emittance of $\sim$ 1 mm mrad. Production of an extremely short bunch at low energy is challenging, especially due to a very strong longitudinal space charge effect. Detailed study and optimisation, including the full effect of wakefields at low energy, is ongoing, and an approach used by Dohlus et al. [89] has been adopted.

4.3 Tolerance studies

Parameter scans of the photoinjector (PI) laser properties, RF voltages and phases, and bunch compressor dipole field from the nominal values of table 4.2 are shown in table 4.3. In each case

2014 JINST 9 T05001

Table 4.3. Tolerance data for the long pulse mode. Each parameter listed is varied over the range stated, change in arrival time, rms energy spread, rms bunch length and mean energy at the exit of Linac 4 are tabulated.

Parameter Varied	**Range**	Δt_{arr} (fs)	$\Delta\delta$E (%)	$\Delta\sigma_{z\mathrm{rms}}$ (%)	ΔE (%)
PI Laser Δx	$\pm$0.1 mm	1.1	1	0.06	0.0004
PI Laser Δy	$\pm$0.1 mm	0.6	0.27	0.08	0.0004
PI Laser Δt	$\pm$300 fs	3	1.8	1.9	0.05
PI Laser $\Delta\sigma$	$\pm$10 %	15	50	9	0.06
Bunch Charge	100 – 300 pC	60	200	25	0.16
Gun ΔV	$\pm$1 %	110	4	4.5	0.06
Gun $\Delta\phi$	$\pm$1 ^{o}	90	3.5	3.5	0.1
Linac 1 ΔV	$\pm$1 %	400	2.6	2.5	0.35
Linac 1 $\Delta\phi$	$\pm$1 ^{o}	250	9	7	0.2
Linac 2 ΔV	$\pm$1 %	50	3	3	0.5
Linac 2 $\Delta\phi$	$\pm$1 ^{o}	550	16	15	0.6
Linac X ΔV	$\pm$1 %	55	1	0.9	0.05
Linac X $\Delta\phi$	$\pm$1 ^{o}	20	3	3	0.02
Linac 3 ΔV	$\pm$1 %	2.5	0.45	0.007	0.4
Linac 3 $\Delta\phi$	$\pm$1 ^{o}	3	0.5	0.0035	0.3
Linac 4 ΔV	$\pm$1 %	0.9	0.4	0.0015	0.4
Linac 4 $\Delta\phi$	$\pm$1 ^{o}	0.7	0.36	0.0025	0.3
BC ΔB	$\pm$0.01 %	10.5	7	6	0.5

we scan over the range quoted and state the maximal variation in four observables, arrival time change, rms energy spread change, rms bunch length change and mean energy change. To assess jitter sensitivity we show the rms change from nominal of the four observables from 50 machines where all parameters are varied according to Gaussians with the standard deviations quoted in table 4.4. Note that these are different from the ranges of the parameter scans which are chosen to be larger to establish trends in the observables.

Table 4.5 shows the resulting rms bunch properties. We see that at $\sim$ 60 fs, the rms arrival time jitter is significantly smaller than the $\sim$ 300 fs flat region of the long pulse bunch, ensuring reliable seed laser pulse overlap, and that the energy and bunch length (hence peak current) jitter satisfy the specification given in section 3.3.5.

4.3.1 Beam based alignment strategy

CLARA will require accurate alignment of the electron beam to ensure the stringent beam properties required for FEL operation are met. The operational strategy for correcting the beam position to the centre of the magnetic elements is based around a combination of Singular Value Decomposition (SVD) trajectory correction, as well as alignment to the magnet centres through beam-based alignment techniques. Trajectory correction on CLARA will be performed through the use of dedicated horizontal and vertical steering dipole magnets. We assume these magnets to be independent of each other but located at the same physical location. The magnets use high-precision power

Table 4.4. The rms values of the Gaussian distributions for the variables used to estimate jitter sensitivity.

rms	Value	rms	Value
$\sigma_{\Delta\sigma\,\mathrm{laser}}$	5%	$\sigma_{\phi G}$	0.1°
$\sigma_{\Delta x\,\mathrm{laser}}$	10%	$\sigma_{V(LS,LX)}$	0.1%
$\sigma_{\Delta y\,\mathrm{laser}}$	10 %	$\sigma_{\phi LS}$	0.1°
$\sigma_{\Delta t\,\mathrm{laser}}$	200 fs	$\sigma_{\phi LX}$	0.3°
$\sigma_{Q\,\mathrm{bunch}}$	2%	$\sigma_{BC\Delta B}$	0.001%
σ_{VG}	0.1%		

Table 4.5. The rms bunch properties of fifty jittered machines with respect to the nominal machine.

Variable	rms
Δt_{arr} (fs)	64.0
$\Delta\,\delta$E (%)	18.6
$\Delta\,\sigma_{z\,\mathtt{rms}}$ (%)	5.0
ΔE (%)	0.10

supplies to provide accurate changes to the beam angle at regular intervals through the lattice. The steering magnets are coupled with BPMs, spread throughout the machine, which provide beam trajectory information. The strip-line BPMs are expected to have $\lesssim 20\ \mu$m resolution in the main part of the machine, with additional high-precision cavity BPMs in the bunch compressor and between all undulators. The cavity BPMs are expected to provide sub-micron resolution in single shot mode. The beam trajectory will be monitored and corrected via the use of SVD of the trajectory response matrix. This method provides a flexible and robust trajectory correction system for the whole machine. Emittance spoiling in the main linacs can be a concern for a low-emittance FEL facility. This is primarily induced by spurious dispersion through the accelerating structures. We assume some form of dispersion minimisation strategy for the linac structures, based around a modified SVD algorithm. Due to their narrow aperture design, and concomitant tight position tolerances, alignment of the FEL undulator modules is expected to be critical to FEL operation. We envisage improved BPM resolutions in the FEL section, primarily by utilising cavity BPM structures, as well as a much stricter pre-alignment strategy to minimise the corrector requirements and BPM offsets. We will use a standard alignment strategy based on powering of quadrupole magnets and analysis of the resulting beam motion on downstream BPMs. We will also further investigate the possibility of photon-beam alignment, whereby downstream photon diagnostics are used in place of electron BPMs and the undulator spontaneous signal can be used as a proxy for the FEL output. The alignment strategy will rely on aligning the beam on an undulator by undulator basis. The beam optics in the FEL section is also of paramount importance. This will be complicated by the continuous FEL gap variability required, and as such, we will require high accuracy beam diagnostic screens throughout the FEL sections.

Finally, for continued stability of the electron beam, we envisage the use of a shot-to-shot feedback system, utilising the steering magnets and BPMs previously described, as well as feed-

forward for the undulator gaps. The intention is to specify components and controls such that shot-by-shot correction at 100 Hz is possible. Feed-back systems for the linac gradients will be performed in the bunch-compressor and dogleg structures, and will be incorporated into the general SVD correction algorithm. Real-time analysis of beam frequency spectra will be used to help diagnose unforeseen noise sources, and the use of feed-forward loops for certain components is expected. Model Independent Analysis methods will be fully utilised throughout.

Chapter 5

Accelerator systems

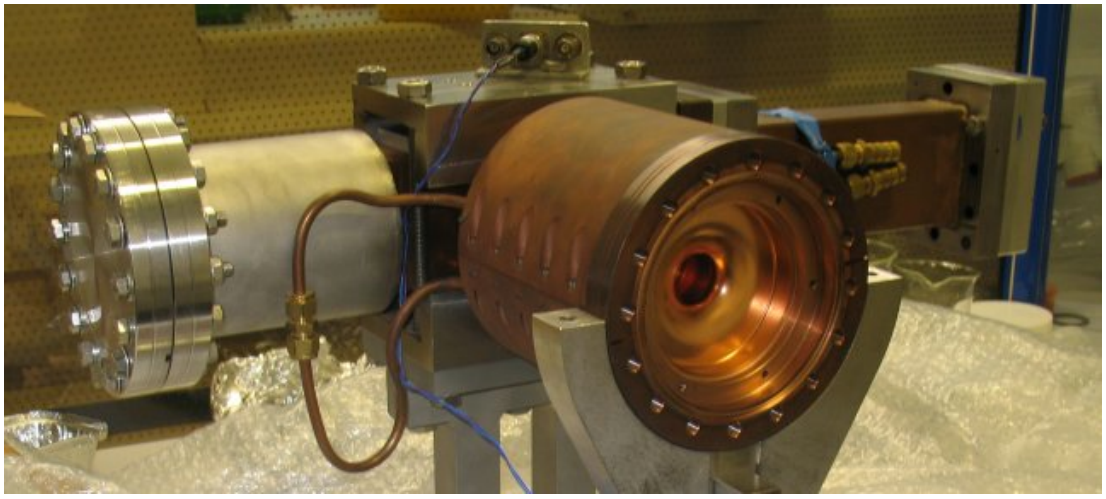

Figure 5.1. The VELA/ALPHA-X photoinjector gun.

5.1 Electron source

The primary electron source of CLARA will be based around a normal conducting S-band photocathode gun with metal and/or alkali photocathodes. This technology has been selected due to the desire to deliver low emittance beams with modest charge and repetition rate. The VELA 2.5 cell gun operated with a fixed copper photocathode is implemented with a maximum field of 100 MV/m and used as a baseline electron source. This gun fulfills the requirements of the seeded, SASE and ultra-short pulse modes of CLARA.

Our vision for the further development of the electron source will be concentrated on the design of a new highly stable, high repetition rate gun with interchangeable photocathodes. This new design would also allow us to increase the operational field to 120 MV/m. A gun with interchangeable photocathodes allows for the use of both metal and alkali photocathodes. The removal of the photocathode cleaning and preparation procedure from the gun will eliminate deterioration of the gun cavity and, as a result, improve the stability of the gun operation. Experimentation of differ-

Table 5.1. Operational power of the CLARA high repetition rate gun at different operation modes.

Repetition Rate	Gradient		*Cavity Design* 1.5 Cell	2.5 Cell
100 Hz	100 MV/m	Pulsed RF Power (MW)	5.7	10.0
		Average Power (kW)	1.7	3.0
	120 MV/m	Pulsed RF Power (MW)	8.2	14.4
		Average Power (kW)	2.4	4.3
400 Hz	100 MV/m	Pulsed RF Power (MW)	5.7	10.0
		Average Power (kW)	6.8	12.0
	120 MV/m	Pulsed RF Power (MW)	8.2	14.4
		Average Power (kW)	9.8	17.3

ent types of metal photocathodes will be possible to reduce the beam emittance and high quantum efficiency alkali photocathodes can also be implemented.

5.1.1 Baseline electron source

The baseline electron source for CLARA will be the VELA photoinjector [90]. The electron gun is a 2.5 cell normal conducting S-band RF design, as shown in figure 5.1. This was originally intended for use on the ALPHA-X laser wakefield acceleration project [91]. The gun is operated with a copper photocathode driven by the third harmonic of a Ti:sapphire laser (266 nm), which is installed in a dedicated thermally stabilized room. The injector will be operated with laser pulses with an energy of up to 1 mJ, pulse duration of 76 fs RMS and a repetition rate of 10 Hz. At a field gradient of 100 MV/m provided by a 10 MW klystron, the gun is expected to deliver beam pulses with energy of up to 6.5 MeV. Modelling with `ASTRA` suggests the length and emittance of the electron bunches at the exit of the gun varies with charge from 0.1 ps at 20 pC to 5 ps at 250 pC and from 0.2 to 0.5 mm-mrad respectively. A solenoid surrounds the gun cavity with a bucking coil to zero the magnetic field on the cathode plane.

5.1.2 Advanced electron source

Further development of the CLARA electron source will be concentrated on the design of a highly stable, high gradient and high repetition rate gun cavity which would allow operation at a field of 120 MV/m at 100 Hz repetition rate and 100 MV/m at 400 Hz. Both 1.5 cell and 2.5 cell designs are under consideration.

Operational field and power

One of the critical limiting factors which restricts performance of normal conducting RF guns is the RF power dissipated inside the cavity. Excess power leads to detuning of the gun and parasitic modulation of the amplitude and phase of the accelerating field. We estimate the operational power of the gun on the basis of existing designs. For a 1.5 cell option we have selected a high repetition rate design [92] with a well-developed cooling system. The proposed cavity can potentially operate with a maximum field of 100 MV/m with 3 μs RF pulses with a repetition rate of 1 kHz. The

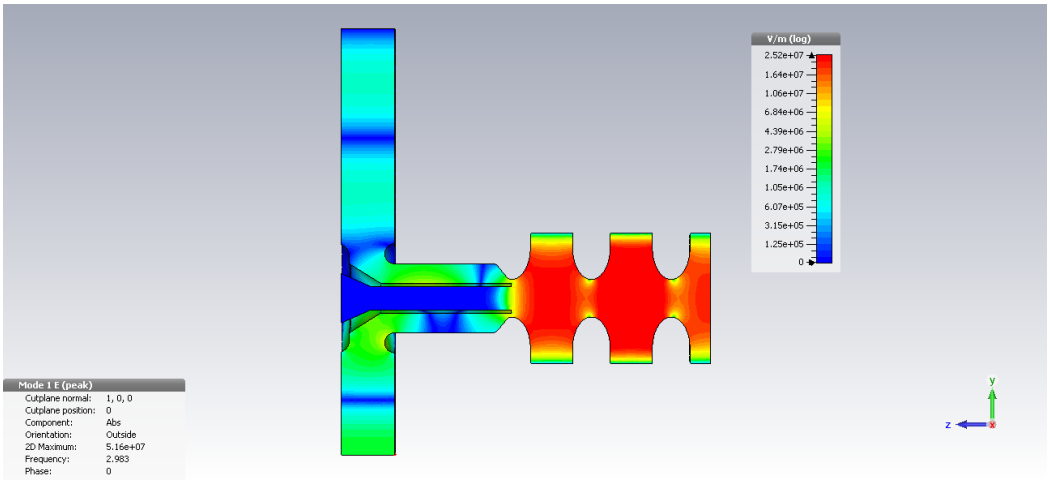

Figure 5.2. CST simulation of the electric field distribution in the VELA/ALPHA-X front-coupled 2.5 cell gun.

maximum cathode field is restricted by the average power dissipated in the cavity which exceeds 17 kW. For a 2.5 cell cavity, the required power may be estimated on the basis of the existing VELA gun cavity [91]. The RF power required to reach a cathode field of 100 MV/m is 10 MW and at a repetition rate of 10 Hz average dissipated power is 300 W.

The results of scaling these design parameters to the CLARA requirements of 100 Hz and 400 Hz repetition rate at two gun cathode fields of 100 MV/m and 120 MV/m are summarized in table 5.1. As may be seen the 1.5 cell design is able to cover all possible operation modes at both peak and average power of 10 MW and 10 kW respectively which can be delivered by the existing VELA RF station. The 2.5 cell design is able to operate in 100 Hz 100 MV/m mode only. All other modes would require an upgrade of the gun RF station.

Dark current generated by field emission is a source of concern for RF guns operating at high field. The S-band gun at LCLS has shown that 0.6 nC is produced over a 2 μs train [93]. Dry ice cleaning was first demonstrated at PITZ, which resulted in a dark current 10 times lower than a similar cavity cleaned with high pressure water rinsing [94]. Collimators in the gun region may also be used to remove unwanted dark current.

Gun stability

Seeded FEL experiments which require interaction between a short laser pulse and the electron bunch place extremely high demands on the RF gun stability. For example, the jitter of the launching phase of the beam in the magnetic bunch compression mode should be less than 300 fs, which, in terms of the S-band RF phase, is 0.32°. To provide such a phase stability the required cavity peak to peak temperature stability should be better than 0.028°C. This is still below the current start-of-the-art performance of thermal stabilisation systems which is 0.04°C [95].

Cavity detuning which is due to a small mechanical deformation caused by the RF heating is a dynamic process and the phase shift changes along the RF pulse following this detuning. For the single bunch modes, the required phase stability may be achieved by proper selection of the bunch launching time within the RF pulse and the introduction of slow feedback from arrival time

2014 JINST 9 T05001

monitors. For the multi-bunch operation mode, the situation is complicated by the rise of the cavity temperature causing detuning and consequent phase shift change along the RF pulse. For the S-band cavities the situation is even more complicated as the time required for deformation to propagate along the cavity wall is comparable to the duration of the RF pulse and for cavity thermal analysis the steady state approximation, typically used for analysis of the long pulse L-band gun, is not applicable. Very careful coupled transient analysis should be performed to satisfy the extremely high phase stability required for CLARA.

The dynamics of pulsed cavity detuning is a new subject and is now under investigation in collaboration with the Institute for Nuclear Research of the Russian Academy of Science. Preliminary analysis indicates that phase instability may be compensated with a feed forward phase correction with Low Level RF and other subsystems.

Cavity design

The RF cavity of the photoinjector must operate in both the 100 Hz 120 MV/m and 400 Hz 100 MV/m regimes, delivering bunches of up to 6 MeV energy.

Two designs are under consideration: a 1.5 cell cavity as seen in the conventional S-band injector design [96] or a 2.5 cell design, similar to the cavity [91] currently used on VELA. In order to provide feedback for stabilising the amplitude and the phase of the RF field in the cavity it will be equipped with pick-up sensors. Initial design simulations suggest that the gradient required to deliver a 6 MeV beam using a 1.5 cell cavity may cause prohibitive heating and resulting frequency instability. The impact of the lower energy delivered by the 1.5 cell gun needs to be investigated.

Two methods of RF power coupling are being considered. One option is to use coaxial coupling which is advantageous because it conserves the axial symmetry of the RF field in the cavity. This scheme may however require a complex engineering design and is also susceptible to multipactor. A coaxial coupler can either be implemented from the front or back of the gun. Front coupling, as in the VELA design (see figure 5.2), is an established technology but may suffer also from heating issues.

The other possibility is to use side coupling with a rectangular waveguide. This has the advantage of simplicity, but compromises the field symmetry in the cavity which is then transmitted to the beam and also restricts the position of the focusing solenoid. In order to compensate the field asymmetry a two-waveguide (as on the LCLS gun [97]) and even four-waveguide scheme may be considered.

Further evaluation is required to narrow down the design choices in terms of numbers of cells and coupling scheme. Alternative design options will also be investigated. Detailed simulation work and optimisation using multiple codes will then be required to find a design that satisfies all the beam physics, RF, cooling, vacuum and mechanical requirements necessary to meet the CLARA specification.

Photocathode and drive laser

The gun photocathode in the initial stage will be driven by an existing frequency-tripled Ti:sapphire laser system with a repetition rate of up to 400 Hz. The maximum pulse energy at 266 nm, at the exit of the laser system, is 1 mJ and the pulse duration is 180 fs FWHM ($\sim$76 fs RMS). The pulse

2014 JINST 9 T05001

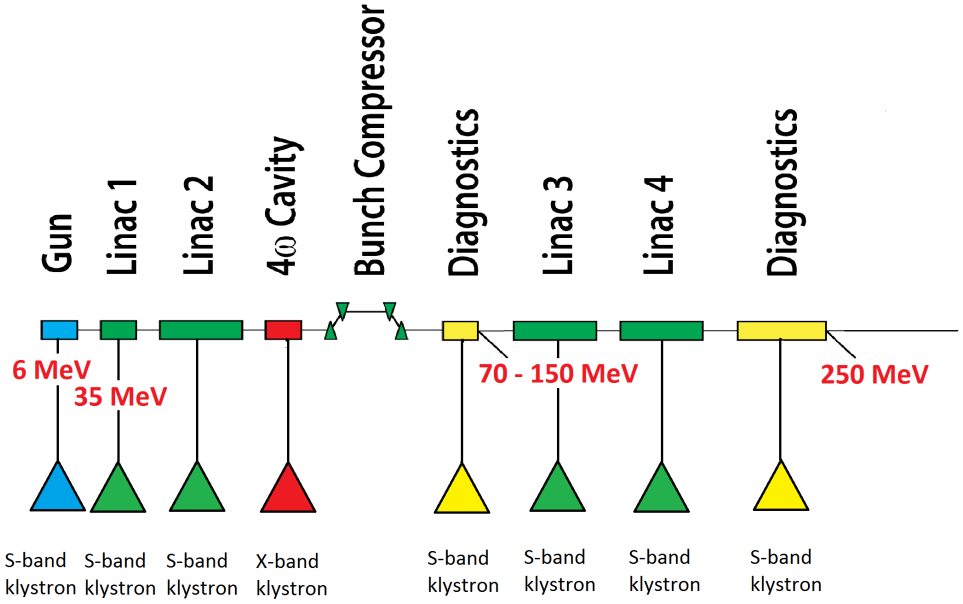

Figure 5.3. RF system layout.

energy is sufficient to deliver 250 pC charge from a metal photocathode without relying on high quantum efficiency, and allowing for unavoidable energy losses in the transport line.

Future developments will look at the use of higher quantum efficiency photocathode materials such as single-crystal Cu and metals such as Mg, Pb, Nb and eventually telluride based photocathodes. In order to transport photocathodes into the gun and easily interchange them, a load-lock system will be used. Such systems were originally developed for GaAs based DC photocathode guns then later were implemented into RF guns [98–100]. The design of the photocathode plug will be chosen to provide reliable RF contact with the gun cavity. Presently two plug designs are widely used: the DESY/INFN-LASA design developed in the framework of the TESLA collaboration [100], now used at FLASH/PITZ, FNAL and LBNL, and the CERN-CTF3 design [99] which has been chosen by PSI for the SwissFEL project. One of these two plug designs will be adopted in order to be compatible with some of the groups listed.

The photocathode plug will be initially prepared in the photocathode preparation system based on the upgraded Vacuum Generators ESCALABII facility being set up at the Accelerator Science and Technology Centre (ASTeC) at Daresbury. Preparation of metal photocathodes will include *ex vacuo* chemical and *in vacuo* thermal cleaning and surface processing with O_3 plasma to remove carbon contaminants. Surface analysis of the prepared photocathodes will be made with high resolution X-ray photoelectron and Auger spectroscopy. Prepared photocathodes will be transported to the accelerator hall with a vacuum transport system which will be attached to the gun load-lock system. This procedure will allow for maintaining ultra-high vacuum conditions in the gun and enable replacement of photocathodes in tens of minutes. A load-lock system will also allow for investigation of a broad range of photocathodes in order to obtain materials for optimal performance at CLARA and future FEL facilities.

2014 JINST 9 T05001

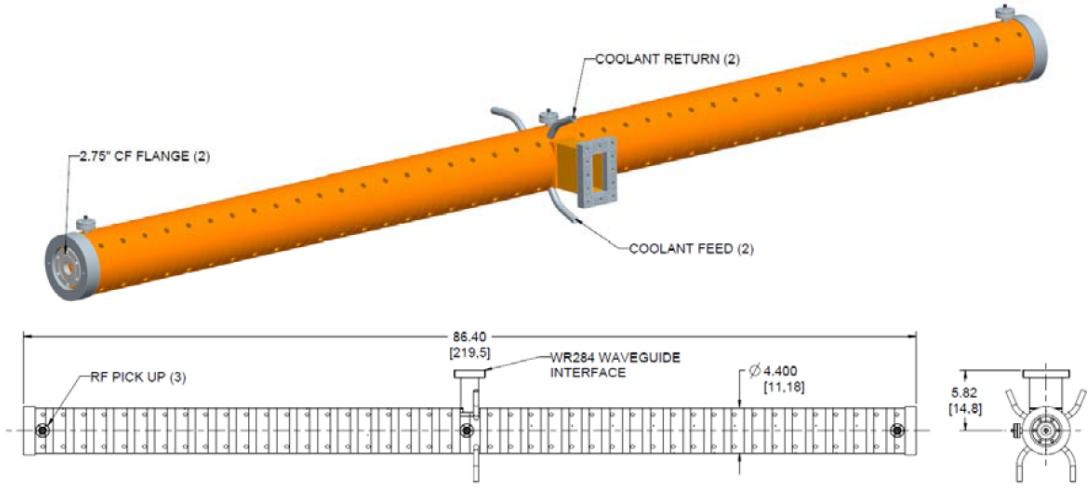

Figure 5.4. Concept design for a 2 m long, 43 cell, high repetition rate linear accelerating structure.

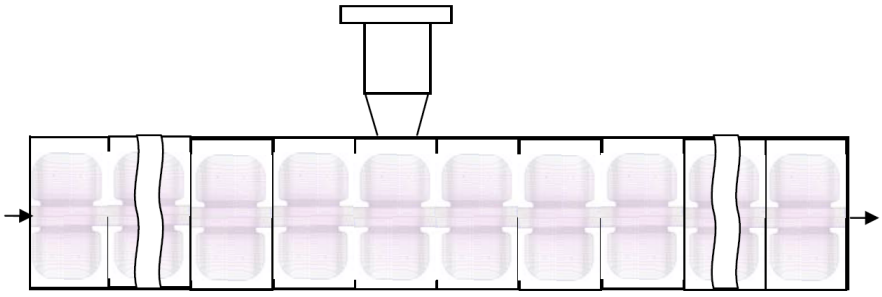

Figure 5.5. Superfish simulation of accelerating cells.

5.2 Radio frequency systems

A review has been performed regarding the frequency options for the CLARA RF system, which assessed the options for S-band, C-band and X-band for both the European and US frequency options. The review assessed the availability of hardware (klystrons and cavity designs) and also considered the various mixes of frequencies. It was concluded that European and US frequencies would not be mixed so as not to cause phase stability issues and limit the buckets that can be filled during operation, and that for hardware availability the most favourable option would be the European S-band and X-band frequencies. Thus the CLARA RF system consists of 4 types of RF cavity structures; an S-band photoinjector gun, 4 S-band linac structures providing acceleration of the electron bunches up to 250 MeV, an X-band cavity for the linearisation of the longitudinal phase space, and 2 S-band TDCs for 6D emittance characterisation of the beam at low and high energy.

The initial photoinjector gun to be installed on CLARA will be the current S-band RF gun installed on VELA, which is the ALPHA-X gun built by Laboratoire de l'Accélérateur Linéaire (LAL) and provided by Strathclyde University.

2014 JINST 9 T05001

Table 5.2. Design specification for Linacs 1–4 and 4th Harmonic Cavity.

	Linac 1	**Linacs 2-4**	**4th Harmonic**
Number of cells	43	122	72
Frequency (MHz)	2998.5	2998.5	11994
Nominal RF voltage (MV/m)	20	20	12
Maximum RF voltage (MV/m)	25	25	16
Nominal RF power (MW)	23	37	6
Max RF power (MW)	32	57	29
Operating Mode	$\pi/2$	$2\pi/3$	$5\pi/6$
Repetition rate (Hz)	100	100	100
Filling time (μs)	$<$1.0	0.995	0.1
Length Flange to Flange (m)	2.15	4.15	0.965
Active Length (m)	2	4.07	0.75
Quality Factor (Q_0)	$\sim$14000	$\sim$15000	
Shunt Impedance (MΩ/m)	82	62	68
Nominal operating temp. ($^\circ$C)	$\sim$25	$\sim$ 35	$\sim$ 35

The photoinjector is a 2.5 cell, 6 MeV gun which operates at repetition rates up to 10 Hz [91, 101]. It is intended that a high repetition rate photoinjector gun is designed and installed to meet the CLARA requirements and is discussed in section 5.1.2.

For each of the individual cavity structures a dedicated high power RF system is to be installed to enable flexibility in providing the required accelerating gradients for the individual CLARA defined requirements as well as the amplitude and phase stability necessary to meet the beam jitter specifications. Additionally, as there is a requirement for a 16 bunch macro-pulse of 2 μs duration a SLED (SLAC Energy Doubler) compression has not been considered as part of the RF design option. The RF layout is shown in figure 5.3.

5.2.1 Linac accelerating structures

Linac section

The initial linac section is to be a 2 m S-band accelerating structure, required to accelerate the electron beam up to 35 MeV, but will be operated in an off-crest mode (up to 30°). A concept design has been produced by Advanced Energy Systems INC (AES) which is a standing wave (SW) structure that operates in the $\pi/2$ mode to provide an accelerating gradient of 25 MV/m with a 3 μs RF pulse at a repetition rate of 400 Hz. Table 5.2 shows the specification for the structure which consists of 43 accelerating cells and 42 on-axis coupling cells, with 3 RF pick-up loops as shown in figure 5.4. Figure 5.5 shows the electrical field modelling work performed on the accelerating cells. To ensure that the filling time is kept to less than 1 μs it will be necessary to have an increased RF power at the beginning of the pulse before reducing to its steady state level. In addition AES have performed a thorough thermal analysis of the structure design to ensure the high average power levels can be dissipated. Further analysis of the requirements is to be performed

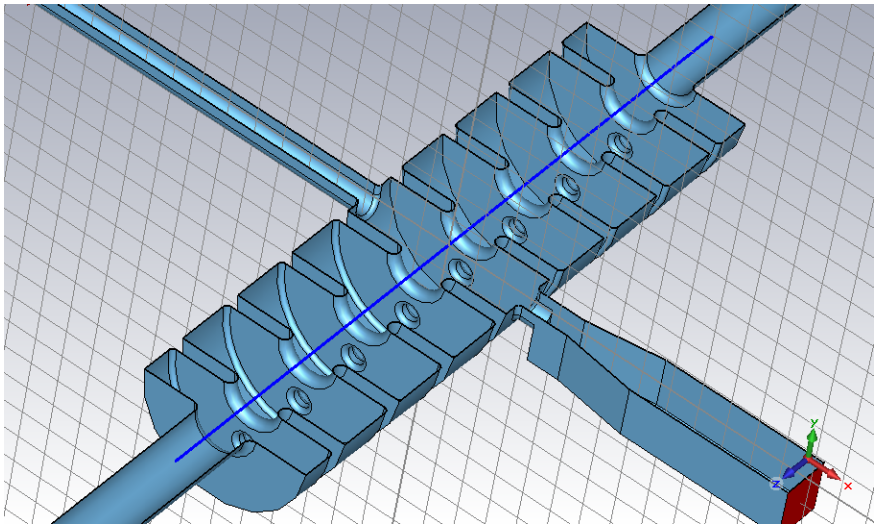

Figure 5.6. 3D model of the transverse deflecting cavity.

Table 5.3. Specification for the transverse deflecting cavity at low energy.

Number of cells	9
Frequency (MHz)	2998.5
Nominal RF voltage (MV)	5
Nominal RF power (MW)	6
Operating Mode	π
Repetition rate (Hz)	10
Nearest mode (MHz)	6.5
Length flange to flange (m)	0.698
Active length (m)	0.5
Quality factor (Q_0)	$\sim$18000
Shunt Impedance deflecting mode R (MΩ)	5.0
Aperture pipe diameter (mm)	35 (Iris 32)
Nominal operating temp. ($^\circ$C)	35
Number of pickups	2 (1 pickup, 1 HOM)

to define whether a SW structure meets the full requirements or whether a travelling wave (TW) would be more suitable, especially with respect to phase stability.

The further 3 linac accelerating sections are to be kindly provided by PSI from the SwissFEL Injector facility. The linac sections are 4.15 m long from flange to flange, and are constant $2\pi/3$ TW structures based on the mechanical design of linac II DESY structures. To meet the SwissFEL requirements the shunt impedance was increased to reduce the peak RF drive power required to provide the accelerating gradient and the RF symmetry is maintained with a split input coupler. However, these structures have been designed for 100 Hz operation, thus for operation at 400 Hz the accelerating gradient will have to be reduced so as not to over dissipate the structures. The parameters for the linac structures are defined in table 5.2 and the designs of these structures are discussed fully in the Swiss FEL Injector Conceptual Design Report [102].

2014 JINST 9 T05001

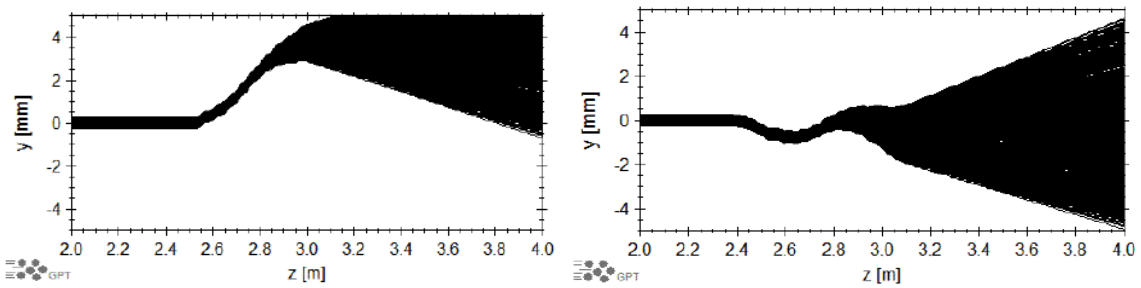

Figure 5.7. Vertical particle trajectories for the TDC (left) without and (right) with beam correction.

Fourth harmonic cavity structure

The X-band, 11,994 MHz, harmonic cavity is required to linearise the longitudinal phase space of the electron beam to correct for the collective instability effects in the successive accelerating stages caused by space charge and wakefields. To meet this requirement a deccelerating gradient of 12 MV/m is needed. There have been a number of X-band structures developed for the European X-band frequency, and a review of these structures has shown that to meet this requirement it will be necessary to use a TW structure compared to a SW structure as these structures are less sensitive to temperature variations. It is proposed to use a modified design for the European X-band frequency based on the SLAC H75 structure, which is a constant gradient, $5\pi/6$ phase advance TW structure comprising of 72 cells [4, 103, 104]. A $5\pi/6$ phase advance TW structure is preferred to a $2\pi/3$ as these structures have proven greater operational reliability. A review of the design will be performed to ensure that the parameters defined in table 5.2 are met. Additionally, an essential part of the design of this structure will be the ability to align the cavity to within 10 μm to ensure accurate beam steering and to enable accurate correction to be applied to the beam.

Transverse deflecting cavities

Two S-band TDCs are required, one at low energy, 70–150 MeV and the second at the full energy of 250 MeV. These will be used to provide longitudinal slice emittance profiling of the electron beam and are required to provide deflecting voltages of 5 MV and 10 MV, respectively.

For VELA a 9-cell TDC has been designed [105] (figure 5.6) which provides a 5 MV transverse kick. Parameters are shown in table 5.3. The cavity has been designed with steering magnets at the entrance and exit and shortened end cells to reduce the effect of the electrical field decay in the beampipes, so as to minimise the effect of the vertical kick on the electron beam trajectory (figure 5.7). A matching short opposite the input coupler has been included to maintain the RF symmetry to minimise the monopole component of the RF fields in the coupling cell.

For the higher energy requirement it will be necessary to investigate whether the cavity is capable of the higher gradient levels or whether it will be necessary to design a higher gradient TW structure.

5.2.2 High power RF systems

For the CLARA design, klystron modulators are being considered in order to provide the pulsed RF power needed to obtain the required accelerating gradients within each of the RF cavity structures.

Figure 5.8. ScandiNova K2 klystron modulator.

A K2 klystron modulator has been supplied by ScandiNova (figure 5.8) and successfully operated on the photoinjector gun cavity on VELA. Additionally a second klystron modulator is being supplied by Diversified Technologies (figure 5.9) for operation on the first linac cavity. Modulator requirements are outlined in table 5.4. Typically the best stability that can be achieved at present is 0.0001 and 0.1° [102] for the amplitude and phase stability respectively, and it will be necessary to compensate for slow fluctuations with a low level RF system. Presently there is ongoing development work being pursued by the modulator manufacturers to achieve greater stability. Progress on this work needs to be reviewed to ensure that this is in line with CLARA requirements. The RF amplitude and phase stability are essentially defined by the stability of the klystron modulator voltage.

5.2.3 Low level RF system

RF reference and timing system

The synchronisation system for CLARA will consist of a very stable, low noise RF reference oscillator system that will be distributed to the acceleration sections (figure 5.10). The RF reference distribution will use a temperature elevated and stabilised environment system running the length of the machine to distribute timing and RF signals. This system will use copper RF cables to provide

2014 JINST 9 T05001

Figure 5.9. Diversified Technologies klystron modulator system.

a baseline system for both RF and timing signals to a level of 50 fs. An automatic phase drift compensation system will be used that should allow stability of less than 10 fs to be achieved [106]. In addition a compensated optical fibre distribution running in parallel with the coax system will offer the ultimate timing performance down to $<$10 fs. This is explained in detail in section 5.5. The decision to use both technologies side by side, although more expensive, should offer the greatest flexibility in initially setting up the machine and achieving the ultimate performance level.

At each acceleration section, low noise local phase locked loops and multiplier/dividers will be used to generate all the required RF frequencies and timing signals locked to the reference system.

Table 5.4. Modulator requirements for photoinjector cavity, Linacs 1–4, 4th harmonic cavity, low energy (LE) TDC and high energy (HE) TDC. Where ranges of values are given these represent the anticipated requirements over a variety of accelerator setups and operating modes.

	Photoinjector	**Linac 1**	**Linacs 2–4**	**4th Harmonic**	**LE TDC**	**HE TDC**
Frequency (GHz)	3	3	3	12	3	3
RF Peak Power (MW)	10	23–32	30–60	6–29	6	21
RF Average Power (kW)	10	21	$<$9	4.5	0.2	0.7
Klystron Voltage Range (kV)	170	280	260–350	331	156	225
Klystron Current Range (A)	125	300	265–415	219	120	215
Flat Top Pulse Length (μs)	3	3	1.5–3	1.5	3	3
Repetition Rate (Hz)	10–400	10–400	10–400	10–100	10	10

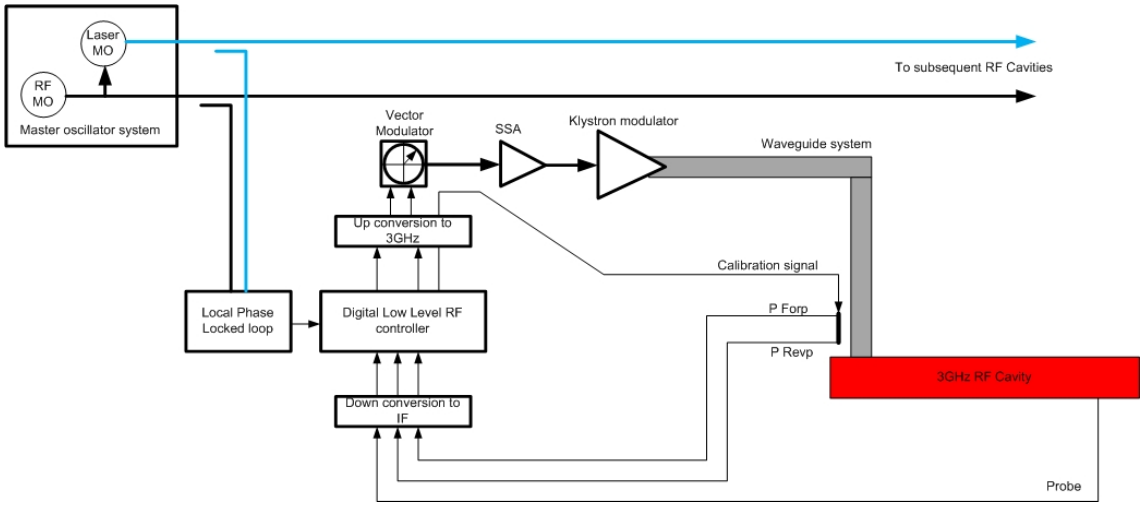

Figure 5.10. Basic RF Control System.

Figure 5.11. An example of a commercial digital LLRF system from Instrumentation Technologies.

Low level RF system

The purpose of the Low Level RF (LLRF) system is to stabilise and regulate the RF fields in the accelerating cavity. Errors in amplitude and phase will cause energy modulation of the beam particularly if the accelerating cavities are running off-crest; this in turn causes timing jitter from pulse to pulse after the bunch compressors. The ability to feed back becomes very difficult, although techniques are now emerging that seek to measure and correct for small errors on a pulse-by-pulse basis [107]. The dominant part of the system that affects the RF fields seen in the cavity is the klystron modulator and drive system. The stability and repeatability of these systems to always produce the same RF field on each pulse is the critical and limiting factor for the short term performance of the machine. The accelerating cavities are equipped with field probes: these can be used to monitor the phase and amplitude inside the structure, providing information on the stability of each cavity over multiple pulses. These signals in conjunction with the forward and reflected power signals will provide the LLRF with information on the state of tune for each cavity and the amount

2014 JINST 9 T05001

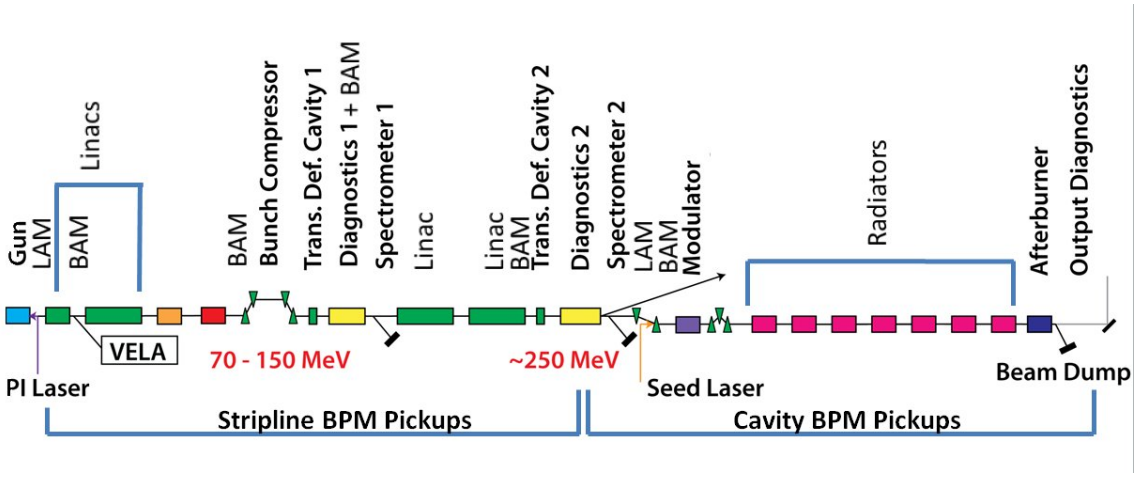

Figure 5.12. Overview of beam diagnostics.

of phase slippage seen by the beam in each accelerating structure. Feed forward calculations can be made and applied to attempt to correct for these issues.

Environmental effects, temperature, humidity and pressure will cause changes to the machine and the RF measurement systems themselves. The accelerator hall, RF modulator areas and all measurement cabling will be held at a precise temperature (to $\pm 0.1^{\circ}$) to combat at least part of these issues, however these environmental changes are slow in nature, and they can be detected in the operation of the machine. To further reduce the effect of these environmental issues, the LLRF system will be equipped with a calibration system [108], this will measure the path length phase and amplitude of the RF drive system on every pulse, monitoring slow changes in the system and applying corrections to the drive set points, this will bring the system long term stability up as high as possible. In addition the use of beam monitoring systems (beam arrival monitors and bunch compression monitors) will provide electron beam measurement and timing stability information that will be used to provide feedback to the RF phase and amplitude at a rate of up to 1/10th of the machine repetition rate [109].

Due to the necessity to interface with calibration systems and electron beam monitoring equipment, digital based systems for RF control will be implemented on CLARA. These systems provide a very flexible and robust solution that can be adapted and upgraded as the machine is operated.

Digital LLRF systems down convert the RF signals from each cavity to an intermediate frequency (IF) of around 50 MHz. The signals are sampled using high speed 14/16 bit Analogue-to-Digital Converters (ADCs) and passed to Field Programmable Gate Array (FPGA) systems for digital processing and adaptive feed forward compensation. The resulting control signals for amplitude and phase are up converted and applied to the klystron modulator for amplification. The hardware for 3 GHz and 12 GHz accelerating cavities will be the same apart from changes to the analog front ends. An example of a commercially available LLRF system is Instrumentation Technologies Libera LLRF system shown in figure 5.11.

It is anticipated that commercially available LLRF hardware will be purchased, that includes highly stable front end systems, low cross talk between RF channels and direct Experimental Physics and Industrial Control System (EPICS) interface. The hardware will allow programming

2014 JINST 9 T05001

and simulation via mathematical program routines (MATLAB etc). By using this commercially designed LLRF hardware we would then be able to focus on the design and implantation of control algorithms in conjunction with the LLRF manufacturer and will be able to update the LLRF hardware and software as the project develops.

It will be possible to use fast analog control loops to monitor and feedback on the klystron modulator [110]. This control loop will be able to reduce modulator noise and remove phase droop during the RF pulse. This control loop requires the use of a high speed phase shifter and locating the electronics very close to the modulator to keep latency times to a minimum.

The performance of the LLRF system in the short term (based on a modulator stability of 4.6×10^{-5} over 1 min) will be 0.035% amplitude stability and 0.05° phase stability.

5.3 Electron beam diagnostics

5.3.1 Bunch charge monitors

Three types of monitors are planned to be used for bunch charge measurement. These will be wall current monitors (WCM) [111], Integrating Current Transformers (ICT) and Faraday Cups (FC) with the FC providing precision and low charge measurements. Four WCMs and ICTs are to be installed after the gun (dark current measurement), after the X-band cavity, and in the low energy and high energy diagnostic sections. The FCs installed at the end of each spectrometer diagnostic section and at the machine end will also serve as full beam dumps.

On the basis of CLARA simulations, shot-to-shot bunch charge stability of better than 1% is required in the high charge operation modes. To provide reliable single bunch charge variation monitoring, monitors of different types will be installed and the most reliable and sensitive monitors will be identified operationally. The ICT is a commercial 'in-flange' device, and the WCM is a FNAL/STFC Daresbury design. The FC and its associated electronics is a further upgrade of an ASTeC design produced for the ALICE (Accelerators and Lasers in Combined Experiments) accelerator. The VELA test facility has enabled full beam testing of FC developments prior to specification for CLARA.

5.3.2 Strip line BPMs

For routine bunch trajectory tracing, twenty five BPMs are spread along the machine (see figure 5.12). The strip line pickups have incorporated survey monuments and can be aligned with respect to the quadrupole magnet axes. The residual zero offset (including BPM electronics zero offset) is expected to be within 0.2 mm. Transverse beam size, varying along the machine, on average is ∼0.2 mm. It is required that the BPMs have a bunch charge range from 250 pC down to several pC. At the lower range of charge, thermal noise will limit strip line BPM accuracy to ∼30 μm, while a resolution of 20 μm is expected for the higher charge modes.

It is intended to use a further development of the in-house designed EPICS based VME BPMs electronics. This system was originally made for single-bunch/turn-by-turn measurements with button pickups on the EMMA (Electron Machine for Many Applications) Accelerator [112, 113]. Advanced testing of the CLARA version of the electronics using strip line pickups will be carried out using VELA. This will provide cross check data with that previously measured from ALICE

Table 5.5. Output spectral ranges and pulse durations that CLARA is expected to deliver in each of the three main types of FEL scheme.

FEL Scheme Type	Output Wavelength range (nm)	Pulse Length Range (fs)
SASE	100–400	20–300
Short Pulse	266–400	2–50
High Temporal Coherence	100–400	30–300

to confirm the achievable BPM resolution. Data Acquisition BPM software already written for EMMA and ALICE will also be used with CLARA.

5.3.3 Cavity BPMs

In the dispersive section of the bunch compressor, and in the inter-undulator/modulator regions, the beam position accuracy and resolution requirements are significantly more challenging than elsewhere in the accelerator. The requirements here are significantly greater than can be provided by a strip line BPM design, and only cavity BPMs can provide the resolution and accuracy required.

A design programme in collaboration with Royal Holloway University London (RHUL) has been instigated to develop a cavity BPM for CLARA, based upon work carried out on a cavity BPM for the International Linear Collider (ILC) final focus model at ATF2 in Japan [114]. Further investigation is still required to confirm that sub-micron resolution with CLARA's low bunch charge is possible. Prototyping and development/testing will be carried out on VELA prior to cavity BPM production.

5.3.4 Screen diagnostic systems

Screen systems employed will incorporate both Cerium doped Yttrium Aluminium Garnet (YAG) and Optical Transition Radiation (OTR) screens as appropriate.

Beam transport systems will be instrumented by a compact standard diagnostic unit based upon designs from FLASH in Germany. These incorporate a number of selectable devices mounted on a linear actuator stage. Each screen 'carriage' that can be inserted orthogonally into the beam holds a 5 μm thick substrate mounted YAG screen or silicon OTR screen.

An additional screen location allows the installation of a calibration graticule screen to provide accurate camera focussing and a dimensioning facility for images. Screens are viewed on a camera system via an offset mirror through a side port in the diagnostic unit. This versatile device is less than 20 cm in length and can also incorporate a wire scanner and button type BPM if required, for example to overcome coherent OTR image distortion [115]. Screen system diagnostics in the intra-undulator sections will be required to image not only the electron beam, but also the photon beam as well. The co-existence of the electron and photon FEL beams requires an advanced multi-beam screen system designed for transverse size and profile measurement on both the electron beam and the FEL radiation. Challenging design constraints at these locations include the requirement to suppress any present coherent OTR, seed laser and minimise any ionizing radiation delivered to the undulators during beam imaging. A novel design for the FERMI@Elettra FEL has been reported, with an optical design resolution of 12 μm [116]. To provide this functionality a similar screen system will be employed on CLARA.

For precise emittance measurement, the electron beam size has to be measured with an error better than 10% of the rms beam size. The standard camera system used by FLASH uses a simple 1:1 lens system and can provide a theoretical resolution of 10 μm/pixel for a beam size $\sim$100 μm. Improved cameras for specific locations such as those in the intra undulator sections where the photon beam is to be imaged on the YAG screens will be required. In conjunction with a distortion minimising lens system, the improvement in signal to noise of the system is such that a theoretical resolution of 8 μm/pixel. In operation this should provide resolutions better than 20 μm, which should be sufficient for precise beam emittance and photon beam measurements.

5.3.5 Beam arrival monitors

Beam Arrival Monitors (BAMs) will be implemented to improve understanding of the beam dynamics and monitor synchronisation points such as the FEL entrance. The BAMs measure the relative delay between the electron bunch centroid and the laser master oscillator. The electron bunch timing is detected with electrodes in the beampipe which pick up the Coulomb field of the passing electron bunch. The output from the electrodes is then sampled by optical clock pulses (see section 5.5) by gating their amplitude in an electro-optic crystal. Measurement of the sampled pulse amplitude then gives a measure of the electron time delay with respect to the master oscillator. Such BAMs have been implemented at DESY and FERMI@Elettra with demonstrated resolutions of better than 10 fs [117].

5.3.6 Bunch compression and temporal profile monitors

The compression of the bunch will be monitored through a pyroelectric detector measuring the CSR power emitted in the final dipole of the compressor. This monitor is not envisaged as providing a quantitative measure of the bunch length, but rather as a means for stabilising the compression at an operationally determined set-point, For quantitative measurement of the temporal profile, a spectral upconversion [118] diagnostic will be used to measure the spectrum of the CSR at the compressor. A second in-beamline spectral upconversion monitor will be located before the FEL modulators. The spectral upconversion systems will be used for non-invasive monitoring and stabilisation of the accelerator and beam transport.

A TDC system is also present in the high energy diagnostic section, and will be used for slice emittance and sliced energy characterisation of the bunch. The spectral upconversion diagnostics will be calibrated against the TDC.

5.3.7 Laser Arrival Monitors

All-optical Laser Arrival Monitors (LAMs) will be used for monitoring the photoinjector laser arrival at the virtual cathode, and the FEL seed lasers at a point close to the injection of the near-IR or mid-IR seed into the electron beamline. The LAMs will be based on optical cross-correlation with the optically distributed RF timing signals (section 5.5).

2014 JINST 9 T05001

Table 5.6. Source parameters derived from a second moment analysis of the simulated output of the CLARA FEL.

Wavelength (nm)		**100**	**266**	**400**
Horizontal	RMS size (μm)	131	243	223
	Position (m)	15.3	11.1	10.9
	M^2	1.25	1.73	1.69
Vertical	RMS size (μm)	112	257	241
	Position (m)	14.9	11.5	11.0
	M^2	1.15	1.62	1.66

5.4 FEL output diagnostics

5.4.1 Introduction

The main aims of the CLARA FEL output diagnostic systems will be to measure the temporal and spectral properties of a single light pulse. The pulse length and spectrum of CLARA FEL output will span a wide range of values depending on the FEL scheme employed (see chapter 3). Table 5.5 summarises the different FEL schemes and the anticipated spectral and temporal ranges of the output.

SASE operation will be the baseline against which the schemes to improve temporal coherence and deliver shorter pulses will be measured. SASE delivers relatively long pulses with complex temporal and spectral profiles. The product of pulse duration and bandwidth will be considerably larger than the transform limit. The diagnostics will give a detailed picture of both the temporal and spectral structure.

Improvements on basic SASE are the core purpose of CLARA. In schemes aimed specifically at delivering shorter pulses (such as Single-Spike SASE and Mode-Locking), the diagnostics will ultimately have to measure pulse durations down to the femtosecond level. Such schemes will also deliver significantly enhanced temporal coherence and spectral and temporal measurement will show how far the pulses deviate from the transform limit. The schemes aimed specifically at delivering the highest temporal coherence (seeding, EEHG etc) will not deliver such short pulses but accurate temporal and spectral measurement will be essential to quantifying how successful the schemes are.

Developing the techniques for achieving a high consistency in FEL output from shot to shot is also a goal of CLARA as this is of critical importance for scientific exploitation of FEL sources. This requires all the output diagnostics to be capable of working on a 'single-shot' basis, ideally at the full repetition rate of the FEL.

The nature of the FEL source needs to be considered when designing the diagnostics. Some sort of focusing of the source will be required and the size and position of the source therefore needs to be known. Source size, position and M^2 factor can be deduced from FEL simulations using a second-moment analysis of the output field files propagated to different distances. Table 5.6 shows the results from simulations of the FEL output in SASE mode with 2.5 m long radiator modules. The position is given relative to the start of the first radiator module. It is expected that these will still be realistic values for operating modes in which the temporal properties are modified as the

spatial properties are not expected to change. The simulations show that the source and position are different in the horizontal and vertical directions and vary with wavelength. It is likely that an adaptive optical scheme will be required to give the correct focusing for the diagnostics.

5.4.2 Spectral diagnostics

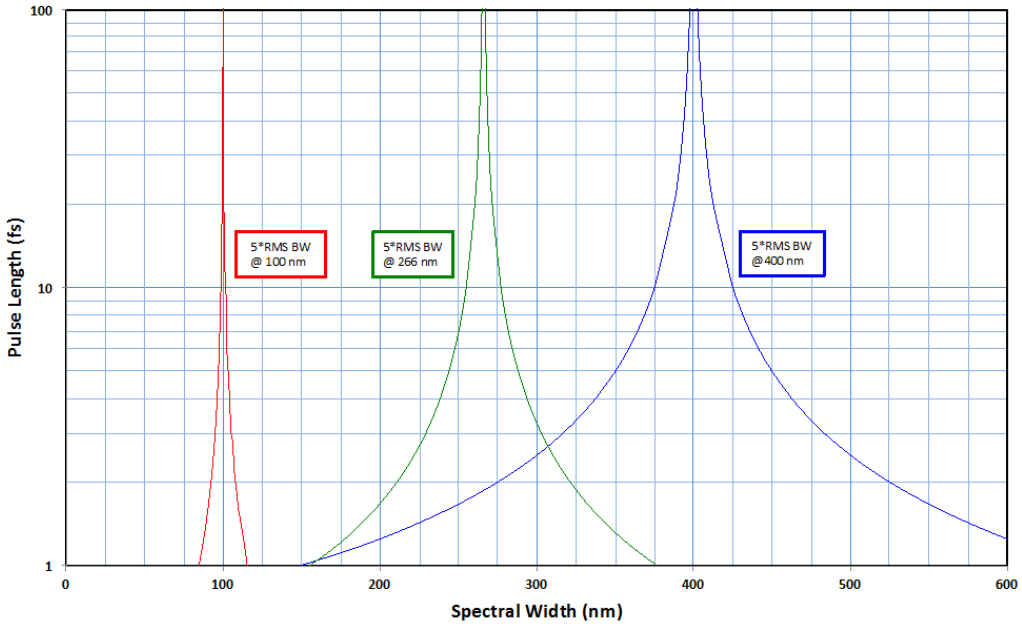

Figure 5.13. Required spectral measurement width for pulses at 100, 266 and 400 nm wavelength.

The aim will be to record the complete spectrum of a single photon pulse from the FEL. This will be accomplished with a flat-field spectrograph and a multi-channel array detector. The spectrograph will be either a commercial instrument or an in-house design using a concave grating with varied-line-spacing to achieve a suitable flat-field. The detector will be a commercial instrument.

The basic requirement for the spectrograph is for the spectral width of the flat-field to be large enough to capture the spectrum of the shortest pulses and the spectral resolving power to be high enough to resolve the longest pulses or spectral structure within SASE pulses. These two requirements are not completely compatible, and some compromise will be necessary if only a single instrument is employed. The priority will be in capturing the full spectrum of ultra-short pulses.

For a temporally coherent pulse, the spectrum and pulse length are linked through the transform limit. For a pulse with a Gaussian temporal profile, the spectrum has a Gaussian profile and the FWHM of the spectral and temporal profiles in nm and fs are related by

$$\Delta\lambda_{\mathbf{FWHM}}\Delta t_{\mathbf{FWHM}} = 1.472 \times 10^{-3}\lambda^2$$

To accurately measure the pulse spectrum, the flat-field of the spectrograph will have to span substantially more than the FWHM of the spectrum. A flat-field width of 5 times the rms width of the spectrum has been chosen as being a sensible design target. Figure 5.13 shows the relation between

pulse length and this target spectral width for wavelengths of 100, 266 and 400 nm. The calculation is for pulse lengths down to 1 fs, but such short pulses will only be feasible for the shortest wavelengths and will not be delivered in the first phase of CLARA operation. Nevertheless, the figure demonstrates the enormous variation in the spectral width of the CLARA output over the possible range of output wavelengths and pulse lengths.

The suitability of various commercial spectrographs has been examined in an internal report [119]. This report also looks at the effect of the spectrograph resolving power and detector array size on the measurability of the longest pulses (i.e. those with smallest bandwidth). The most suitable instrument considered is the Jobin Yvon VTM300 vacuum spectrograph [120], which operates over the wavelength range 60 to 300 nm with a flat-field width of approximately 60 nm. It will be able to record the 5σ width of a 1 fs FWHM pulse at 70 nm, a 1.4 fs pulse at 170 nm and a 3.6 fs pulse at 270 nm. Suitable CCD array detectors can be bought commercially, for example the Greateyes GE 1024 256 BI UV1 or UV3 1024 by 256 pixel cameras [121].

5.4.3 Temporal diagnostics

The ultimate aim will be to develop and implement single-shot diagnostics with the capability of extracting the full spectral phase information of a photon pulse with duration as short as 1 fs FWHM at a wavelength near 266 nm. Measuring (and generating!) such short pulses will be very challenging so the first target will be to reliably measure pulses with durations down to $\sim$10 fs and then to improve the technique to measure shorter pulses. Single-shot measurements of pulses of this duration at shorter wavelengths will not be in the baseline specification unless such an extension proves to be trivial.

The diagnostic approach will be derived from the established Frequency Resolved Optical Gating (FROG) technique, which allows the complete spectral phase information of the pulse to be recovered. However, even without the full analysis, the technique is a powerful window on the correlation of spectral and temporal information in the FEL pulse because the FROG measurement gives an immediate picture of how the spectrum in the pulse changes along the pulse length. For example, it will be possible to see the spectrum of each spike in a SASE pulse.

FROG has already been used to measure pulses of 8 fs duration at 270 nm [122]. However, for CLARA with pulses potentially as short as 1 fs, some modifications and developments to the technique are required. The very large relative bandwidth contained in sub-10 fs UV pulses means that propagation through even short air paths will stretch the pulse through dispersion. For example, even a ‘long’ pulse of 10 fs FWHM duration at 266 nm would be stretched to about 30 fs after passing through 1 m of air. Because the light is generated in an accelerator, the beam path on CLARA will be several meters in length, and so the entire beam path will have to be in vacuum.

Dispersion will also stretch the pulses if transmissive optics (windows, lenses, polarisers, beam splitters etc) are inserted in the beam path. For example, transmission through 1 mm of fused silica will stretch a 10 fs pulse at 266 nm to $\sim$55 fs. Therefore beam focusing will have to be done with mirrors and regions of ultra-high and medium vacuum will have to be separated by differential pumping rather than with windows. The latter point is easily satisfied as the lattice of narrow-gap undulator vessels is expected to provide an adequate buffer to the parts of the machine requiring the highest vacuum. More significantly however, the non-linear beam mixing that is at the heart of the FROG technique (or any optical auto- and cross-correlation technique) cannot be done within any

2014 JINST 9 T05001

practical transmissive medium without changing the pulse as it is being measured. It is therefore proposed to exploit non-linear interactions at surfaces.

A key challenge for the diagnostic on CLARA is that the initial operation in the mode-locked scheme will produce a pulse train of ultra-short pulses with spacing of just 167 fs. Unless the detector is gated at an impossibly high rate of 6 THz, even a 'single-shot' autocorrelation technique will give an average result over all pulses in the train because both the probe and measured beams have an identical pulse structure [123]. To measure either one pulse or a short sequence of pulses in the train without this averaging requires the probe beam to have a single pulse per macro pulse of the FEL so that the probe acts as the detector gate.

It is conceptually feasible to take the part of the FEL beam to be used as the probe and condition it to a single pulse by gating with fast switching mirrors, accomplished by exploiting transient reflectivity triggered by another laser. This approach will be technically very challenging and probably quite 'lossy', and thus may leave insufficient probe beam intensity. So it is therefore proposed to use cross-correlation with the probe beam derived from the Ti:sapphire laser used to generate seed pulses for the FEL, which will be naturally synchronised and have one pulse per FEL macropulse.

The disadvantages of the cross-correlation approach are that the probe pulse will be longer than the measured pulse and that the temporal phase of the probe must be accurately known before the cross-correlation signal can be unravelled to extract the temporal phase of the FEL pulses. However, by using the probe at the native 800 nm or frequency doubled to 400 nm we can use conventional FROG to characterise the beam.

There will need to be some experimental work undertaken to develop the cross-correlation technique for these very demanding measurements. The most important aspect is to decide the nature of the non-linear interaction that will be exploited and to find a suitable surface. We are currently conducting experiments using the VELA photoinjector laser to see if we can exploit difference frequency generation (DFG) between 800 nm and 266 nm light. The advantage of DFG over sum frequency generation (SFG) is that the correlation signal will be in the visible and therefore the detection will be more straightforward and cheaper.

5.4.4 Photon flux and pulse energy monitoring

Detectors are required to measure the photon output flux. High sensitivity detectors will be needed to monitor the spontaneous flux from the undulator prior to lasing. An absolute measurement is not required since the aim is to detect an increase in signal indicative of the start of lasing as machine parameters are adjusted. Once lasing is established, the absolute energy of the FEL pulse is of more interest than the average flux and so detectors that are able to respond to a single photon pulse are required. This will be straightforward in FEL modes that emit a single pulse per electron bunch (e.g. SASE or single-spike SASE) but more challenging in the schemes that generate trains of pulses (e.g. the mode-locked schemes). In the latter case, absolute detectors are likely to be limited to measuring the integrated energy in the pulse train. However, comparison with the diagnostics that can resolve the individual spikes (either temporally or spectrally) should enable some information on the energy in each pulse in the train to be deduced.

The type of detector used will depend also on the spectral range of the output. A significant part of the FEL operating range is at optical wavelengths and so conventional laser pulse energy

2014 JINST 9 T05001

detectors can be used. These tend to be thermal in operating principal and so quite slow responding, but this will be acceptable for CLARA repetition rates. The FEL output can be extracted from the vacuum via a suitable window for which transmission and reflection losses have been measured. The only caveat is that the shortest pulses have a very large bandwidth and so accurate compensation for window losses may be difficult. Dispersive changes to the pulse profile will not impact on the pulse energy. Non-linear interactions in the windows will need to be considered as well, but as the FEL pulse energies are in the μJ range are unlikely to be an issue. Similarly, the spontaneous output can be monitored in air using conventional detectors such as APDs. These should have sufficient sensitivity to detect the weak spontaneous output.

At the shortest wavelengths that CLARA can reach, the measurements will have to be performed *in vacuo*. The vacuum requirements of CLARA are not stringent, but nonetheless, most conventional airside detectors will be unsuitable. Spontaneous output can still be monitored with APDs (which are easily adaptable to vacuum use) or with electron multipliers (CEMs or MCPs) which can be purchased with coatings to enhance their photon responsivity. The measurement of the absolute pulse energy *in vacuo* is more challenging. Essentially, the same detectors will be used as for measuring the spontaneous output. Absolute pulse energy will be deduced by prior calibration of the detectors response. The main challenge will be correctly accounting for any spectral dependency of the response over the large bandwidth of the shortest pulses.

5.5 Optical timing and synchronisation

The timing and synchronisation system for CLARA will fulfil two main functions. The first is to generate and deliver a stable clock signal to all the accelerator subsystems that require synchronisation, and the second is to use that reference to monitor and or improve the accelerator timing stability at the subsystem. A combination of RF and optical timing techniques will be adopted to achieve the required timing and control tolerances.

5.5.1 Synchronisation targets

To meet CLARA's aims in beam and photon output stability the synchronisation of various subsystems is critical. In particular, synchronisation at the following locations will have the most stringent timing targets.

- RF cavities to electron beam: 0.02°.
- Seed laser pulse to electron beam: 200 fs rms
- FEL output to user experiments when in seeding mode: 10 fs rms

Certain diagnostics also have tight timing tolerances such as electron beam arrival monitors and laser arrival monitors. These diagnostics will primarily aid in the understanding of CLARA's performance, but could also potentially be used as feedback signals to advance stability.

5.5.2 Timing system architecture

The baseline timing system architecture is shown in figure 5.14. The system will operate from a Laser Master Oscillator (LMO) which will be phase locked to a RF Master Oscillator (RFMO)

2014 JINST 9 T05001

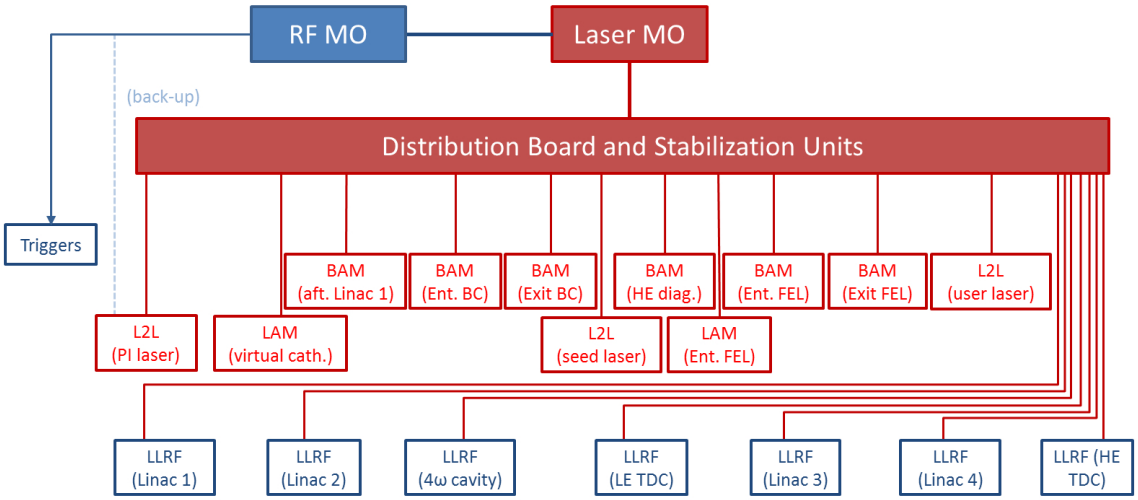

Figure 5.14. Architecture of the timing and synchronisation system.

to reduce drift. Timing jitter between the LMO and the RFMO is expected to be <35fs [124]. Both the RFMO and the LMO, along with the optical distribution and stabilization boards, will be situated in a common temperature stabilised ($\pm 0.1^{\circ}$C) EMC shielded synchronisation room. The optical distribution cables running the length of the accelerator will also use a temperature elevated and stabilised environment system. Distribution lines from the LMO will supply five types of end stations:

1. Laser-to-laser locking (L2L)
2. BAM
3. LAM
4. LLRF cavity controls
5. Triggered systems

In all except the triggered systems, which has the most relaxed timing tolerances, monitoring and feedback techniques will be used to maintain synchronisation of the relevant subsystem with the delivered clock and hence with the oscillators and other subsystems.

The system will use the LMO as the common reference for the LLRF stations, the L2L of the laser systems and time critical diagnostics such as the LAMs and BAMs. Each of these will receive its reference through parallel optical fibre links split from an optical distribution board near the LMO. This prevents the accumulation of jitter in the links and will be actively stabilized against timing delays that can arise from thermal drifts and vibrations along its distribution. BAMs and LAMs will be supplied with synchronised and stabilized links that are length adjusted to match the nominal propagation time of photons and electron beams along CLARA. This will reduce the effect of any phase instabilities in the LMO by correlating all measurements for a single bunch to the same source pulse. Thus all the BAMs will be able to be considered as time-of-flight monitors with

respect to the first LAM. Signals for the triggered systems will be distributed through conventional copper cables.

Similar optical timing systems with demonstrated femtosecond level performance have largely followed two types of schemes. Pulsed schemes which stabilise the group delay of the distribution link such as that at DESY [125], and continuous wave (CW) schemes which stabilise phase delay such as that at LBNL [126]. While both have their merits, CLARA will adopt a pulsed scheme because it delivers short optical pulses which enable direct implementation of established arrival time monitoring techniques with high fidelity. It is noted that some facilities such as FERMI@Elettra and SwissFEL have adopted a hybrid scheme using a lower cost CW distribution for the higher tolerance RF stations. However, due to the smaller size of CLARA with only 7 LLRF stations, the reduced cost of supplying these with a CW distribution is considered to be outweighed by the need to develop and implement a second stabilised distribution scheme.

5.5.3 RF Master Oscillator

The RFMO for CLARA will consist of a 10 MHz source with a Global Positioning System (GPS) reference that will provide a stability of $< 2 \times 10^{-12}$ (100 seconds Allen variance) and a yearly stability of $< 5 \times 10^{-10}$. This RF source will be used with a phase locked oscillator and multipliers to produce a frequency for locking to the LMO.

5.5.4 Laser Master Oscillator

The LMO will be a passively mode-locked fibre ring laser with a pulse repetition rate at a subharmonic of the cavity RF frequency. These lasers are obtainable commercially and provide excellent jitter performance at high frequencies (>10 kHz). However at low frequencies (<10 kHz), the LMO is prone to drifts in cavity length and will need to be phase locked to the RFMO to reduce drifts in the LMO repetition rate.

5.5.5 Optical clock distribution

The optical reference clock will be distributed across CLARA through single mode fibre. The propagation time through the fibre, which is vulnerable to temperature and humidity fluctuations and vibrations, will be stabilized by reflecting a portion back from the end of the distribution link and comparing its return time with reference pulses maintained in the synchronisation room. The comparison is achieved with a balanced optical cross-correlator (BOXC) which uses a periodically-polled $KTiOPO_4$ crystal (PPKTP) to generate a second harmonic signal from the overlap between the reference and the return pulses, thus measuring their relative timing [127]. The BOXC signal will be used to feedback on delay controls in each of the links compensating for any delay changes.

The fibre and propagation lengths joining the stabilized clock signal to the required end station will necessarily be outside the stabilisation loop. These lengths will be kept to a minimum and housed in temperature controlled casing.

5.5.6 Laser-to-laser synchronisation

Laser-to-laser locking will be the most important of the synchronisation end stations. It will ensure that the photoinjector laser, which instigates electron bunch timing, is synchronised to the rest of

2014 JINST 9 T05001

the accelerator as a whole. L2L locking will also be implemented for the FEL seed laser and the external laser to enable synchronisation of the FEL photon output when operating in the seeded mode. The output of the slave laser will be referenced to the delivered optical clock pulses with a two-colour BOXC, which uses sum frequency generation between the laser and the clock pulses in a similar configuration to the link stabilisation [128]. The error signal from the BOXC will be used in a feedback loop to adjust the slave laser cavity and lock its timing with respect to the LMO.

5.5.7 Beam Arrival Monitors

BAMs will be implemented to improve understanding of the beam dynamics and monitor synchronisation points such as the FEL entrance. The BAM locations are shown in figure 5.12. Further details on BAM operation are described in section 5.3.

5.5.8 Laser Arrival Monitors

Arrival monitors will be implemented just before the gun and at the laser seed entry point. The purpose of the first arrival monitor will be to assess the laser jitter level of the source as well as provide a 'zero' time reference for all BAMs downstream. The seed LAM will be used in conjunction with a BAM preceding the FEL to enable and monitor synchronisation of the bunch seeding. Nonlinear materials will be implemented in a cross-correlator arrangement to detect relative delay between the delivered optical clock and the signal to be monitored.

5.5.9 Referencing of LLRF

The LLRF systems will stabilise and regulate the RF fields in the accelerating cavities to reduce amplitude and phase errors. Such errors in the cavity fields would cause an energy modulation on the electron beam which would convert to timing errors after the bunch compressor. The RF fields will be measured through probes in the accelerating cavities and stabilised in amplitude through the local LLRF feedback system. The LLRF will also stabilise the measured phase by referencing it to the transmitted clock through a phase locked loop. Details of the LLRF system are given in section 5.2.3.

The pulsed optical links will need to convert the delivered optical pulses into an RF signal onto which the LLRF systems can be phase locked. The laser to RF clock conversion will be done through a low noise photodiode and filtered at 3 GHz for the LLRF stations. The optical to RF conversion process is expected to introduce very little jitter in itself, although some may be introduced through amplification of the required harmonic. The optical links supplying the LLRF stations will have higher tolerances than the timing diagnostics stations. As such, it may be considered sufficient for these pulsed links to be stabilised through a more cost-effective RF harmonic comparison scheme [129].

5.6 Lasers

5.6.1 Seed lasers for FEL modulation

Several operating modes call for seed laser pulses with mid-IR to far-IR wavelengths. It is proposed to generate these from a combination of optical rectification of a Ti:sapphire system, and difference

frequency mixing of intermediary wavelength laser pulses generated in Ti:sapphire driven Optical Parametric Amplifiers (OPA). Separate experiments require an 800 nm wavelength ultra-short pulse for the seed, which will be provided from the same Ti:sapphire system used for the long wavelength generation.

The FEL Mode-Locking scheme specifies a seed wavelength between 50-30 μm, as well as potential experiments at a longer wavelength of 120 μm. EEHG experiments are targeted at a seed wavelength of 800 nm.

Generation of 120 μm wavelength seed

For modulation at a wavelength of 120 μm, corresponding to a frequency of 2.5 THz, pulses energies of 10 μJ or greater are specified (see chapter 3). Demonstrations of μJ level THz generation based on optical rectification have been reported, although the focus has generally been on obtaining the highest electric field strengths in quasi-single-cycle pulses. In contrast, the requirement of the CLARA seed is for quasi-monochromatic pulses at approximately 2.5 THz, with the number of cycles in the pulse matching or exceeding the number of undulator periods.

Efficient THz generation by optical rectification in $LiNbO_3$ is achievable with 800 nm Ti:sapphire tilted pulse front pumping. Pulse energies of 10 μJ were obtained when pumping with 20 mJ of 800 nm pulses [130], although the central frequency of 0.5 THz ($\lambda = 300\,\mu$m) is considerably lower than required for the CLARA seed.

Even higher pulse energies have been demonstrated, with 50 μJ reported by Stepanov et al. [131], and 125 μJ achieved by Fulop et al. [132]. Despite these demonstrations of high power being at the relatively low frequency of approximately 0.5 THz, tunability through the pulse front tilt offers some potential for 2.5 THz $LiNbO_3$ sources with only moderately reduced efficiency [133]. High pulse energy THz pulses with bandwidth extending out to 3 THz have been produced by optical rectification in ZnTe, for example 1.5 μJ THz pulse energy for an excitation with 48 mJ pump energy has been reported [134].

While the above systems have the advantage of being able to be directly pumped by Ti:sapphire pulses at 800 nm, the limitations on bandwidth ($LiNbO_3$) or efficiency (ZnTe) place these as secondary solutions that would require further development before being considered base-line sources.

An alternative approach is the use of the organic crystals DAST [135] or OH1 [136], together with an OPA for conversion of the Ti:sapphire to more optimum wavelength of 1.5 μm. Hauri et al. [135] report THz pulse energies of 20 μJ for approximately 1 mJ pump energy at a wavelength of 1.5 μm. The spectrum of the THz pulses extends over 0.5–5.0 THz, with a peak at approximately 2.1 THz. Whilst this demonstration was targeted at short single-cycle THz pulses with high field strengths, the demonstrated efficiency (>2% efficiency in energy conversion) and large spectral bandwidth highlight its potential for quasi-monochromatic cycle generation in the target region of 2.5 THz.

The baseline 2.5 THz (50 μm) seed system will involve THz generation in DAST, pumped by 1.5 μm wavelength pulses. The 1.5 μm laser will itself be generated by an OPA pumped by a Ti:sapphire that can deliver up to 20 mJ at the 400 Hz repetition rate of CLARA. To provide the THz central frequency and bandwidth tunability, a chirped pulse beating (CPB) arrangement will be used. In the CPB, the broad bandwidth 1.5 μm pulse is linearly chirped to approximately 2 ps, split into two pulses which are then recombined with a fixed time delay [137, 138]. The time delay

2014 JINST 9 T05001

between the two pulses provides a constant frequency shift between them, which is converted into the central THz frequency when driving the optical rectification process. The bandwidth of the THz pulse can also be tuned by the choice of chirped pulse duration.

Generation of 50 μm–30 μm wavelength seed

The seed-modulated Mode-Locked FEL experiments described in section 3 are based on a seed wavelength of 50 μm, 10 μJ and approximately 3 cycles, or 500 fs, in duration. It is also possible that with further investigation these experiments may be carried out at shorter wavelengths, down to approximately 30 μm.

While an approach similar to that described for optical rectification will be used for the seed generation, changes are required as the non-linear material phase-matching differs significantly at these wavelengths. Phonon resonances, generally in the region of 6-10 THz, give rise to both THz absorption, and a THz refractive index varying rapidly with THz frequency. The transverse-optical resonance in ZnTe lies at 5.3 THz, and rules out the use of this material for generation of the 6 THz seed. A potential 6 THz source proposed by Stepanov et al. [139] involves optical rectification of 800 nm pulses in a multilayer DAST/SiO_2 structure. While the 800 nm and THz pulses are not phase matched in DAST, the alternating layers of SiO_2 allow the different wavelengths to re-phase in a non-active medium, before re-entering the subsequent DAST layer for further coherent, in-phase, generation of THz. An efficiency approaching 1 % has been calculated. While this approach appears promising, further investigations and experimental validation is required to confirm the capability. Broadband THz generation (0.1-10 THz) and high pulse energy THz generation (45 μJ at $\sim$2.5 THz) have recently been separately demonstrated [140] and a development programme is currently underway to optimise excitation conditions to obtain comparable pulse energies (10 μJ) at the frequency target of 6 THz.

For higher frequencies (shorter wavelengths) the generated radiation lies above the phonon resonances, avoiding problems of THz absorption, and opening further opportunities for difference frequency mixing. Extremely high electric field strengths exceeding 100 MV/cm, over a tunable range of 10–72 THz (λ=30–4μm) have been demonstrated by difference frequency mixing in GaSe [141]. In this demonstration, difference frequency generation between two distinct wavelengths of ultra-fast lasers, the first at 1100 nm, the second tunable from 1100-1500 nm. Pulse energies of 1.7 μJ at 30 THz ($\lambda = 10\,\mu$m) have been reported for relatively modest 0.3 mJ pulse energy in each of the OPA output lasers pulses.

800 nm seed

For the FEL experiments involving sub-50 fs seed pulses, the Ti:sapphire output at a wavelength of 800 nm will be used. The pulse energy requirement will be significantly below that needed for the far-IR conversion schemes.

Seed transport

Under the FEL schemes to be tested with CLARA, it is foreseen to only require a single wavelength to be provided at a given time. The seed transport will be a single vacuum transport line, where if needbe the optics will be interchangeable between near-IR (800 nm) and its harmonics, and for the

2014 JINST 9 T05001

transport of the long wavelength sources. To allow for in-situ electro-optic characterisation of the far-IR THz seed, facility will be made for the simultaneous transport of the μJ level 800 nm pulses.

5.6.2 Photoinjector laser system

The photoinjector laser system for CLARA will be the existing Ti:sapphire system used for VELA, with modifications and enhancements as required to satisfy CLARA operating modes. The existing system, supplied by Coherent Inc, delivers 11 mJ pulse energy at a wavelength of $\lambda = 800$ nm, at a repetition rate up to 400 Hz. High conversion efficiency to the $\lambda = 266$ nm third harmonic is achieved by using short 45 fs FWHM pulses in the conversion stage, with UV pulse energy up to 2 mJ possible. The UV pulses have a broad bandwidth exceeding 1.5 nm, and a pulse duration of approximately 180 fs FWHM.

The VELA system does not include temporal pulse shaping. To provide this capability for CLARA, a UV fourier-plane-filtering system similar in concept to that developed by FERMI@Elettra is planned.

To prevent degradation of the transverse beam quality through non-linear effects, as much of the $\simeq$14 m long transport path as possible is in vacuum, with final entry into the accelerator beam transport through a differential pumping section rather than through a window. The laser transport includes relay imaging with reflective optics.

Burst mode for RAFEL

The RAFEL mode of CLARA requires a train of $\sim$20 bunches, of up to 25 pC per bunch, with the spacing of approximately 120 ns set by the cavity round trip time. The total bunch charge required is within that deliverable with the Ti:sapphire and a copper cathode. One option for delivering this multi-bunch structure is using an arrangement of beam splitters and optical delays lines. Maintaining a stable optical pulse train with a sequence of optical delay lines of (round trip) length 35 m will have significant engineering challenges. Controlling the transverse diffraction of the beams will require an imaging system within the delay lines. Whether achieving the required stability and intra-pulse variation is feasible in practise requires further investigation.

If the delay line approach proves not to be feasible, the alternative would be to provide a different laser system that operates in the required 8.5 MHz burst mode. Laser systems have been demonstrated that provide confidence that such an option is technically feasible. On the ALICE energy recovery linac, a Nd:YVO_4 system operates at 81.25 MHz, and is able to provide pulse trains of length from single pulse, up to 100 μs, and with repetition rate selectable from 81.25 MHz to 1.2 MHz (in discrete steps of $81.25/n$, $n = 1 \ldots 64$). The FLASH and XFEL photoinjector systems at DESY demonstrate the production of higher pulse energy trains at a repetition rate of 1 MHz. High pulse energies and ps pulse durations, in trains with approx 6 MHz repetition rate, are also being developed for laser wire applications. The choice of approach for a burst mode laser system will be tightly coupled to the choice of photocathode material, and cannot be made at the current time.

5.6.3 Lasers for FEL photon diagnostics

The temporal characterisation of the FEL UV output will be via difference frequency cross-correlation with ultra-fast Ti:sapphire pulses. Initially the laser pulses at a wavelength of 800 nm or

Table 5.7. Specifications for the modulator and radiator undulators.

	Modulator	**Radiator**
Type	Planar	Planar, Vertical Linear Polarisation
Number of Modules	1	7
Module Length (m)	∼1.0	1.5
Period (mm)	∼200	27
Number of Periods	4	53
Minimum Gap (mm)	20	6
Minimum Wavelength (nm)	800	100
Maximum Wavelength (nm)	120000	400
Maximum K	∼25	3.3

its harmonics will be split from the Ti:sapphire system that generates the FEL seed radiation, with pulse energies of less than 1 mJ expected to be required.

5.6.4 Laser synchronisation

The photoinjector and seed laser system will be locked to the accelerator RF thorough the optical timing distribution system. The timing of the 1.5 μm wavelength optical pulses that are distributing the RF clock, and the pulse train of the 75-100 MHz oscillators of Ti:sapphire systems will be locked with a balance optical cross-correlator, and a feedback loop acting on the Ti:sapphire oscillator cavity length.

The selection of individual pulses from the RF-locked oscillator train for amplification requires only ns stable triggering. However, additional ps level drifts and timing noise can be introduced from the laser amplifiers and the laser transport. LAMs, based on optical cross-correlation between the amplified pulses and the optical timing distribution, will be located near the gun and the seed injection point. The LAMs will be used to correct drifts in the timing of the amplified laser pulses.

5.7 Undulators

As explained in chapter 3 there are three distinct undulator systems planned for CLARA; the modulator, the radiators, and the afterburner. Our studies so far have focussed on the modulator and radiator sections as the afterburner is not a core part of the facility and will likely not be satisfied by just one device type but will itself be changed to suit the particular experiment being proposed. The specifications for the modulator and radiator undulators are given in table 5.7. The modulator must cover a wide range of seed input wavelengths, leading to a large K requirement. Fortunately one of our existing insertion devices, available from the decommissioned Daresbury SRS, seems very well suited to meeting these requirements and we are currently assuming that this device can be used for this purpose, further FEL studies will be carried out to confirm this in the future. The SRS device [142] has a period length of 200 mm and 4 periods and will be able to achieve the required K value easily. One possible issue which will be considered further is that to operate at 800 nm the magnet gap will be rather large (∼200 mm) and so fringe fields must be carefully assessed and magnet clamp plates retrofitted if necessary.

Another option which will be considered in the future is to operate the modulator over a more restricted wavelength range but to then seed on a higher harmonic of the device. In order to interact with the 800 nm input laser the modulator could be tuned to a fundamental of 4000 nm, for example, and the seed interact at the 5th harmonic. A demonstration of the principle has previously been made at UCLA [143].

The radiator undulators will be planar hybrid types utilising NdFeB permanent magnets and steel poles. In order to optimise the optical transmission of the FEL photon output into the diagnostic area, which requires large angle horizontal reflections, the radiators will be designed to generate vertical linear polarisation. In practice this means that the magnet arrays will generate a horizontal magnetic field and the gap adjustment will also be in the horizontal plane. It is not envisaged that this arrangement will cause any particular engineering difficulty when compared to the more common vertical gap adjustment mechanisms. Note that the modulator polarisation is independent of this specific radiator polarisation requirement since it is the electron modulation effect caused by the laser-modulator interaction which is required, and not the actual radiation generated in that section. We are assuming a modulator with horizontal linear polarisation at present.

The radiator undulators are separated by the inter-undulator sections. These sections must contain several pieces of equipment to ensure the optimum operation of the FEL, the total space required for each section is presently assumed to be 1.1 m. Each section will contain a quadrupole to match the electron beam properties along the length of the FEL, a phasing unit to ensure the radiation phase from each module can be independently adjusted, horizontal and vertical steerers to maintain good electron beam orbit control, an electron and photon beam screen diagnostic, and a cavity BPM. Space must also be included in the design for vacuum pumps and gauges. This space allowance is consistent with other FEL projects.

Detailed resistive wall wakefield studies must be carried out for the different bunch types interacting with the narrow gap undulator vessel. Initial simulations for the Ultra-short mode, which is expected to be the worst case, with a peak current of over 1500 A and 100 pC bunch charge show that the induced energy spread is significant and could impact on the FEL performance at short wavelength. Further studies will be carried out to assess more carefully the energy spread change in detail as an induced linear chirp could be compensated by undulator gap tapering, for example. Mitigation strategies exist if the FEL performance is disrupted significantly. The undulator vessel size could be increased, for example, as this is entirely compatible with 100 nm operation.

As well as requiring undulators for the FEL, CLARA will be an excellent facility for testing advanced undulator designs. ASTeC has a strong track record in developing short period, narrow gap, permanent magnet undulators [144] and also in high-field superconducting undulators [145]. Exotic ideas, such as RF or laser driven undulators, which would be too risky for an operating user facility to try, can be tested on CLARA.

5.8 Control system

5.8.1 Introduction

The control system plays a central role in all accelerator facilities. The CLARA control system will be a facility wide monitoring and control system integrating all parts of the CLARA accelerator. The control system will extend from the interface of the equipment being controlled through

2014 JINST 9 T05001

to the operator, technical expert or physicist. It will include all hardware and software between these bounds including computer systems, networking, hardware interfaces, programmable logic controllers (PLCs) and fieldbuses.

The Personnel Safety System (PSS) will be interfaced to, and monitored by, the CLARA control system. Timing and synchronisation of the lasers and RF systems is covered in section 5.5 and is not considered to be part of the control system. A separate event synchronisation system will be implemented as part of the control system to ensure synchronisation of critical control operations and to provide a common high resolution time-stamping capability.

The CLARA control system will benefit from existing control system equipment standards and knowledge gained from the recently implemented VELA facility.

5.8.2 Architecture

The CLARA control system will use the EPICS software toolkit. EPICS has been successfully applied at Daresbury in the ALICE, EMMA and VELA facilities and on numerous accelerator projects worldwide. EPICS is a proven software toolkit with well-defined interfaces at both the client and server and will enable fast integration and development. Due to its collaborative nature, using EPICS enables us to take advantage of work done at other laboratories.

The various elements of the control system will be connected to a high speed Ethernet local area network. This will consist of several class C subnets connected to the main site network. Access will be provided to the control system data via EPICS gateway systems running access security.

Whenever possible, wireless access will be provided in the accelerator complex to enable quick commissioning and maintenance to be carried out using laptop/tablet PCs.

The hardware interface layer of the control system will provide the connection to the underlying sub-systems. This will consist of a modular hardware solution of commercial rack mount PCs and VME systems running the Linux operating system connected to a range of I/O types directly or via selected fieldbuses.

Application software will be installed on central file servers to ensure consistent operation from any console on the control system network. The control system will be implemented in such a way that it can be incrementally expanded and upgraded as the project proceeds. The control system must be able to be extended to new hardware and software technology during the project phase and later.

A number of EPICS Channel Access client interfaces will be supported for controls and physics application development in high-level languages. These will include C#/VB via .NET, Matlab, Mathematica and Python.

5.8.3 Controls hardware

The network hardware and commercial PC hardware of the CLARA control system will use standards defined by the STFC Network and IT Support departments.

As far as possible controls hardware used on the VELA facility should be preferred to take advantage of existing expertise and proven hardware standards. This hardware includes:

2014 JINST 9 T05001

- *Commercial rack mount PC systems running a Linux operating system with real-time kernel:* existing EPICS support is available for interfacing many I/O types including analogue, digital and serial (RS232/422/485) along with status/interlocking via Ethernet connected PLCs.

- *Omron CJ series PLCs:* status and interlock systems for digital control and component protection of vacuum subsystems, magnets, power supplies etc.

- *Motion control systems:* fieldbus based systems interfaced to the control system via EtherCAT. These shall be jointly developed in collaboration with PSI for use also on the SwissFEL facility.

Any special control requirements would be solved by using dedicated real-time controllers (for example VME based or FPGA based). Examples of such systems could include geographically isolated devices or systems that require the computing speed of a dedicated CPU. Any dedicated controllers would be integrated into the EPICS environment and software build processes.

5.8.4 Timing and synchronisation system

One of the major challenges with a network distributed control system is the synchronisation and accurate time-stamping of events spread across several physically and logically separated systems. An example of this is the simultaneous measurement of beam diagnostic information along an entire beam transport system. This operation will typically involve collecting data from a number of front-end server systems.

Commercially available synchronisation hardware, as used on SLS, LCLS and other projects, is available for a number of platforms and provides timing outputs with a sufficient resolution for CLARA applications. It will be important to ensure that the master clock used by the control system is locked to the RF and laser systems of CLARA.

5.8.5 Interlock systems

The control system will provide a comprehensive interlock and protection system ranging from the enforcement of sensible operating limits right through to the protection of the whole accelerator against excessive beam loss. This section excludes the PSS which is described in section 6.2. Note that full monitoring of the PSS will be provided by the control system.

High integrity

This will be used to provide high-speed and fail-safe local protection in situations where serious damage to equipment is likely to occur. A typical example would be protection of undulator magnet arrays from excessive beam losses. Embedded micro-controllers could be used for this purpose.

Routine

This level of protection is intended to prevent minor damage to individual machine components or sub-systems. The Omron CJ series PLC based interlock system developed for the VELA facility will be used for this purpose.

2014 JINST 9 T05001

Both interlock systems will operate independently of EPICS with monitoring and control requests marshalled to the interlock systems via EPICS for processing via internally programmed logic.

In addition, but not described here, there will also be local systems that supervise individual components such as RF structures.

5.8.6 Feedback systems

Digital feedback will be required in a number of places on CLARA. The primary requirements are as follows:

Global transverse trajectory stabilisation

This will take the transverse beam position information from strip-line BPMs spread throughout the machine along with high-precision cavity BPMs in the bunch compressor, and derive correction settings to remove the effects of thermal drift, mechanical vibrations, electrical noise and other sources of disturbance.

Undulator transverse trajectory stabilisation

The stability requirements within the undulators will be particularly demanding. Transverse beam position must be stabilised in order to maintain FEL gain. Cavity BPMs will be used to provide positional reference information.
Low latency feedback systems will be required to satisfy the transverse stability requirements of CLARA on a shot-to-shot basis.

Stabilisation of the RF fields within the accelerating structures

The requirements for a proposed digital LLRF system are described in section 5.2.3. The necessary control loops for RF stabilisation will be implemented within the LLRF system and will be tightly integrated into the control system.

2014 JINST 9 T05001

Chapter 6

Radiation safety

6.1 Shielding requirements

6.1.1 Radiological classification of areas

A Radiological Classification of Areas considers all identified areas within a given facility and specifies a radiation zone for each area based on discussions with the designers of the facility, with regard to the following key drivers from the perspective of dose control:

- Expected occupancy levels,
- Prompt radiation levels during electron beam operations,
- Residual radiation levels following beam shutdown.

Minimisation of exposure to ionising radiation is aided by the classification of facility layouts according to the radiation levels expected in each area and the access or restriction requirements. These classifications assist in the production of a rational shielding design and dose saving strategy that will facilitate normal operational dose control. At this stage of the CLARA project, a full Radiological Classification of Areas has not been developed. In order to determine the bulk shielding requirements annual whole body effective doses of 1 mSv within the site boundary and 0.3 mSv outside of the site boundary have been assumed in accordance with the relevant STFC Safety Code. Taking account of reasonable occupancy levels to the side and on the roof of CLARA the following dose rate criteria have been assumed:

- 1 μSv/hr at the cold-side of the shielded enclosure walls;
- 2.5 μSv/hr at the cold-side of the shielded enclosure roof.

6.1.2 Source and material data

All of the source terms are directly derived from the operating modes described in chapter 3. Three scenarios have been assessed as these are thought to be those which represent realistic worse case situations. These are:

- Beam Dump: 250 MeV electrons, 25 pC$\times$20, 100 Hz, 12.5 W,

2014 JINST 9 T05001

- Beam Dump: 100 MeV electrons, 250 pC, 400 Hz, 10 W,

- Beam Collimator: 130 MeV electrons, 25 pC$\times$20, 100 Hz, 6.5 W.

In order to perform shielding calculations it is necessary to specify the isotopic compositions and densities of the shielding materials employed. All standard elemental compositions (e.g. Iron) have been taken from the FLUKA code [146]. The composition of concrete assumed is a pessimistic, dry composition, with a density of 2.32 g/cm^3. A simple, non-optimised, beam dump has been assumed which is an iron cylinder of 15 cm radius and 55 cm length with a 20 cm recess where the electrons first strike the material. This iron is then encased within a concrete cylinder of 45 cm radius and 85 cm long.

6.1.3 Shielding calculations

Dose rates have been assessed on the exterior of the shield surface where the maximum dose rate would be experienced whilst CLARA is operating. All dose rates have been calculated using the FLUKA Monte Carlo code. Independent cross-checks of calculations have been performed using MCNPX [147] and these demonstrate good agreement with the FLUKA calculations.

The results for the beam dump scenarios show that the 250 MeV case is bounding when compared with the 100 MeV case. Therefore, bulk shielding requirements will be driven by the 250 MeV case. The results indicate that 150 cm of concrete would be adequate to reduce dose rates to less than 1 μSv/hr (i.e. through the walls), or 125 cm to reduce the dose rate to less than 2.5 μSv/hr (i.e. through the roof). Beam dump optimisation could result in further reductions in bulk shielding thickness.

For the collimator scenario an impact angle of 11.3° was assumed, corresponding to a failure of a dipole magnet and the electron beam striking the steel vacuum vessel in an uncontrolled manner. Note that this scenario assumes all of the beam is lost so it would be a fault condition and not a long term operational scenario. In this case the calculations indicate that 160 cm of concrete would be required for the walls and 150 cm for the roof. If a continuous beam loss of 10% is assumed as opposed to 100%, the shielding thicknesses reduce to 130 cm (walls) and 115 cm (roof). Note that no additional local shielding has been assumed in these collimator calculations and so these remain rather pessimistic.

In summary, for the scenarios considered so far, the simulations suggest that a concrete wall thickness of 150 cm and roof thickness of 125 cm should ensure that the dose rates are within acceptable limits. Future studies will consider further optimisation of the beam dump and other locations where fractional continuous beam loss is expected, such as the collimator sections. In addition, the personnel labyrinth locations and geometries will need to be modelled and verified as well as the penetrations for cabling, waveguide, etc. Consideration will also be given to the anticipated levels of dark current and their sources to ensure that this additional source does not impact on the bulk shielding definition.

2014 JINST 9 T05001

6.2 Personnel safety system

6.2.1 Purpose

The purpose of the PSS for CLARA is to provide engineering control measures and interlocks that work together with radiation shielding and administrative procedures to ensure the safety of all personnel working on, or in close proximity to, the facility. The high-level functionality of the system must meet the legal requirements laid down in the Ionising Radiation Regulations, 1999 (IRR99). Also, an Approved Code of Practice (ACOP) to IRR99 provides guidance and advice on the design, operation and test of compliant systems.

6.2.2 Design requirements

In order to meet the requirements of IRR99 and its ACOP a number of key design features need to be present in the CLARA PSS. These can be summarised as:

- Warning devices giving a clear indication of the operating mode,
- Fail-safe Interlocks to ensure that persons cannot gain access to areas where exposure to ionising radiation is possible,
- A monitored search procedure to ensure that no one is trapped in the area when ionising radiation is being generated,
- Emergency Off buttons,
- Radiation Monitors to ensure that radiation levels are not significantly above expected design levels,
- Key activated permit switches to provide a means of easily authorising or disabling the facility or selected sub-systems. Also, over-ride key switches to permit, for example, low power RF to be enabled while trained staff are performing measurement and test within the machine.

Several additional design features cover functionality that is not required by legislation but which significantly improve operational usability:

- Integration with the CLARA control system so that the state of all interlocks and permits can be monitored, displayed and recorded,
- Use of permanently installed radiation monitors to ensure that measured radiation levels do not significantly exceed pre-determined limits,
- Use of modular hardware to simplify future expansion, fault-finding and maintenance,
- Provision of ‘Limited Access’ operation to allow controlled access to one or more machine areas under safe conditions without compromising the integrity of the search process.

2014 JINST 9 T05001

6.2.3 Implementation

In order to meet these requirements the PSS for CLARA will use a Commercial-Off-The-Shelf safety-rated PLC system to provide a modular, programmable and expandable system. This technology has been available for a number of years and is widely used in manufacturing industry to implement high-integrity safety systems for production lines, chemical processes and dangerous machinery. Although the use of such systems for radiation protection is relatively new this approach is currently being used on VELA and initial experiences are very encouraging so it is expected that a suitably scaled system will be a good solution for CLARA.

Chapter 7

Potential upgrades and future exploitation

The primary motivation for CLARA is firstly as an FEL test facility, but the availability of bright bunches of electrons at a range of energies may also enable other challenging areas of accelerator research to be developed which would otherwise not be possible. This chapter puts forward a number of areas which have come to our attention during the design of CLARA and that are worthy of further study. There may well be other applications possible which could be proposed in the future, so the ideas described here should be treated as a sample of possible applications, and not as a well-defined priority list or roadmap.

To enable these opportunities to be feasible in the future, space has been reserved within the CLARA shielding area for a 250 MeV beam transport line with beam extraction from CLARA, close to or possibly part of the high-energy spectrometer line. The shielded enclosure has room for at least one beamline parallel to the FEL and the option of taking additional beamlines into a new shielded area is also practical within the confines of the existing building.

7.1 Plasma accelerator research

High-gradient plasma accelerators hold the promise to minimize the scale and cost of future accelerators: it is possible to achieve accelerating gradients from 1 GV/m to 100 GV/m using relativistic plasma waves. Beam-driven plasma wakefield acceleration has achieved many significant breakthroughs [148, 149]. Proton-driven wakefield acceleration is proposed in the AWAKE project [150] to demonstrate high gradients for future high-energy colliders, as well as proposals such as LUNEX5 [151] which seeks to demonstrate lasing using a laser wakefield accelerated beam. This ongoing research will give significant boost to plasma accelerator research.

The beam parameters of CLARA are ideal to demonstrate plasma wakefield acceleration. A Plasma Accelerator Research Station (PARS) based at the CLARA facility will allow us to study the key issues in electron-driven wakefield acceleration. This will be the first UK-based beam driven plasma wakefield accelerator facility and will yield information essential for longer-term development of such facilities [152].

Preliminary studies show that a 250 MeV electron will obtain energy doubling with a ∼20 cm plasma cell. One-bunch electron-beam driven wakefield acceleration could be demonstrated in any of the three operating regimes of CLARA: long pulse (bunch length: 250–800 fs); short pulse (250 fs); and ultra-short pulse (30 fs), albeit using different bunch charges. The diverse beam operating modes of CLARA will allow the testing of scaling laws of plasma wakefield acceleration. It will also be possible to test many other interesting concepts such as: two-bunch experiments (crafting two bunches using a collimator, one for driving the plasma wakefield, and the other for sampling the wakefield); beam shaping studies for high transformer ratio (beam density profile shaping by shaping the laser pulse — multiple bunches or hard-edged beams can be near-ideal drivers); self-modulation of a long electron bunch can provide inputs to the CERN proton-driven PWFA experiment, AWAKE; use of CLARA as an electron injector for laser-driven wakefield acceleration (combined with LWFA research).

The beam will be switched to PARS at a full energy of 250 MeV. The proposed dogleg beam line design using π transform between the dipoles (using two FODO doublets) limits the transverse beam emittance blow up which arises from coherent synchrotron radiation; studies have assumed a 250 pC bunch charge and 250 fs bunch length, or 20 pC at 30 fs. The possibility of using an additional take-off line at lower angle ($\simeq 6^\circ$) from the 30° dipole for a high-energy diagnostics spectrometer is also being investigated. The proposed beamline is contained within the CLARA shielding area with a transverse centre-to-centre offset of approximately 1.5 m. In addition to PARS, this beamline could also be used for other experiments mentioned in this section as well as other future exploitation of the high-quality beam from CLARA.

7.2 Ultrafast Electron Diffraction

Electron beams with sub-angstrom wavelength and sub-100 fs bunch lengths, available from photoinjectors such as the CLARA gun, provide a cost-effective alternative to X-ray FELs for time-resolved structure determination. Ultrafast electron diffraction (UED) provides spatial information with atomic resolution on the time scale of the making and breaking of chemical bonds.

Similar photoinjector based accelerators for UED are being developed at DESY (Germany) [153], UCLA (US) [154] and Osaka University (Japan) [155] amongst others, together with the requisite detection and diagnostics instrumentation. The development of such a facility formed a core part of the NLS science case [17] where the accelerator provided the probe electron diffraction beam to monitor structural change as it evolved.

The initiation of change is with a pump laser derived from the photoinjector laser system and therefore a fundamental requirement is to obtain sufficiently high quality diffraction data in a single shot, as in most cases the sample is irreversibly changed by the pump laser. This can be achieved with only ∼1 pC charge.

The basic layout for UED is a sample chamber located at a position where the electron beam has low energy (few MeV), low divergence ($< 50\,\mu$rad) and short bunch length (<100 fs). The chamber allows a pump laser to be focussed onto the sample such that it is coincident with the electron beam. An electron collimator before the sample will allow beam shaping to provide a beam diameter of ∼0.5 mm at the sample, smaller than the diameter of the pump laser spot. This collimator will be sufficiently thick to prevent X-rays generated within it emerging and contami-

2014 JINST 9 T05001

nating the diffraction pattern on the downstream fluorescent screen; this screen is viewed with an image-intensifying CCD camera that allows single electron imaging [156].

The CLARA design allows the first linac to be used for velocity bunching, and the sample chamber can be located before Linac 2, which would be used as a drift section for the diffracted beams to be transported to the detection screen; the required diagnostics include beam arrival time monitoring. Key developments (which are also being pursued elsewhere, see for example Byrd [157]) are to reduce the RF jitter which limits the ultimate temporal resolution.

7.3 Compton photon production

It will be possible to generate photons with very high energies by Compton-scattering an intense longer-wavelength laser with the high-energy CLARA electron bunches: the naturally-short bunches will mean that, even in a head-on scattering geometry, the generated photons will be confined to pulses as little as 100 fs in length. 800 nm photons from a Ti:sapphire laser scattering from CLARA electrons at up to 250 MeV will generate a maximum photon energy around 1.5 MeV. By using a longer wavelength laser or lower energy electrons, the photon energy can be easily reduced to the keV region.

Dedicated Compton scattering facilities, such as ThomX in France [158] and ELI-NP [159] in Romania, are now being developed, demonstrating that there is a demand for short pulses of photons in the keV to MeV region. The electron beam brightness of CLARA is very competitive with these projects and so it will be capable of generating similar quality output.

7.4 Dielectric Wakefield Acceleration

Research into dielectric wakefield acceleration (DWA) has steadily increased over the past decade. This interest is driven by the prospect of developing advanced accelerators with accelerating gradients greater than $\sim$ 1 GV/m that will dramatically reduce the size and cost of high energy linear colliders, and that will also lead to the development of compact light sources. DWA concepts compare favourably with traditional metal accelerating structures, which are typically limited to gradients less than 100 MeV/m.

The wakefield in a DWA structure is generated by a drive bunch of relatively low energy (tens or hundreds of MeV), short length ($<$ 1 ps) and large bunch charge (many nC). A trailing bunch with the correct phase with respect to the drive bunch will then be accelerated by a high gradient wakefield [160]. The DWA structures currently being investigated are of simple cylindrical or planar designs with sub-mm apertures and fundamental frequencies in the THz range. Recent experimental progress in DWA research is impressive. Breakdown limits of 14 GV/m on the dielectric surface of a cylindrical dielectric structure have been demonstrated [161]. Trailing bunches have been accelerated in planar DWAs, albeit so far with modest $\sim$10 MeV/m gradients [162, 163]. Strong wakefield-induced energy modulation of the longer bunches has been demonstrated, the aim being to generate density-modulated electron beams on the sub-ps scale for production of coherent THz radiation [164]. A number of other experimental and theoretical DWA-related studies have been conducted. New enhanced DWA structures are under development and several experimental programmes are proposed, including those to be conducted at AWA (Argonne), FACET (SLAC)

2014 JINST 9 T05001

and FLASH (DESY). Near-term R&D encompasses the development of accelerator systems that can provide independent pairs of drive/witness bunches for DWA experiments, methods of shaping the drive bunch to increase the so-called transformer ratio (dual-frequency linacs, emittance exchange mechanisms etc.), and the construction and characterisation of novel DWA structures. For example, DWA structures are being investigated at AWA [165] as an alternative to metal RF structures in two-beam accelerator schemes such as CLIC.

The CLARA design parameters (up to 250MeV beam energy, sub-ps bunch lengths, low transverse emittance) and its flexibility in beam manipulation are ideal for conducting DWA-related R&D. Since the majority of the near-term DWA studies will be proof-of-concept experiments, the sub-nC bunch charges from CLARA should not be a particularly detrimental factor as long as the wakefield effects can be properly characterised. There are presently a limited number of suitable test facilities worldwide at which DWA research can be conducted. Therefore the initiation of DWA R&D on CLARA would potentially attract collaborations both nationally (with for example the Cockcroft and John Adams institutes) and internationally. Dielectric wakefield acceleration is a new and exciting area of research with far-reaching practical applications; it complements the mainstream FEL-related studies intended on CLARA, thus increasing this test facility efficiency and elevating its profile in the international accelerator physics community.

7.5 Nonequilibrium electron rings

Although 4th-generation sources of synchrotron radiation are primarily considering the use of FELs to provide ultra-bright pulses of photons to users, there remains a strong demand for radiation with other properties such as high average intensity, or which give other wavelengths. Indeed, the UK's first 3rd-generation source - DIAMOND - was only brought into operation six years ago, and is just entering its final phase of insertion device installation before it reaches full capacity. A programme of studies is underway to explore the possibility to upgrade the DIAMOND lattice with completely new magnets to give a so-called 'ultimate storage ring' with very small emittance for users. Similarly, several UK-led projects have proposed construction of facilities (such as DAPS, 4GLS and NLS) to service the VUV and soft X-ray research communities with radiation sources optimised for their needs.

Recent work carried out by ASTeC and the Cockcroft Institute [166] has suggested a new approach using nonequilibrium (NEQ) rings. Rather than allowing electron bunches to reach equilibrium as occurs in a normal electron storage ring, nonequilibrium rings store bunches for only a few thousand turns and use ultrafast kickers (already under intensive development for use in particle physics collider damping rings) to inject and extract them from the ring. With sufficient kicker speed and a good electron injector with high repetition rate, currents of up to 100 mA or more may in principle be achieved, the ring giving intense beams of photons with smaller emittances than would be achievable from a storage ring of the same size, but without the beam power problems inherent in high-energy ERLs. For example, ring designs similar to the Swedish MAX-II (90 m) or MAX-III (36 m) designs may be used to generate photons of energy ~ 2 keV but with 1 nmrad emittance. Even shorter wavelengths are possible by incorporating superconducting dipoles into the ring optics.

2014 JINST 9 T05001

CLARA's initial energy and repetition rate are insufficient to deliver high currents or short wavelengths, but a first demonstration of the nonequilibrium principle could be conducted using the 250 MeV electron energy; a future upgrade of CLARA to energies of 500 MeV or greater, and repetition rates great than 100 Hz, would allow a full test of a non equilibrium ring for synchrotron radiation production. A test electron ring could also be used for other purposes, as detailed in the following section.

7.6 Exotic storage ring concepts

A number of interesting demonstrations would be enabled by a small electron ring ∼50 m circumference that used CLARA as an injector. Firstly, an electron storage ring with electron energy of a few hundred MeV, in which electron polarisation naturally develops in the stored beam over a few hours, could be used as a calculable source of synchrotron radiation in the UV/VUV photon range by standards bodies such as the National Physical Laboratory; similar rings such as the German Metrology Light Source [167] have recently been constructed for just this purpose. The electron energy may be measured to high precision using a now-standard method to synchronously depolarise the beam.

Secondly, an electron ring of modest energy could be used to provide the first experimental demonstration of optical stochastic cooling (OSC) in an electron beam [168, 169]. Also proposed as a method to improve the beam brightness in hadron colliders, OSC could be used as a method to reduce the beam emittance in electron storage rings to improve the brightness of synchrotron radiation [170]. NEQ operation may be used to alleviate the increased Touschek scattering and short lifetime brought about by such small beam emittances, but another method which may be explored is the recent work to design the so-called Integrable Optics Test Accelerator (IOTA) [171, 172]. Proposed as an add-on to the Fermilab ASTA project, IOTA would utilise special nonlinear magnetic lattice elements to give a storage ring with very large dynamic aperture, allowing scatted electrons to survive to damp back down into the beam core. Combined with beam cooling this could be an alternative approach to providing good beam quality and long beam lifetime in a low-energy electron ring. It is possible that a single electron ring design could be used to test the NEQ, OSC, and IOTA principles at CLARA, whilst also being used as a standards radiation source.

7.7 Industrial exploitation

Whilst fundamental enabling research into next generation light sources remains the core driver of the CLARA facility, it will also be possible to harness the unique characteristics of the facility for industrial exploitation. Extensive market research for VELA [24] has identified that a high-power beam at energy up to 100 MeV would be optimum. Operation at 100 MeV, rather than 250 MeV, allows the maximum repetition rate to be increased from 100 Hz to 400 Hz without placing excessive thermal load on the accelerating structures. The bunch charge can be up to 250 pC to maximise the beam power if required and the other parameters can be optimised to meet the requirements of individual users. CLARA will build on the successful industrial engagement processes which are currently being implemented for first exploitation of the VELA accelerator facility in the summer 2013, whereby a variety of technology development groups have identified

2014 JINST 9 T05001

an effective route to utilise the flexible electron-beam delivery facility in order to validate new technologies or processes. Being able to offer similar levels of beam performance at higher beam energies and intensities will be the primary advantage of CLARA for industrial exploitation.

The fundamental accelerator technology systems required for the majority of the industrial accelerators globally can be effectively developed and demonstrated utilising the VELA/CLARA facilities: from electron beam sources, beam acceleration and diagnostics systems, magnets and UHV vacuum components, laser optics, beam control and feedback systems. The VELA Market Research Survey [24] identified a number of application areas where the increased electron beam energy of CLARA may enable access to markets beyond those currently enabled through VELA. These include a further enhancement of cargo scanning applications, enabling access to a greater range of treatment-applicable radioisotopes, high-energy medical sterilisation and a broader applicability of electron beams to environmental clean-up and purification challenges, all of which require accelerator technology sub-systems which can be developed and demonstrated using the CLARA experimental facility.

Whilst the exploitation of the photon output from CLARA for commercial use is not covered within the scope of the project, the inherent flexibility of the facility layout and infrastructure does not preclude future commercial photon exploitation work, should a suitable application and business case arise. From the broader perspective of the ASTeC facility portfolio, establishing the CLARA facility will further enhance the capabilities of the existing VELA facility by driving performance improvements to the equipment installed in the shared accelerator hall, and through the transfer of electron beam optimisation and development work to the new facility, thereby enabling a greater proportion of the VELA running time to be dedicated to industrial exploitation.

2014 JINST 9 T05001

Bibliography

[1] P. Emma et al., *First lasing and operation of an angstrom-wavelength free-electron laser*, *Nat. Photon.* **4** (2010) 641.

[2] H. Tanaka et al., *A compact X-ray free-electron laser emitting in the sub-angstrom region*, *Nat. Photon.* **6** (2012) 540.

[3] M. Altarelli et al. (eds). *XFEL: The European X-ray free-electron laser technical design report*, Technical Report DESY 2006-097, DESY, 2007.

[4] R. Ganter ed., *SwissFEL Conceptual Design Report*, Technical Report PSI Bericht Nr. 10-04, Paul Scherrer Institut, April 2012. ftp://ftp.psi.ch/psi/SwissFEL_CDR/SwissFEL_CDR_V20_23.04.12.pdf.

[5] W. Ackermann et al., *Operation of a free-electron laser from the extreme ultraviolet to the water window*, *Nat. Photon.* **1** (2007) 336.

[6] C.J. Bocchetta et al., *FERMI@Elettra Conceptual Design Report*, Technical Report ST/F-TN-07/12, Sincrotrone Trieste, 2007.

[7] P. Emma et al., *Femtosecond and subfemtosecond x-ray pulses from SASE based free electron laser*, *Phys. Rev. Lett.* **92** (2004) 074801.

[8] P. Emma et al., *Attosecond X-Ray Pulses in the LCLS Using the Slotted Foil Method*, in proc. of *FEL 2004*, 2004.

[9] E. L Saldin et al., *Terawatt-scale sub 10-fs Laser Technology - Key to Generation of GW-level Attosecond Pulses in X-ray Free Electron Lasers*, *Opt. Commun.* **237** (2004) 153.

[10] E.L. Saldin et al., *A New Technique to Generate 100 GW-level Attosecond X-ray Pulses from the Xray SASE-FELs*, *Opt. Commun.* **239** (2004) 161.

[11] A.A. Zholents and G. Penn. *Obtaining Attosecond X-ray Pulses using a SASE-FEL*, *Phys. Rev. Spec. Top. Acc.* **8** (2004) 050704.

[12] A. Zholents, *Methods of Attosecond X-Ray Pulse Generation*, in proc. of *IEEE, Particle Accelerator Conference* (2005) 39.

[13] E. Saldin, E. Schneidmiller and M. Yurkov. *Self-amplified spontaneous emission FEL with energy-chirped electron beam and its application for generation of attosecond x-ray pulses*, *Phys. Rev. Spec. Top. Acc.* **9** (2006) 1

[14] A.A. Zholents and M.S. Zolotorev. *Attosecond X-ray pulses produced by ultra short transverse slicing via laser electron beam interaction*, *New J. Phys.* **10** (2008) 025005.

[15] N.R. Thompson and B.W.J. M^{c}Neil. *Mode locking in a free-electron laser amplifier*, *Phys. Rev. Lett.* **100** (2008) 203901.

2014 JINST 9 T05001

[16] D.J. Dunning, B.W.J. M^{c}Neil, and N.R. Thompson. *Few-Cycle Pulse Generation in an X-Ray Free-Electron Laser*, *Phys. Rev. Lett.* **110** (2013) 104801.

[17] J. Marangos, R. Walker and G. Diakun eds., *NLS Project: Science Case and Outline Facility Design*, STFC, 2009.

[18] P.B. Corkum and F. Krausz. *Attosecond Science*, *Nat. Phys.* **3** (2007) 381.

[19] F. Krausz and M. Ivanov. *Attosecond physics*, *Rev. Mod. Phys.* **81** (2009) 163.

[20] H. Kapteyn et al., *Harnessing Attosecond Science in the Quest for Coherent X-rays*, *Science* **317** (2007) 775.

[21] *The Versatile Electron Linear Accelerator (VELA)*, http://www.stfc.ac.uk/ASTeC/Programmes/EBTF/38426.aspx.

[22] *FACET-II Facility for Accelerator Science and Experimental Test Beams-II*, Technical report, SLAC, 2013. https://portal.slac.stanford.edu/sites/ard_public/facet/Documents/FACET-II%20Proposal%20v6.pdf.

[23] L.T. Campbell and B.W.J. M^{c}Neil. *Puffin: a three-dimensional, unaveraged free-electron laser simulation code*, *Phys. Plasmas* **19** (2012) 093119.

[24] Inventya Ltd, *ASTeC–The Electron Beam Test Facility, Market Research* (2012).

[25] A.M. Kondratenko and E.L. Saldin, *Generation of coherent radiation by a relativistic electron beam in an ondulator*, *Part. Accel.* **10** (1980) 207.

[26] R. Bonifacio, C. Pellegrini and L. Narducci, *Collective Instabilities and High-Gain Regime in a Free-Electron Laser*, *Opt. Commun.* **50** (1984) 373.

[27] J.B. Murphy and C. Pellegrini, *Laser Handbook Vol. 6*, pages 9–69. North-Holland, 1990.

[28] R. Bonifacio et al., *Physics of the high-gain free electron laser and superradiance*, *Riv. Nuovo Cimento* **13** (1990) 1.

[29] E.L. Saldin E.A. Schneidmiller and M.V. Yurkov, *The Physics of Free Electron Lasers*, Springer, 2000.

[30] W.A. Barletta et al., *Free electron lasers: Present status and future challenges*, *Nucl. Instrum. Meth.* **A 618** (2010) 69.

[31] B.W.J. M^{c}Neil and N.R. Thompson, *X-ray Free-Electron Lasers*, *Nat. Photon.* **4** (2010) 814.

[32] H.H. Braun, *The Future of X-Ray FELs*, in proc. of *IPAC2012* (2012) 4180. http://accelconf.web.cern.ch/AccelConf/IPAC2012/papers/fryap01.pdf.

[33] B.W.J. M^{c}Neil, *A simple model of the free electron laser oscillator from low into high gain*, *IEEE J. Quant. Electron.* **26** (1990) 1124.

[34] D.C. Nguyen et al., *First lasing of the regenerative amplifier FEL*, *Nucl. Instrum. Meth.* **A 429** (1999) 125.

[35] B. Faatz et al., *Regenerative FEL amplifier at the TESLA Test Facility at DESY*, *Nucl. Instrum. Meth.* **A 429** (1999) 424.

[36] Z. Huang and R.D. Ruth, *Fully coherent X-ray pulses from a regenerative amplifier free electron laser*, *Phys. Rev. Lett.* **96** (2006) 144801 [physics/0602076].

[37] B.W.J. M^{c}Neil et al., *A Design for the Generation of Temporally-Coherent Radiation Pulses in the VUV and Beyond by a Self-Seeding High-Gain Free Electron Laser Amplifier*, *New J. Phys.* **9** (2007) 239.

2014 JINST 9 T05001

[38] D.J. Dunning, B.W.J. M^{c}Neil and N.R. Thompson, *Short Wavelength Regenerative Amplifier Free-Electron Lasers*, *Nucl. Instrum. Meth.* **A 583** (2008) 116.

[39] R. Colella and A. Luccio, *Proposal for a free electron laser in the X-ray region*, *Opt. Commun.* **50** (1984) 41.

[40] K.-J. Kim et al., *A Proposal for an X-Ray Free-Electron Laser Oscillator with an Energy-Recovery Linac*, *Phys. Rev. Lett.* **100** (2008) 244802.

[41] S. Reiche, *GENESIS 1.3: A fully* $3-D$ *time dependent FEL simulation code*, *Nucl. Instrum. Meth.* **A 429** (1999) 243. Code available at http://genesis.web.psi.ch/.

[42] J. Marangos et al., *New Light Source Conceptual Design Report*, Technical report, 2010. www.newlightsource.org.

[43] G. Stupakov, *Using the Beam-Echo Effect for Generation of Short-Wavelength Radiation*, *Phys. Rev. Lett.* **102** (2009) 1.

[44] D. Xiang and G. Stupakov, *Echo-enabled harmonic generation free electron laser*, *Phys. Rev. Spec. Top. Acc.* **12** (2009) 1.

[45] I. Martin, *Preliminary Studies of the Tapered Undulator Short Pulse Scheme Applied to the CLARA FEL*, Technical Report CLARA-FEL-REP-001/AP 500, STFC, 2012.

[46] I.P.S. Martin and R. Bartolini, *Comparison of short pulse generation schemes for a soft x-ray free electron laser*, *Phys. Rev. Spec. Top. Accel. Beams* **14** (2011) 030702.

[47] M. Borland, *ELEGANT - Electron Generation and Tracking*, 2000. APS-LS-287.

[48] R. Bonifacio, L.D. Salvo, P. Pierini, N. Piovella and C. Pellegrini, *Spectrum, Temporal Structure and Fluctuations in a High-Gain Free-Electron Laser Starting from Noise*, *Phys. Rev. Lett.* **73** (1994) 70.

[49] D.J. Dunning et al., *Start-to-end modelling of a mode-locked optical klystron free-electron laser amplifier*, *Phys. Plasmas* **18** (2011) 073104.

[50] E. Kur et al., *A wide bandwidth free-electron laser with mode locking using current modulation*, *New J. Phys.* **13** (2011) 063012.

[51] R. Bonifacio et al., *Generation of XUV light by resonant frequency tripling in a two-wiggler FEL amplifier*, *Nucl. Instrum. Meth.* **A 296** (1990) 787.

[52] I. Ben-Zvi, L.F. Di Mauro, S. Krinsky, M.G. White and L.H. Yu, *Proposed UV FEL user facility at BNL*, *Nucl. Instrum. Meth.* **A 304** (1991) 181.

[53] L.H. Yu, *Generation of intense UV radiation by subharmonically seeded single-pass free-electron lasers*, *Phys. Rev.* **A 44** (1991) 5178.

[54] L.-H. Yu et al., *High-Gain Harmonic-Generation Free-Electron Laser*, *Science* **289** (2000) 932.

[55] J. Feldhaus et al., *Possible application of X-ray optical elements for reducing the spectral bandwidth of an X-ray SASE FEL*, *Opt. Commun.* **140** (1997) 341.

[56] E.L. Saldin, E.A. Schneidmiller, Y. Shvydko and M.V. Yurkov, *X-ray FEL with a meV bandwidth*, *Nucl. Instrum. Meth.* **A 475** (2001) 357.

[57] G. Geloni et al., *A novel self-seeding scheme for hard X-ray FELs*, *J. Mod. Opt.* **58** (2011) 1391.

[58] J. Amann et al., *Demonstration of self-seeding in a hard-X-ray free-electron laser*, *Nat. Photon.* **6** (2012) 693.

[59] N.R. Thompson et al., *Improved Longitudinal Coherence in SASE FELs*, in proc. *IPAC2010* (2010) 2257 TUPE050.

2014 JINST 9 T05001

[60] J. Wu, A. Marinelli and C. Pellegrini, *Generation of Longitudinally Coherent Ultra High Power X-Ray FEL Pulses by Phase and Amplitude Mixing*, in proc. of *FEL 2012*, 2012. also SLAC-PUB-15348.

[61] D. Xiang et al., *Purified self-amplified spontaneous emission free-electron lasers with slippage-boosted filtering*, *Phys. Rev. Spec. Top. Acc.* **16** (2013) 010703.

[62] B.W.J. M^{c}Neil, N.R. Thompson and D.J. Dunning, *Transform-Limited X-Ray Pulse Generation from a High-Brightness Self-Amplified Spontaneous-Emission Free-Electron Laser*, *Phys. Rev. Lett.* **110** (2013) 134802.

[63] D.J. Dunning, N.R. Thompson and B.W.J. M^{c}Neil, *Design Study of an HHG-Seeded harmonic cascade free-electron laser*, *Journal of Modern Optics*, 58(16):1362, 2011.

[64] N.M. Kroll, P.L. Morton and M.N. Rosenbluth, *Free-electron lasers with variable parameter wigglers*, *IEEE J. Quantum Electron.* **17** (1981) 1436.

[65] R. Bonifacio and F. Casagrande, *The superradiant regime of a free electron laser*, *Nucl. Instrum. Meth.* **A 239** (1985) 36.

[66] L. Giannessi et al., *Nonlinear pulse evolution in seeded free-electron laser amplifiers and in free-electron laser cascades*, *J. Appl. Phys.* **98** (2005) 043110.

[67] T. Wanatabe et al., *Experimental Characterization of Superradiance in a Single-Pass High-Gain Laser-Seeded Free-Electron Laser Amplifier*, *Phys. Rev. Lett.* **98** (2007) 034802.

[68] I. Martin, *Feasibility Studies of Echo-Enabled Harmonic Generation on CLARA*, Technical Report CLARA-FEL-REP-002/AP 500, STFC, 2013.

[69] B.W. J. M^{c}Neil, G. R. M. Robb, D.J. Dunning and N.R. Thompson, *FELO: A One-Dimensional Time-Dependent FEL Oscillator Code*, in proc. of *FEL2006* (2006) 59.

[70] B W J M^{c}Neil et al., *A design for the generation of temporally-coherent radiation pulses in the vuv and beyond by a self-seeding high-gain free electron laser amplifier*, *New J. Phys.* **9** (2007) 239.

[71] B.W.J. M^{c}Neil and N.R. Thompson, *Cavity resonator free electron lasers as a source of stable attosecond pulses*, *Europhys. Lett.* **96** (2011) 54004.

[72] J. Wu, C. Pellegrini and A. Marinelli, *Generation of Longitudinally Coherent Ultra High Power X-Ray FEL Pulses by Phase and Amplitude Mixing*, in proc. of *FEL 2012* (2013) 237 TUPD07.

[73] J. Wu and C. Pellegrini, private communication.

[74] R. Santer and N.R. Thompson, *High-Brightness SASE Studies for the CLARA FEL*, in proc. of *FEL* (2013) 1274 TUPEA061.

[75] J.K. Jones et al., *A Compact, Modular Electron Beam Delay Line for Use in Novel Free-Electron Laser Schemes*, in proc. of *IPAC2012* (2012) 1759 TUPPP069.

[76] H.L. Owen and P.H. Williams, *A Modular Path Length Corrector for Recirculating Linacs*, *Nucl. Instrum. Meth.* **A 662** (2012) 12 [arXiv:1108.1709].

[77] H. Geng et al., *Polarization Analysis for Seeded FELs in a Crossed-Planar Undulator*, in proc. of *IPAC2010* (2010).

[78] D. Angal-Kalinin et al., *Design of the Production and Measurement of Ultra-Short Electron Bunches from an S-band RF Photoinjector*, in proc. of *IPAC12* (2012) 1560.

[79] S. Lebet et al., *A Multi Purpose X Band Accelerating Structure*, in proc. of *IPAC12* (2012) 70.

2014 JINST 9 T05001

[80] P.H. Williams, J.K. Jones and J.W. McKenzie, *Comparison of Compression Schemes for CLARA*, in proc. of *IPAC12* (2012) 1756 TUPPP068.

[81] K. Flöttmann, *Astra - a space charge tracking algorithm, 2000*, http://www.desy.de/∼mpyflo.

[82] J.W. McKenzie and B.L. Militsyn, *A Velocity Bunching Scheme for Creating Sub-picosecond Electron Bunches from an RF Photocathode Gun*, in proc. of *IPAC11*.

[83] S. Di Mitri, *Machine Design and Electron Beam Control of a Single-Pass Linac for Free Electron Laser: the FERMI@Elettra Case Study*, Ph.D. thesis, U. Groningen, 2011.

[84] S. Di Mitri et al., *Electron beam optics and trajectory control in the fermi free electron laser delivery system*, *Phys. Rev. Spec. Top. Acc.* **15** (2012) 012802.

[85] P. Craievich et al., *A Transverse RF Deflecting Cavity for the FERMI@Elettra Project*, in proc. of *DIPAC 2007*.

[86] D. Dowell, *The limits of beam brightness from photocathode rf guns*, in proc. of *Free Electron Laser Conference 2010*, FEL 2010.

[87] J.T. Moody et al., *Longitudinal phase space characterization of the blow-out regime of rf photoinjector operation*, *Phys. Rev. Spec. Top. Acc.* **12** (2009) 070704.

[88] R. Luus and T.H.I. Jaakola, *Optimization by direct search and systematic reduction of the size of search region*, *AIChE J.* **19** (1973) 760.

[89] M. Dohlus et al., *Start-to-end simulations of SASE FEL at the TESLA Test Facility, phase 1*, *Nucl. Instrum. Meth.* **A 530** (2004) 217.

[90] B.L. Militsyn et al., *Photoinjector of the EBTF/CLARA facility at Daresbury*, in proc. of *LINAC 2012*, 2012.

[91] F.B. Kiewiet, *Generation of Ultra-short, High Brightness, Relativistic Electron Bunches*, Ph.D. thesis, Technische Universiteit Eindhoven, 2003 ISBN 90-386-1815-8.

[92] J.-H. Han et al., *Design of a high repetition rate S-band photocathode gun*, *Nucl. Instrum. Meth.* **A 647** (2011) 17.

[93] D.H. Dowell et al., *Measurement and Analysis of Field Emission Electrons in the LCLS Gun*, in proc. of *PAC07*, Albuquerque, New Mexico, USA, 2007.

[94] F. Stephan et al., *New Experimental Results from PITZ*, in proc. of *LINAC08*, Victoria, BC, Canada, 2008.

[95] T. Asaka et al., *Stability Performance of the Injector for SACLA/XFEL at SPring-8*, in proc. of *LINAC12*, Tel-Aviv, Israel, 2012.

[96] K. Batchelor et al., *Development of a High Brightness Electron Gun for the Accelerator Test Facility at Brookhaven National Laboratory*, in proc. of *1st European Particle Accelerator Conference* Rome, Italy (1988) 954.

[97] R. Akre et al., *Commissioning the Linac Coherent Light Source injector*, *Phys. Rev. Spec. Top. Acc.* **11** (2008) 030703.

[98] J.-P. Carneiro et al., *Beam Transport, Acceleration and Compression Studies in the FERMILAB High-Brightness Photoinjector*, in proc. of *LINAC98* (1998) 878.

[99] E. Chevallay et al., *Photo-Cathodes for the CERN CLIC Test Facility*, in proc. of *LINAC98* (1998) 872.

2014 JINST 9 T05001

[100] S. Schreiber et al., *On the photocathodes used at TTF photoinjector*, in proc. of *PAC03* (2003) 2071, see also http://wwwlasa.mi.infn.it/ttfcathodes.

[101] J. Rodier, *Construction of The Alpha-X Photo-injector Cavity*, in proc. of *EPAC13* (2006) 1277.

[102] *Swiss FEL Injector Conceptual Design Report*, Technical report, Paul Scherrer Institut, July 2010.

[103] M. Dehler et al., *A Multipurpose X-band Accelerating Structure*, in proc. of *IPAC2012* (2012) 70.

[104] M. El Ashmawy, *Electron Beam Dynamics in CERN-PSI-Elettra* $5\pi/6$ *Travelling Wave X-band Linearizer*, in proc. of *IPAC2010* (2010) 4662.

[105] G. Burt et al., *A Transverse Deflecting Cavity for the Measurement of Short Low Energy Bunches at EBTF*, in proc. of *IPAC2012* (2012) 3335.

[106] P. Kownacki, *Reflectometer System for Active Phase Drift Compensation in Coaxial Cables*, in proc. of *LLRF11* DESY, October 2011.

[107] M. Hoffman et al., *Precision LLRF Controls for the S-Band Accelerator REGAE*, in proc. of *IPAC 2013*, 2013.

[108] M. Milloch et al., *LLRF Performance Results in Fermi@Elettra*, in proc. of *LLRF11* DESY, October 2011.

[109] T. Schilcher, *First Results of the SwissFEL Injector Test Facility LLRF System*, in proc. of *LLRF11* DESY, October 2011.

[110] A. Gallo et al., *Laser and RF Synchronization Measurements at SPARC*, in proc. of *PAC07* (2007) 992.

[111] J. Crisp and B. Fellenz, *Tevatron Resistive Wall Current Monitor*, 2011 *JINST* **6** T11001.

[112] A. Kalinin et al., *Diagnostic System Commissioning of the EMMA NS-FFAG Facility at Daresbury Laboratory*, in proc. of *IPAC10*, August 2010.

[113] D. Angal-Kalinin et al., *ALICE ERL Intra-Train Variation Investigation Using Bunch-by-Bunch BPMs*, in proc. of *IPAC13* (2013).

[114] D. Lipka, *Cavity BPM Designs, Related Electronics and Measured Performances*, in proc. of *DIPAC09* (2009).

[115] J. Bodewadt et al., *A Compact Electron Photon Diagnostic Unit for a Seeded FEL*, in proc. of *DIPAC09* (2009).

[116] M. Veronese et al., *Intra Undulator Screen Diagnostics for the FERMI@Elettra FEL*, in proc. of *IBIC2012* (2012).

[117] A. Angelovski et al., *High bandwidth pickup design for Bunch Arrival-time Monitors for Free-Electron Laser*, *Phys. Rev. Spec. Top. Acc.* **15** (2012) 112803.

[118] S.P. Jamison et al., *Upconversion of a relativistic Coulomb field terahertz pulse to the near infrared*, *Appl. Phys. Lett.* **96** (2010) 231114.

[119] M.D. Roper, *Spectral photon diagnostics for CLARA; General requirements and suitability of commercial spectrometers*, Technical Report CLARA-PHOT-DIAG-RPT-0002, STFC, 2012.

[120] Horiba Scientific, *VTM 300 - Vacuum Toroidal Monograph 300*, VTM300.

[121] Greateyes, *Scientific Full-Frame CCD Cameras for VUV, EUV, X-Ray Imaging and Spectroscopy*, GE 1024 1024 series.

[122] C.G. Durfee et al., *Intense 8-fs pulse generation in the deep ultraviolet*, *Opt. Lett.* **24** (1999) 697.

2014 JINST 9 T05001

[123] M.D. Roper, *Photon diagnostics for CLARA: Temporal diagnostics for mode-locked FEL scheme*, Technical Report CLARA-PHOT-DIAG-RPT-0001, STFC, 2012.

[124] Onefive GmbH, http://www.onefive.com/sync.html.

[125] S. Schulz et al., *Progress towards a permanent optical synchronization infrastructure at FLASH*, in proc. of *FEL* (2009).

[126] R. Wilcox et al., *Stable transmission of radio frequency signals on fiber links using interferometric delay sensing*, *Opt. Lett.* **34** (2009) 3050.

[127] J. Kim et al., *Long-term femtosecond timing link stabilization using a single-crystal balanced cross correlator*, *Opt. Lett.* **32** (2007) 1044.

[128] S. Schulz et al., *All-optical synchronisation of distributed laser systems at FLASH*, in proc. of *PAC* (2009). TH6REP091.

[129] T.T. Ng and S.P. Jamison, *Optical Clock Distribution at the ALICE Energy Recovery Linac*, in proc. of *IPAC* (2011). MOPC148.

[130] K.-L. Yeg et al., *Generation of 10 μ ultrashort terahertz pulses by optical rectification*, *Appl. Phys. Lett.* **90** (2007) 171121.

[131] A.G. Stepanov et al., *Mobile source of high-energy single-cycle terahertz pulses*, *Appl. Phys.* **B 101** (2010) 11.

[132] J.A. Fulop et al., *Generation of sub-mJ terahertz pulses by optical rectification*, *Opt. Lett.* **37** (2012) 557.

[133] J. Hebling et al., *Tunable THz pulse generations by optical pulse generation of ultrashort laser pulses with tilted pulse fronts*, *Appl. Phys.* **B 78** (2004) 593.

[134] F. Blanchard et al., *Generation of 1.5 μJ single-cycle terahertz pulses by optical rectification from a large aperture ZnTe crystal*, *Opt. Express* **15** (2007) 13212.

[135] C.P. Hauri et al., *Strong-field single-cycle THz pulses generated in an organic crystal*, *App. Phys. Lett.* **99** (2011) 161116.

[136] C. Ruchert, C. Vicario and C.P. Hauri, *Scaling submillimeter single-cycle transients toward megavolts per centimeter field strength via optical rectification in the organic crystal OH1*, *Opt. Lett.* **37** (2012) 899.

[137] Z. Chen et al., *Generation of high power tunable multicycle teraherz pulses*, *Appl. Phys. Lett.* **99** (2011) 071102.

[138] J.R. Danielson et al., *Intense narrow band terahertz generation via type-II difference-frequency generation in ZnTe using chirped optical pulses*, *J. App. Phys.* **104** (2008) 033111.

[139] A.G. Stepanov, L. Bonacina and J.-P. Wolf, *DAST/SiO_2 Multilayer Structure for efficient Generation of 6 THz Quasi-Single Cycle Pulses via Cascaded Optical Rectification*, in proc. of *37th International Conference on Infrared, Millimeter and Terahertz Waves (IRMMW-THz)*, IEEE, 2012.

[140] C. Vicario et al., *High-Field Laser-Based Terahertz Source for Swiss-FEL*, in proc. of *FEL13* (2013).

[141] A. Sell, A. Leitenstorfer and R. Huber, *Phase-locked generation and field-resolved detection of widely tunable terahertz pulses with amplitudes exceeding 100 MV/cm*, *Opt. Lett.* **33** (2008) 2767.

[142] J.A. Clarke et al., *Final measurements of the SRS multipole wigglers*, in proc. of *PAC 99* (1999) 2656.

2014 JINST 9 T05001

[143] S. Ya. Tochitsky et al., *Efficient harmonic microbunching in a 7th-order inverse-free-electron laser interaction*, *Phys. Rev. Spec. Top. Acc.* **12** (2009) 050703.

[144] B.J. A. Shepherd and J.A. Clarke, *Design, measurement and correction of a pair of novel focusing undulators for the ALPHA-X project*, *Nucl. Instrum. Meth.* **A 654** (2011) 8.

[145] D.J. Scott et al., *Demonstration of a High-Field Short-Period Superconducting Helical Undulator Suitable for Future TeV-Scale Linear Collider Positron Sources*, *Phys. Rev. Lett.* **107** (2011) 174803.

[146] A. Fasso et al., *FLUKA-2011: a multi-particle transport code*, Technical Report CERN-2005-10, CERN, 2005.

[147] *MCNPX Version 2.7.0*, Technical report, LANL, 2011.

[148] M. Hogan et al., *Plasma Wakefield Experiment at FACET*, in proc. of *IPAC2011* (2011) 715.

[149] E. Kallos et al., *High-gradient plasma-wakefield acceleration with two subpicosecond electron bunches*, *Phys. Rev. Lett.* **100** (2008) 074802.

[150] A. Caldwell et al., *Proton Driven Plasma Wakefield Acceleration*, *Nature Phys.* **5** (2009) 363.

[151] M.E. Couprie et al., *LUNEX5: A FEL project towards the fifth generation in France*, in proc. of *FEL2011* (2011) 208.

[152] G. Xia et al., *A Proposed Plasma Accelerator Research Station at CLARA Facility*, in proc. of *IPAC2013* (2013) 1280 TUPEA064.

[153] S. Manz et al., *Towards ultrafast electron diffraction and dynamic microscopy with REGAE*, http://regae.desy.de/e135097/e135098/.

[154] P. Musumeci et al., *High quality single shot diffraction patterns using ultrashort megaelectron volt electron beams from a radio frequency photoinjector*, *Rev. Sci. Instrum.* **81** (2010) 13306.

[155] Y. Murooka et al., *Transmission-electron diffraction by MeV electron pulses*, *Appl. Phys. Lett* **98** (2011) 251903.

[156] R.K. Li, *Imaging single electrons to enable the generation of ultrashort beams for single-shot femtosecond relativistic electron diffraction*, *J. Appl. Phys.* **110** (2011) 074512.

[157] J. Byrd, *Strategies for achieving femtosecond synchronization in Ultrafast Electron Diffraction*, in *Workshop on Ultrafast Electron Sources for Diffraction and Microscopy Applications*, 2012 http://pbpl.physics.ucla.edu/UESDM_2012/Program.html.

[158] A. Variola, *The THOMX Project*, in proc. of *IPAC2011* (2011) 1903.

[159] ELI - The Extreme Light Infrastructure, http://www.eli-np.ro/.

[160] W. Gai et al., *Experimental Demonstration of Wake Field Effects in Dielectric Structures*, *Phys. Rev. Lett.* **61** (1988) 2756.

[161] M.C. Thompson et al., *Breakdown Limits on Gigavolt-per-Meter Electron-Beam-Driven Wakefields in Dielectric Structures*, *Phys. Rev. Lett.* **100** (2008) 214801.

[162] S. Antipov et al., *Experimental demonstration of wakefield effects in a THz planar diamond accelerating structure*, *App. Phys. Lett.* **100** (2012) 132910.

[163] A. Andonian et al., *Dielectric wakefield acceleration of a relativistic electron beam in a slab-symmetric dielectric lined waveguide*, *Phys. Rev. Lett.* **108** (2012) 244801.

[164] S. Antipov et al., *Experimental observation of energy modulation in electron beams passing through teraherz dielectric wakefield structures*, in proc. of *IPAC2012* (2012) 595.

2014 JINST 9 T05001

[165] M.E. Conde et al., *A test-bed for future linear collider technology: Argonne Wakefield Accelerator facility (AWA)*, in proc. of *IPAC2012* (2012) 2778.

[166] H.L. Owen, P.H. Williams and S. Stevenson, *Nonequilibrium electron rings for synchrotron radiation production*, *Phys. Rev. Lett.* **110** (2013) 154801.

[167] R. Klein et al., *Operation of the metrology light source as a primary radiation source standard*, *Phys. Rev. Spec. Top. Acc.* **11** (2008) 110701.

[168] A.A. Mikhailichenko and M.S. Zolotorev, *Optical stochastic cooling*, *Phys. Rev. Lett.* **71** (1993) 4146.

[169] M.S. Zolotorev and A.A. Zholents, *Transit-time method of optical stochastic cooling*, *Phys. Rev. E* **50** (1994) 3087.

[170] E.G. Bessonov, M.V. Gorbunkov and A.A. Mikhailichenko, *Enhanced optical cooling system test in an electron storage ring*, *Phys. Rev. Spec. Top. Acc.* **11** (2008) 011302.

[171] V. Danilov and S. Nagaitsev, *Nonlinear accelerator lattices with one and two analytic invariants*, *Phys. Rev. Spec. Top. Acc.* **13** (2010) 084002.

[172] S. Nagaitsev, A. Valishev, V.V. Danilov and D.N. Shatilov, *Design and Simulation of IOTA - a Novel Concept of Integrable Optics Test Accelerator*, arXiv:1301.7032.

2014 JINST 9 T05001